AD NUMBER: AD0250673

LIMITATION CHANGES

TO:

Approved for public release; distribution is unlimited.

FROM:

Distribution authorized to U.S. Gov't. agencies and their contractors; Administrative/Operational Use; 31 DEC 1960. Other requests shall be referred to Office of Naval Research, Arlington, VA 22203.

AUTHORITY

ONR ltr dtd 4 May 1977

FINAL REPORT ON

CONTRACT Nonr-3109(00)

Investigations on the Direct Conversion of Nuclear Fission Energy to Electrical Energy in Plasma Diode

December 31, 1960

Research Laboratories

General Motors Corporation

MASTER DISTRIBUTION LIST

Contract Nonr-3109(00)

	No. of Copies
Power Branch (Code 429) Office of Naval Research Washington 25, D. C.	2
Cognizant ONR Area Branch Office	1
U. S. Naval Research Laboratory Technical Information Division Washington 25, D. C.	6
Naval Research Laboratory Code 6430 Washington 25, D. C.	1
Commanding Officer Office of Naval Research Branch Office Box 39 Navy #100 Fleet Post Office New York, N. Y.	2
Office of Technical Services Department of Commerce Washington 25, D. C.	1
Armed Services Technical Information Agency Arlington Hall Station Arlington 12, Virginia	10
National Aeronautics & Space Administration 1512 H. Street Washington 25, D. C. Attn: James J. Lynch	1
National Aeronautics & Space Administration Lewis Research Center 2100 Brookpark Road Cleveland 35, Ohio Attn: Frank Rom Roland Breitwieser Bernard Lubarsky	3
Chief, Bureau of Ships Department of the Navy Washington 25, D. C. Attn: Code 342B Code 1500, LCDR J. H. Weber	2

Chief of Naval Operations (OP-07G) Department of the Navy Washington 25, D. C.	1
Division of Reactor Development U. S. Atomic Energy Commission Washington 25, D. C. Attn: LCOL G. M. Anderson Doyle Rauch	2
Wright Air Development Division (WWRMFP) Wright Patterson Air Force Base Ohio	1
Air Force Cambridge Research Center (CRZAP) L. G. Hanscom Field Bedford, Massachusetts	1
Power Information Center (SP-01) University of Pennsylvania Moore School Building 200 South 33rd Street Philadelphia 4, Pennsylvania	1
Mr. A. F. Underwood Manager, General Motors Research Labs. 12 Mile and Mound Road Warren, Michigan Attn: Dr. D. H. Loughridge	1
Atomics International P. O. Box 309 Canoga Park, California Attn: Dr. N. S. Rasor	1
General Atomic P. O. Box 608 San Diego 12, California Attn: Dr. R. W. Pidd Dr. R. C. Howard	2

Republic Aviation
Farmingdale
Long Island, N. Y.
Attn: A. Schock — 1

Director of Special Projects (SP-01)
Department of the Navy
Washington 25, D. C. — 1

North Carolina State College
Raleigh, North Carolina
Attn: Dr. A. C. Menius — 1

Allied Research Associates, Inc.
43 Leon St.
Boston 15, Massachusetts
Attn: Dr. P. Goodman — 1

Ford Instrument Company
3110 Thomas Ave.
Long Island City, N.Y.
Attn: T. Jarvis — 1

Armour Research Foundation
10 W. 35th St.
Chicago 16, Illinois
Attn: Dr. D. W. Levinson — 1

Jet Propulsion Laboratory
California Institute of Technology
4800 Oak Grove Drive
Pasadena, California — 1

RCA Laboratories
David Sarnoff Research Center
Princeton, New Jersey
Attn: Dr. L. S. Negaard — 1

Los Alamos Scientific Laboratory
P. O. Box 1663
Los Alamos, New Mexico
Attn: Dr. George M. Grover — 1

Thermo Electron Engineering Corporation 85 First Avenue Waltham 54, Massachusetts Attn: Dr. George N. Hatsopolus	1
The Martin Corporation Baltimore 3, Maryland Attn: D. N. Tolat	1
Argonne National Laboratory 9700 South Cass Ave. Argonne, Illinois Attn: Aaron J. Ulrich	1
Hughes Research Laboratories 3011 Malibu Cannon Road Malibu, California Attn: Dr. R. C. Knechtli	1
Thomson Ramo Wooldridge, Inc. 7209 Platt Ave. Cleveland 4, Ohio Attn: Wm. J. Leovic	1
General Electric Research Laboratory Schenectady, New York Attn: Dr. V. C. Wilson	1
Westinghouse Electric Co. Research Laboratories Beulak Road Churchilboro Pittsburgh, Pennsylvania Attn: Dr. Max Gavbuny	1
Total - - - - -	55

Abstract. Contract Nonr-3109(00)

1. Experimental & theoretical studies on the fission fragment, noble gas plasma diode for direct conversion of nuclear energy to electrical energy.
2. Electron emissivity measurements in connection with material research on uranium bearing cathodes.
3. Spectral measurements of cesium plasmas yielding data on electron temperatures and ion number densities.
4. Preliminary measurements of a pulsed noble gas plasma diode.

Abstract. Contract Nonr-3109(00)

1. Experimental & theoretical studies on the fission fragment, noble gas plasma diode for direct conversion of nuclear energy to electrical energy.
2. Electron emissivity measurements in connection with material research on uranium bearing cathodes.
3. Spectral measurements of cesium plasmas yielding data on electron temperatures and ion number densities.
4. Preliminary measurements of a pulsed noble gas plasma diode.

Abstract. Contract Nonr-3109(00)

1. Experimental & theoretical studies on the fission fragment, noble gas plasma diode for direct conversion of nuclear energy to electrical energy.
2. Electron emissivity measurements in connection with material research on uranium bearing cathodes.
3. Spectral measurements of cesium plasmas yielding data on electron temperatures and ion number densities.
4. Preliminary measurements of a pulsed noble gas plasma diode.

Abstract. Contract Nonr-3109(00)

1. Experimental & theoretical studies on the fission fragment, noble gas plasma diode for direct conversion of nuclear energy to electrical energy.
2. Electron emissivity measurements in connection with material research on uranium bearing cathodes.
3. Spectral measurements of cesium plasmas yielding data on electron temperatures and ion number densities.
4. Preliminary measurements of a pulsed noble gas plasma diode.

Abstract. Contract Nonr-3109(00)

1. Experimental & theoretical studies on the fission fragment, noble gas plasma diode for direct conversion of nuclear energy to electrical energy.
2. Electron emissivity measurements in connection with material research on uranium bearing cathodes.
3. Spectral measurements of cesium plasmas yielding data on electron temperatures and ion number densities
4. Preliminary measurements of a pulsed noble gas plasma diode.

Abstract. Contract Nonr-3109(00)

1. Experimental & theoretical studies on the fission fragment, noble gas plasma diode for direct conversion of nuclear energy to electrical energy.
2. Electron emissivity measurements in connection with material research on uranium bearing cathodes.
3. Spectral measurements of cesium plasmas yielding data on electron temperatures and ion number densities
4. Preliminary measurements of a pulsed noble gas plasma diode.

Abstract. Contract Nonr-3109(00)

1. Experimental & theoretical studies on the fission fragment, noble gas plasma diode for direct conversion of nuclear energy to electrical energy.
2. Electron emissivity measurements in connection with material research on uranium bearing cathodes.
3. Spectral measurements of cesium plasmas yielding data on electron temperatures and ion number densities.
4. Preliminary measurements of a pulsed noble gas plasma diode.

Abstract. Contract Nonr-3109(00)

1. Experimental & theoretical studies on the fission fragment, noble gas plasma diode for direct conversion of nuclear energy to electrical energy.
2. Electron emissivity measurements in connection with material research on uranium bearing cathodes.
3. Spectral measurements of cesium plasmas yielding data on electron temperatures and ion number densities.
4. Preliminary measurements of a pulsed noble gas plasma diode.

TABLE OF CONTENTS

Introduction

1. . The effect originally noticed by Edison in which an electric current flows between a hot and a cold electrode in an evacuated space, has long been recognized as potentially providing the means for direct conversion of heat energy to electrical energy.(1) In recent years, an increasing amount of effort has been applied to the problem, particularly within industrial and government laboratories.(2)-(6) At the present time, the thermionic approaches to the problem can be roughly divided into the high vacuum diodes and the gas filled diodes. Within the latter class, the use of cesium gas has attracted the greatest attention. It was originally shown by Langmuir and Kingdon(7) that when cesium impinges on a hot tungsten filament (1200° K or more) the atoms are converted practically completely into cesium ions. Similar effects would be expected in the case of any metal whose work function is higher than the ionization potential of the impinging atom. However, the presence of such positive ions on the surface of the metal lowers the work function of that metal and results therefore in reducing the efficiency of the ionization process when a sufficiently large fraction of the metallic surface is thus covered by the atoms. (About 20% coverage in the case of cesium on tungsten.)(6)

In the summer of 1958, it was suggested, at the General Motors Laboratories, that the fission fragments produced in the fissioning of a uranium cathode might produce sufficient ionization density in a noble gas to cause the formation of a plasma. A diode of this type, having a uranium containing cathode, would release fission fragments of sufficient energy to ionize readily the noble gas in the diode even though the ionization potential of the noble gas is high in comparison to that of cesium.(8) A group was established by GM Management to investigate the field of thermionic direct conversion, and it was determined that the first objective would be the study of conversion of nuclear heat by the fission fragment, noble gas, diode concept. A contract between GM and the University of Michigan for the use of the latter's research reactor and hot cells was consummated during the fall of 1958. By late spring of 1959, the first noble gas diode with a UC cathode was designed, fabricated and ready for test.

2. . Investigators Responsible for the Work

The work described in this report has been carried out in the Physical Research Department of the General Motors Laboratories. The work has been directed by Dr. Donald H. Loughridge, Department Head. The research scientists and engineers active in the various investigations described in this report are: Dr. Frank E. Jamerson, Dr. Robert Silver, Mr. Charles B. Leffert, Mr. Richard H. Abrams, Jr., Mr. Robert Donohue, Mr. Robert Hill, and Mr. William J. LeGray. Technical assistants are Mr. Richard Dusman, Mr. James Bedard, Mr. Charles Williams, and Mr. Arthur Dolenga, glass blower.

(1) W.Schlichter, dissertation, University of Gottingen (1915)
(2) H.Moss, Brit. J.Electronics 2, 305, 1957
(3) M.J.O. Strutt, Proc.Inst. Radio Engs. 40, 601, 1952
(4) G.Medicus & G. Wehner, J.Appl.Phys. 22, 1389, 1951
(5) Hernqvist, Kanefsky & Norman, RCA Review, 19, 244, 1958
(6) V.C.Wilson, J.Appl.Phys. 30, 475, 1959
(7) I.Langmuir and K.H.Kingdon, Science, 57, 58, 1923
(8) Jablonski, Leffert, Silver, Hill, Loughridge, J.Appl.Phys. 30, 2017, 1959

Cooperating Groups

In the work described in this report, the following consultants were made available by contract with the General Motors Research Laboratories:

Professor W.P. Allis of the Massachusetts Institute of Technology contributed to the development of the theory of direct conversion diodes.

Dr. K. H. Kingdon has contributed to the work on cesium diodes and the pulsed diode concept.

Dr. Hans Griem, University of Maryland, has been a consultant to the work on plasma spectroscopy.

The University of Michigan reactor engineers have provided valuable cooperation.

A contract between Battelle Memorial Institute and General Motors has furnished investigations, and development, of various suitable cathodes and materials.

The G.M. Research Departments of Metallurgy, Physics, and Processing have greatly aided in material research, spectroscopic studies, and construction of laboratory devices, respectively.

Reactor Experiment I

Fig. 1 is a diagram of the first experimental cell. The UC cathode for this cell was prepared by the Argonne National Laboratory and was made by reducing UO_2 with excess C at 1900° C. Subsequent analysis showed about 0.3% UO_2 remaining, with some free carbon. The uranium carbide button was formed in two layers, the bottom being $U^{238}C$ while the upper layer was $U^{235}C$, since the 10 grams of U^{235} required to provide sufficient nuclear heat made the button too thin to handle. Initial calculations in the fall of 1958 had indicated that a plasma density approximating that of current cesium diodes could be produced in argon at 1 atmosphere pressure by a neutron flux of 10^{12} neutrons per second per square centimeter, which is the flux available in the University of Michigan "swimming pool" research reactor. Based on the plasma thermocouple theory of Lewis & Reitz(9)-(10), an aluminum water cooled anode was utilized since it minimized reactor design problems. Subsequently, however, the plasma thermocouple concept has been shown to be incapable of explaining presently known facts.

(9) H. W. Lewis & J. R. Reitz, Los Alamos Memo T-DO, July 25, 1958
(10) H. W. Lewis & J. R. Reitz, J. Appl. Phys. 30, 1439, 1959

A considerable amount of effort went into the heat transfer aspects of the cell design. Fig. 1 shows the tantalum radiation shields which surround the cathode. For radiation with neutrons, the entire assembly was placed at the bottom of an aluminum chamber 3 ft long by 3 in O.D., and the latter connected to a 20-ft length of aluminum tube which supported the device within the reactor core under 16 ft depth of water, and carried all the necessary electrical wiring and controls. See Fig. 2.

Only a limited amount of thermionic data on the reactor cell cathode disc were obtained in the laboratory prior to the reactor run, since the $U^{235}C$ sample provided by Argonne began to show signs of spallation at the edges after heat treatment. The disc, which ultimately fractured prior to assembly, was bonded to a tantalum holder with a niobium-titanium alloy to remove the tendency to spall at the edge.

Cathode disc temperature was measured by thermocouples and indicated 1900° K at full reactor power. Short circuit currents up to 0.02 amperes and open circuit voltages of about 1 volt were measured. Cell resistance was measured as a function of reactor power level and 30 ohms were recorded as a minimum value. Unexpectedly the major current flow was to an electrically insulated radiation shield which could be connected to the cathode. A series of separate reactor runs were made under varying cathode-anode gap and gas conditions. The results of successive runs indicated that the UC was being lost from the cathode. See Fig. 3. This situation was very definitely confirmed on the fifth run where the temperature was much lower than in former runs at the same reactor power. During the subsequent disassembly in the hot cell, the UC was found to be in pieces.

The first inpile experiment allowed the following conclusions to be drawn:

(a) Cathodes containing UC must be fabricated in such a way as to better withstand the effect of thermal cycling.

(b) Temperatures high enough for satisfactory electron emission from small cathodes can be produced in UC with a neutron flux of about $10^{12} n/cm^2$ sec.

(c) Low work function material must be used in the anodes.

(d) Improved outgassing and construction techniques, which will ensure a minimum of oxygen contamination, must be utilized.

(e) Pre-inpile emission studies of cathodes are desirable in order to show the expected increase in diode current due to the formation of plasma and also to check the constancy of diode properties by means of post-inpile emission runs.

(f) The noble gas plasma diode required an analysis different from other thermionic diode converters. The cathode-anode gap is filled with a noble gas which becomes ionized by fission fragments from the cathode. This generates a plasma of low fractional ionization which, under the influence of the contact potential difference and a sufficiently small cell resistance, allows the diode to operate as a direct converter of heat to electricity.

The theory of this diode, as developed by Dr. F. E. Jamerson, in collaboration with Prof. W. P. Allis, Consultant, is given in Appendixes I and II.

Reactor Experiment II

The objective of the next experiment was to study the increase in cathode-anode current obtained when a plasma is produced by fission fragments being introduced into the interelectrode region of a noble gas diode which had as cathode and anode tungsten impregnated with barium. Each of these electrodes could be separately electrically heated. See Fig. 4. The tube itself was of aluminosilicate glass and was baked out at 450° C. All metallic parts were either hydrogen fired, when their material properties allowed, or were induction heated when sealed on the pumping system. The uranium foil (0.032 gr U^{235}) 0.0025 cm thick is attached to the inside diameter of a tantalum cylinder which is 3 times larger in area than the foil and surrounds the cathode and anode. This thickness of U is about 2-1/2 times the fission fragment range. The neutron flux available in the U. of Mich. reactor is about 3×10^{12} neutrons/cm^2sec and the nuclear heat developed in the uranium foil was estimated at 9 watts/cm^2; the heat sink radiated 0.9 watts/cm^2. The total emissivity of Ta is about 0.15, in the temperature range of interest, which resulted in a uranium foil temperature of about 1000° K. Uranium vapor pressure considerations show that at this temperature the uranium foil should be quite stable. In addition to nuclear heat, there was the heat radiated from the cathode and anode that was intercepted by the foil. The cathode and anode were molybdenum of total emissivity 0.15. The cathode at 1450° K radiated 4 watts and the anode at 900° K about 0.5 watt. Thus an additional 0.45 watt/cm^2 added to the 0.9 watt/cm^2 from heat of fission gave a calculated foil temperature of around 1100° K. (U melts at 1400° K). The gas filling was Ne:A (10^3:1) at a pressure of 20 mm Hg. Conduction and convection losses would maintain the foil temperature below the 1100° K mentioned above, and indeed this was the case as during the reactor runs the foil temperature attained a maximum value of approximately 800° K. Voltage-current curves, recorded on an X-Y recorder, yielded the following results:

(a) Diode characteristics taken prior to and after inpile operation showed the usual retarding field and space charge characteristics, indicating the cathode surfaces to be stable under neutron radiation.

(b) Diode measurements with reactor power off indicated negligible gamma ionization effects.

(c) Inpile V-I characteristic showed an increase on short circuit current of a factor of 30 over the out of pile characteristic at the same temperature. See Fig. 5. The inpile data are similar to that obtained in the case of an auxiliary plasma diode operated in the laboratory, indicating the presence of a plasma in the inpile experiment of comparable density. The plasma number density, as computed from the measured saturated electron current and with electron temperature equal to cathode temperature, ranged from 4×10^{10} to 2×10^{11} ions/cm^3 over the temperature range 1150° K to 1450° K for a neutron flux (as experimentally calibrated) of 5×10^{12} n/sec cm^2 at the uranium foil in the diode.

(d) Diode saturated current measured with +10 volts accelerating potential on the anode during reactor startup showed an increase which varied as the square root of the power level, indicating that plasma density is recombination controlled. See Appendix III.

(e) More quantitatively, the saturated diode current was measured to be 1/10 of the saturated cathode emission at 1150° K, and 1/50 of the saturated cathode emission at 1450° K. The maximum current densities, measured over this temperature range, were 10^{-2} amps/cm^2 to 10^{-1} amps/cm^2.

In order to explain the low diode saturation current (I_{s-}) observed (1/10 to 1/50 of the saturated cathode emission I_e) it is assumed that the emission is held back by a negative potential, ΔV where (See Appendix III)

$$\frac{\Delta V}{T_e} = \ln \frac{I_{s-}}{I_e}$$

If it is further assumed that the space around the electrodes (see Fig. 4), where the fission fragments are densest and most of the ionization is taking place, is at cathode potential, or at a constant difference from cathode potential, then the voltage ΔV will pull ions into the interelectrode space and may cause the observed increase in

I_s with temperature. This interpretation leads one to recognize the relatively large effect of ion diffusion on the present results. It should be pointed out in this connection that the cylindrical geometry of this tube with the relatively small cathode-anode spacing of 1 mm causes the latter to act somewhat as a slit, and therefore the full number of fission fragments per sq cm do not pass through the slit region, but do maintain a higher flux density in the relatively unimpeded region in front of the uranium ring. This undesirable effect on the fission fragment flux should not obtain in a future diode where the cathode itself will be furnishing the fission fragments, and the latter will be emitted directly into the cathode anode gap. See Fig. 6 which is the design of a ceramic noble gas plasma diode experiment now in progress.

Reactor Experiment III

The question naturally arises as to the effect of fission gases upon the emission properties of uranium bearing (or other type) cathodes and anodes. To this end, a simple diode of barium impregnated tungsten cathodes, of 1 mm separation, was constructed but within a glass envelope which also held a small container filled with 1.2 gr of U^{235}. See Fig. 7. The container was provided with some small holes to allow fission gases to emerge into the diode region, but not release any appreciable number of the fission fragments. The diode gas filling was Ne:A (10^3:1) to a pressure of 20 mm of Hg. Either anode or cathode could be independently heated electrically. Runs were again made in the U. of Mich. research reactor in an experimental setup similar to Reactor Experiment II. The objectives of this experiment were to

1. Determine the effect of fission products on barium impregnated tungsten emitters.

2. Determine whether cesium released in fission would convert a noble gas plasma diode to a cesium diode.

3. Determine the effect of gamma induced ionization in a noble gas plasma diode.

Three runs were made with this tube while at the U. of Michigan reactor. Two were inpile and the third out of pile.

The V-I characteristics for a "cold" reactor and for increasing power levels up to 1 MW are given in Fig. 8 for nearly the same cathode temperature over the power range shown. It is interesting to note the saturated characteristic similar to that observed with Reactor Experiment II. See Fig. 5. This is a positive indication that

electrons arising from gamma ray collisions with tube structure are causing ionization within the tube. Another interesting feature of these data is the increase in back emission with power level. This is presumably true anode back emission since the ratio of forward to back emission is much less than the factor of 200 called for when positive ions simply make up the back current. For example, at 1 MW, the anode temperature, T_a, = 1015° K. At that temperature, the anode should yield a saturated emission of 0.8 ma and about 0.5 ma was measured at -10 volts, indicating that initially the anode surface was properly activated.

It was observed, however, that the back emission changed with time and this observation is plotted in Fig. 9 for the tube parameters indicated. The back emission appears to level off with time, and is still greater than leakage (measured as 30×10^{-9} amp at -10 volts). The ratio of the last data point, 0.006 ma, to the forward emission, 1.2 ma, is 200^{-1}, thus indicating that electron emission from the anode is now small and the back current is presumably ion current alone. The forward emission and the open circuit voltage, V_{oc}, are seen in Fig. 9 to be constant with time. Since the current is still plasma limited, the saturated forward emission is a measure of plasma density which is observed to be constant at positive voltages during this observation period.

To determine whether the anode surface could be reactivated, its temperature was raised to 1473° K for several minutes. Fig. 10 indicates the increase in back emission after the reactivation. However, it did not approach the original value of 0.5 ma in Fig. 8.

Four days after the above run, data were taken on the same tube at the side of the reactor pool. The initial runs showed the usual retarding and space charge type characteristic of the diode in the absence of ionization. The back current for T_c = 1415° K, T_a = 738° K was observed to be roughly twice leakage, i.e. 0.070 μa. At this anode temperature, the expected anode emission would be 0.3 μa, so the anode was still in the deactivated condition.

To observe whether or not residual fission products gases had any effect on the activation of the stem cathode at this point, the time dependence of voltage and current was measured at short circuit current. As seen in Fig. 11, there is not much change with time, even though the stem cathode temperature was low (1000° K) where sensitivity to deactivation should be high. The sign on the voltage graph is such as to correspond to a decrease in V with an increase in I corresponding to a reactivation.

Finally, the boat cathode was operated at 1400° K for 30 minutes showing essentially no change in forward or back emission with time. Both cathodes are fully activated then at this time.

The next run was an inpile experiment the following day. Pre-inpile V-I characteristics looked similar to Fig. 7, i.e. normal in the absence of plasma.

The time variation of saturated currents and V_{oc} was observed for a cathode temperature of 1180° K, and is given in Fig. 12. A decay in back current is observed similar to that of Fig. 9 observed at 1380° K. The decay is slower in the 1180° K case, and the current after 100 minutes is essentially constant, making the ratio of forward to back emission around 70, again less than $\sqrt{\frac{m_{neon}}{m_e}} = 200$. Forward emission and V_{oc} were nearly constant as seen previously.

Assuming that gases released from the hot uranium are responsible for poisoning the anode, it seems reasonable that the cathode surface would be poisoned as well, provided its temperature was low enough so that self-activation did not take place. A slight decrease in forward emission and V_{oc} with time was observed at T_c = 975° K, while back emission was relatively constant, as seen in Fig. 12. The reference for the time scale was selected as the time when the filament current was adjusted to give the temperature indicated.

By turning off both filaments an "ion chamber" current was measured. Because of the fission heat source in the tube, the cathodes were not cold, $T_{stem\,c}$ = 780° K $T_{boat\,c}$ = 850° K. These temperatures correspond to saturated emission of 0.002 ma and 0.02 ma respectively, whereas the measured values were 0.006 ma and 0.01 ma. The measured stem cathode value would correspond to ion current then, whereas the boat cathode value would correspond to ion current plus boat cathode emission.

The data and analysis give the following results:

1. The release of gases from uranium at 950° C reduces the emission of a barium impregnated tungsten surface, though it is possible to reactivate it by heating during inpile operation. The rate of change of emission is a function of surface temperature. At 1380° K the change in emission corresponded to a calculated 0.5 volt decrease in work function in 30 minutes.

2. For the 11-1/2 hour period at full reactor power, there was no evidence of increase in saturated output with time that would indicate operation of the tube as a cesium diode converter.

3. A saturated current was measured indicating that a weak plasma was being generated by electrons arising from gamma ray collisions with tube structure. The ion densities were smaller by a factor of ten or more than those observed for a fission fragment generated plasma.

4. For this period of operation, ion number density, as measured at saturation positive voltages, was unaffected by the fission products generated and released.

Thermionic Emission Studies of the UC-Nb Cermet Cathodes

Cathode life in any direct conversion device utilizing high temperature cathodes will always be affected by the vaporization of the cathode material. UC appears at present, from the studies at Los Alamos(11) and NRL(12) to be quite satisfactory from the standpoint of electron emissivity, but theoretically would be expected to have too short an operating lifetime due to its relatively high vapor pressure. With the objective of maintaining the good emission properties, but increasing the cathode lifetime, a contract with Battelle Memorial Institute was established to produce, for experimental study, various ceramic and cermet cathodes utilizing their high-pressure high-temperature autoclave techniques. The ceramic materials of interest were pure UC and mixtures of UC and ZrC prepared from both elemental and prealloyed powders in the ratio of 25 a/o uranium, 25 a/o zirconium, and 50 a/o carbon. The cermet materials investigated were 80 v/o UC in both niobium and rhenium.

The four materials listed in Table I were prepared by first hot pressing at 2200° F under a pressure of 3000 psi. The three ceramic type materials were then

Table I

	Composition			Estimated Core Density Per Cent Theoretical		
	Weight Per Cent	Atomic Per Cent	Volume Per Cent	Before Pressure Bonding	After Pressure Bonding	Remarks
.	76.1 UC(8.74 w/o C); 23.9 Zr	25 U; 25 Zr; 50C		50 to 55	Center 60 Edge 100	Slight core cracking
.	Arc melted$(U\text{-}Zr)C_2$	25 U; 25 Zr; 50 C		65 to 70	85	Slight core cracking
.	70.8 UC(4.85 w/o C); 29.2 ZrC (9.9 w/o C)	25 U; 25 Zr; 50 C		57 to 62	95	Moderate core cracking
4.	86.4 UC(4.85 w/o C); 13.6 Nb		80 UC; 20 Nb	67	99	No core cracking

sintered for 1 hour at 1930° C with little or no densification being observed. The four cores were then placed in a tantalum container and pressure bonded at 1320° C for 3 hours under a continuous pressure of 10,000 psi.

(11) R.W.Pidd, G.M.Grover, D.J.Roehling, E.W.Salmi, J.D.Farr, N.H.Krikorian, and W.G.Witteman, J.Appl.Phys. 30, 1575 (1959)

(12) George A.Haas and John T.Jensen, Jr, J.Appl.Phys. 31, 1231 (1960)

Various degrees of densification took place during pressure bonding as shown in Table I. The four specimens listed in the table were cycled three times between room temperature and 1700° C at a heating and cooling rate of approximately 72° C/min. Visual examination of the ceramic specimens suggested some reaction at the cladding interface. The cermet specimen seemed unaffected by the cycling. After metallographic examinations, the specimens were further cycled 10 times to 1700° C. By this time the cores numbered 1 and 3 had completely separated from the tantalum cladding; the cores 2 and 3 showed the presence of a second phase, while core 4 showed the appearance of a dark phase in and around the niobium in the core.

The above results showed that the UC-Nb cores stood the thermal cycling better than the other specimens. Hence two more were prepared by mixing 80 v/o UC-Nb powders (325 mesh size) for 2 hrs in an argon-filled dry box, after which samples of the mix were removed from the dry box and immediately covered with a 3 w/o cetyl alcohol-petroleum ether. After complete evaporation of the ether, the mix was pressed at 40,000 psi in an 0.1985" diameter die. The cores were immediately loaded into a niobium rod fitted with a niobium end cap which was in turn all fitted into a stainless steel tube. The stainless steel tube was sealed by welding on two stainless steel end plugs, one of which had an attached evacuation tube. The assemblies were evacuated and pressure bonded for 3 hrs at 1150° C under a helium gas pressure of 10,000 psi. This pressure bonding operation provided a bond between the niobium container and the niobium end cap so that the stainless steel tubing could be stripped off to prevent any reaction from occurring between the niobium and the stainless steel during subsequent pressure-bonding. Next the niobium clad cores were further pressure bonded for 3 hrs at 1320° C under a helium gas pressure of 10,000 psi to ensure densification of the cermet core. With the aid of radiographs, the emitter core was ground and polished by metallographic techniques to the required finished size.

A study of the thermionic emission properties of these cermets is being carried out at GMR. Data have been obtained for one of the cermets in a parallel plate diode geometry. A 2 cm molybdenum anode with a large mass and radiating surface was used in order to operate the anode as cool as possible, and to reduce cathode temperature fluctuations due to back radiation. The cathode to anode spacing was 0.05 cm. The diode was enclosed in a glass envelope, evacuated on a glass vacuum system, baked out and then sealed off. The seal off pressure was about 10^{-7} mm of Hg.

Voltage-current characteristics were taken by sweeping the anode voltage from 0 to 3000 volts and displaying the voltage on the x axis and the current on the y axis of an oscilloscope. See Fig. 13. Data were limited to 3000 volts due to breakdown in the tube. This upper limit of field strength (60,000 volts/cm) is not high enough to ensure that the slope of the voltage current curve is far enough into the Schottky region. Thus the temperatures calculated from the Schottky slope were lower

than the measured values. A Schottky plot of the data is shown in Fig. 14. The solid lines are the Schottky slopes fit to the experimental points. The dashed lines are the slopes expected from the experimentally observed temperatures. A Richardson plot using the observed temperatures and the saturated current values obtained from the observed temperature slopes is shown in Fig. 15. It is of interest to compare these results to those obtained at Los Alamos[11] for uranium carbide. Parallel plate geometry was used. Fig. 16 gives a plot of this Los Alamos data in which the maximum field strength was about 6000 volts/cm. The present data are shown on the same graph and indicate that the UC-Nb compares favorably with UC, as an electron emitter, at temperatures up to at least 1500° K. Both the present data and Los Alamos data suffer from insufficiently high field strengths to go far enough out on the Schottky curves. Thus the A and ϕ values obtained from these experiments are not reliable, but the present results do show very close equivalence between UC and UC-Nb as electron emitters.

Additional UC data have been obtained by Haas and Jensen at the Naval Research Laboratory [12] with electric field strengths of 220,000 volts/cm in cylindrical geometry. They obtain values of A and ϕ, in the Richardson equation, for UC of 33 amps/cm^2 K°^{2} and 2.94 electron volts, respectively.

Thus we conclude that UC-Nb cathodes are roughly equivalent to UC in their electron emissive powers, and are superior as far as thermal cycling is concerned.

Ceramic Noble Gas Diode

The results of the various experiments carried out up to this stage of progress in the work now gave encouragement that a ceramic noble gas filled diode could be designed and constructed with a cathode of UC-Nb cermet, and an anode of barium impregnated tungsten. (Philips type). The design of the tube is shown in Fig. 17. The UC-Nb cathode was fabricated at Battelle Memorial Institute using their high pressure, high temperature, bonding technique, and contained 20 grams of U^{235}. The cathode and anode are each 1" in diameter and separated by a 3 mm gap. This gap is maintained by 3 sapphire rods. The various metal to metal seals were formed by brazing techniques utilizing induction heating. All metallic parts were hydrogen fired before assembly. The various metal to metal seals were formed by hydrogen brazing techniques utilizing induction heating. An x-ray examination after assembly and leak test revealed that the cathode had expanded greatly in volume and completely filled the anode-cathode gap. This unexpected result has been attributed to a

(11) loc cit
(12) loc cit

hydriding reaction in the UC-Nb cermet during the final hydrogen braze. The reaction very probably is the following:

$$UC + Nb = NbC + U$$

$$2U + 3H_2 = 2UH_3$$

The UH_3 has a density of about 1/3 that of UC, which results in the large expansion. As a consequence, the ceramic tube is being rebuilt but will not be ready for test within the period required for inclusion in this report. A supplement to the present report will be provided as soon as the results become available.

Plasma Spectroscopic Studies

The satisfactory interpretation of much of the data from direct conversion devices requires a knowledge of the ion and electron densities as well as their temperatures. In order to satisfy such needs, a program for the experimental investigation of cesium plasmas was established. The object of this section is to present a brief outline of the theory and experimental techniques employed in the program.

The physical quantities desired are:

a. Temperature of the electrons
b. Number density of electrons and ions
c. Temperature of atoms and ions
d. Number density of neutral atoms

All of these variables are desired as a function of the distance between cathode and anode. Furthermore, the question of thermal equilibrium between ions, electrons and atoms is important.

Electron temperatures are obtained by measuring the ratio of intensities of the two cesium lines 8521 A° and 4555 A°. The electron temperature, T, is obtained from the following equation:(13)(14)

$$\frac{I_{8521}}{I_{4555}} = 9.26\, e^{\frac{14700}{T}}$$

(13) "The Electric Arc." J. M. Somerville, Pg. 25
(14) "Absolute Values of Transition Probabilities for Members of the Principle Series of Cesium Lines". Leningrad Univ., 1952

The temperature of the ions and the number densities of the electrons are obtainable from the profile of the 4555 A° line. Ion temperatures related to the Doppler width of the line are given by (15)

$$T_i = \text{const} \frac{\Delta\lambda_D^2}{\lambda} \quad \text{where } \Delta\lambda_D \text{ is the Doppler half width of the line.}$$

Dr. Hans Griem has shown theoretically(16) that the electron density is given by

$$N_e = 10^{17}\Delta\lambda_c \quad \text{where } \Delta\lambda_c \text{ is the collision half width, and}$$

is in angstrom units. The latter is obtained from the wings of the 4555° line using the Voight formula(15) to represent the intensity, J, of the line as a function of wave length within the line breadth.

$$\lim_{\Delta\lambda \to \infty} J = \frac{\Delta\lambda_c}{(\Delta\lambda)^2}$$

Actually, $\Delta\lambda \to \infty$ only indicates measurement in the wings of the line breadth. Here it is assumed that the electron and ion densities are equal.

The number density of neutral atoms is determined from the absolute intensity of the infra red line and the electron temperature, T,

$$N_0 = C_1 e^{\frac{1.69 \times 10^4}{T}} \quad (13)$$

where N_0 = number density of neutral atoms

C_1 = a constant of the radiating energy state and the geometry of the experimental tube

The experimental apparatus is shown in Fig. 18 and consists of a Bausch & Lomb Littrow-Echelle spectrograph tube and oven. The plasma tube consists of a ten mil diameter tungsten filament 2 cm in length serving as a cathode, and is surrounded by a concentric nickel anode 2 cm in diameter. The filament is heated by a battery. An optically flat window serves as the optical exit from the pyrex tube, and thus allows viewing with the optical path parallel to the filament and anode surfaces. The entire

(13) loc cit
(15) "Quantitative Molecular Spectroscopy & Gas Emissivities", S. S. Penner; Addison-Wesley; Reading, Mass; 1959, Ch 3, eq 3-30; 3-34
(16) Unpublished communication with Dr. Hans Griem

tube is mounted in an electrically heated oven and temperatures are recorded by thermocouples at four positions on the tube. The tube contains only cesium, the pressure being determined by the temperature of the housing in which the tube is mounted. The lowest thermocouple reading is taken to be the cold spot temperature and thus yields the cesium vapor pressure from known data. The radiation from the plasma is focused on the slit of the spectrograph. The radiation can pass through two optical systems on its way to the exit where it activates a photographic plate.

The first system is a quartz prism (Littrow) with a mirror behind it. Light from the entire cathode-anode gap is split into its components and is recorded on the plate. This system yields line intensities for short exposure times.

The second system is the same prism with a grating (Echelle) behind it. The radiation is moderately resolved (60,000 in the red) so that the line profile can be recorded on the plates. Only a small portion ($\sim$ 20 microns) of the cathode-anode gap can be recorded during one exposure, and the exposure time is about one hour for the blue lines and less than one minute for the infra red lines

Measurements of the line intensities and profiles were taken with this instrument for the following diode operating parameters:

1. T_{fil} = 2770° K
2. T_{bath} = 360° C
3. I_{fil} = 8.2a
4. V_{fil} = 6.0 volts
5. I_{C-A} = 1.0 amps

Typical results of these measurements were:

1. T_{el} = .69 ev = 8000° K
2. T_i = .52 ev = 6050° K
3. T_{SA} = .62 ev = 7200° K
4. $N_{el} = N_{ions}$ = 2.6×10^{15}/cm
5. $P_{el} + P_{ions}$ = 5.3 mm of Hg
6. P_{VP} = 7.0 mm of Hg

Figure 19 is a plot of the electron temperature as a function of the cathode to anode gap.

One can see that the ion and electron temperatures agree reasonably well (within experimental error which is about 20%). T_{SA} is the temperature determined from the Saha[17] equation using our values for N_a, N_i, and N_o. T_{SA} and T_{el} are nearly equivalent, a fact which indicates the consistency of the data.

The consistent agreement between the values presented suggest that the theory and technique of this experiment yield a reasonable picture of the physical phenomena which are occurring in the tube.

A further study is now being made in which the cathode of the diode is heated by a half-wave rectifier and measurements on line intensities made both during the heating part and the unheated part of the 60 cycle wave. Preliminary results show that the intensities of the lines vary during the entire pulse, and it is expected that such time dependent measured intensities will aid in answering the question of thermal equilibrium.

Present Material Program at BMI

In the studies with UC-Nb systems, Battelle has shown that it is necessary to use UC containing excess carbon to prevent the formation of free uranium by the reaction

$$UC + Nb \longrightarrow U + NbC$$

This was accomplished by establishing niobium carbide barriers between the UC and Nb metal. However, it is difficult to supply sufficient excess of carbon to satisfy completely the niobium reaction. In order to obtain improved UC containing cathode materials, it was found desirable to initiate a new program at BMI with the aim of establishing a material system that will stabilize the UC.

A review of the ternary phase diagrams was conducted by BMI in an effort to select other promising UC cermet systems. It seems possible at this time to place the refractory metals in three categories: (1) those metals that form very stable carbides, such as niobium and zirconium which would be expected to form free uranium in a UC-metal system; (2) those metals that form less stable carbides, such as molybdenum, which upon equilibrium would contain free refractory metal in a UC-metal system; and (3) those materials, such as rhenium, which form very unstable carbides.

BMI is presently conducting a program that will give preliminary information on the last two types of material systems. The niobium system (type 1) has been

completed in the first phase of our materials program. In this study, it is planned to prepare cermet cathodes consisting of 80 v/o UC in molybdenum, rhenium and tungsten, and to compare the stability of these systems with that of the UC-Nb system. This should provide us with the most useful data for planning future material programs, and should make a valuable contribution to the field of UC cathode development.

Future Program

During the calendar year 1961 the program for development of thermionic energy converters will be a continuation of the inpile experiments on fission-fragment-noble-gas-plasma converters; increased emphasis on the noble gas pulsed diode converter; continued spectroscopic studies of cesium plasmas, and possible also plasmas of other alkali metals.

The General Motors Research Laboratories has contributed additional laboratory space which will provide roughly three times the area for experimental work. Continuing recruiting of competent investigators is being carried out by the Personnel Department. Very appreciable additions to the experimental equipment required for such an expanding program are being provided.

The contribution to the support of the work during calendar year 1960 by the Office of Naval Research under contract Nonr-3109(00) is greatly appreciated, and has resulted in more rapid progress than would otherwise have been attained. It is hoped that such additional support to the GM program on direct conversion will be continued.

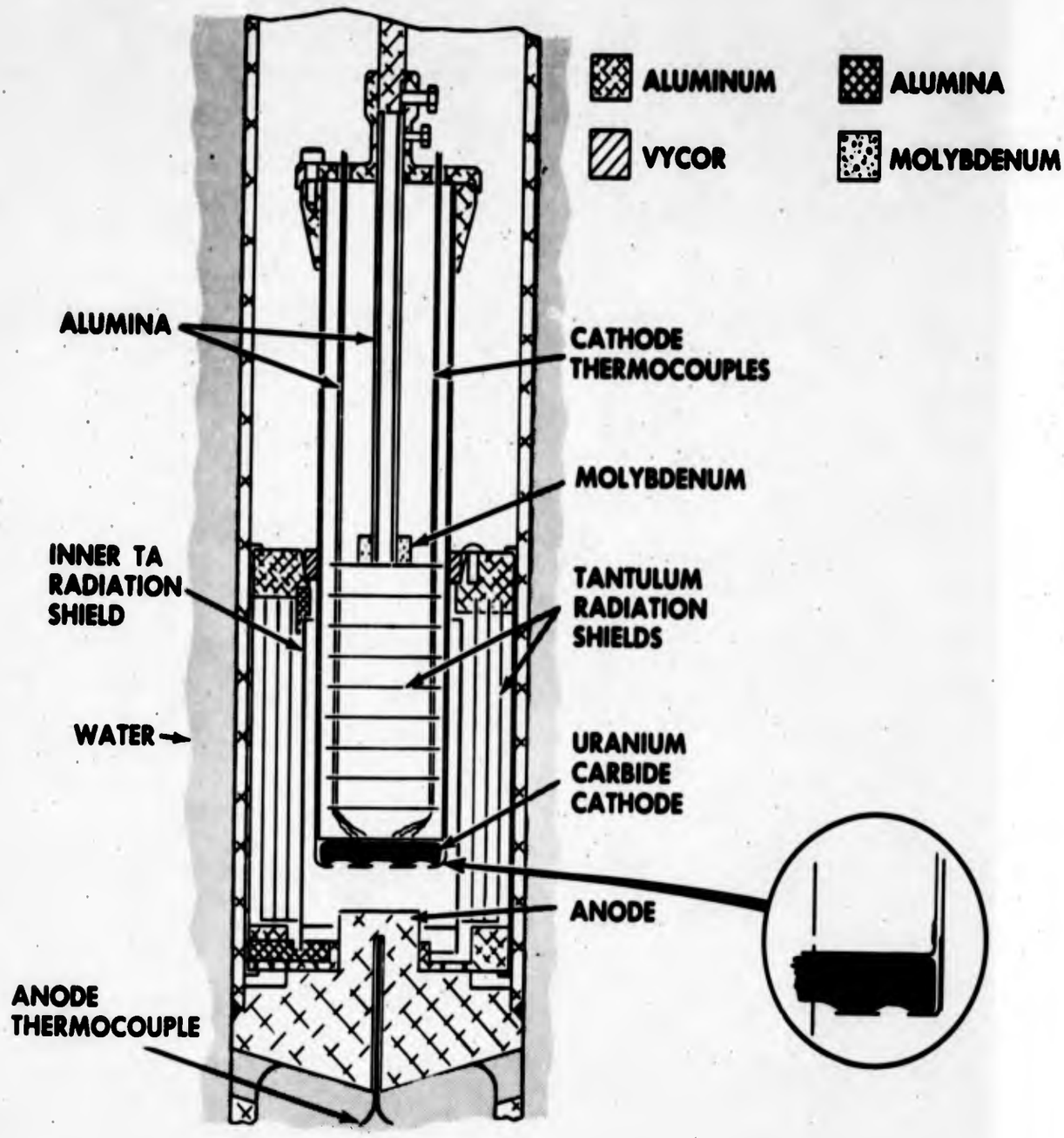

Figure 1
Diode 1. Sub-Assembly

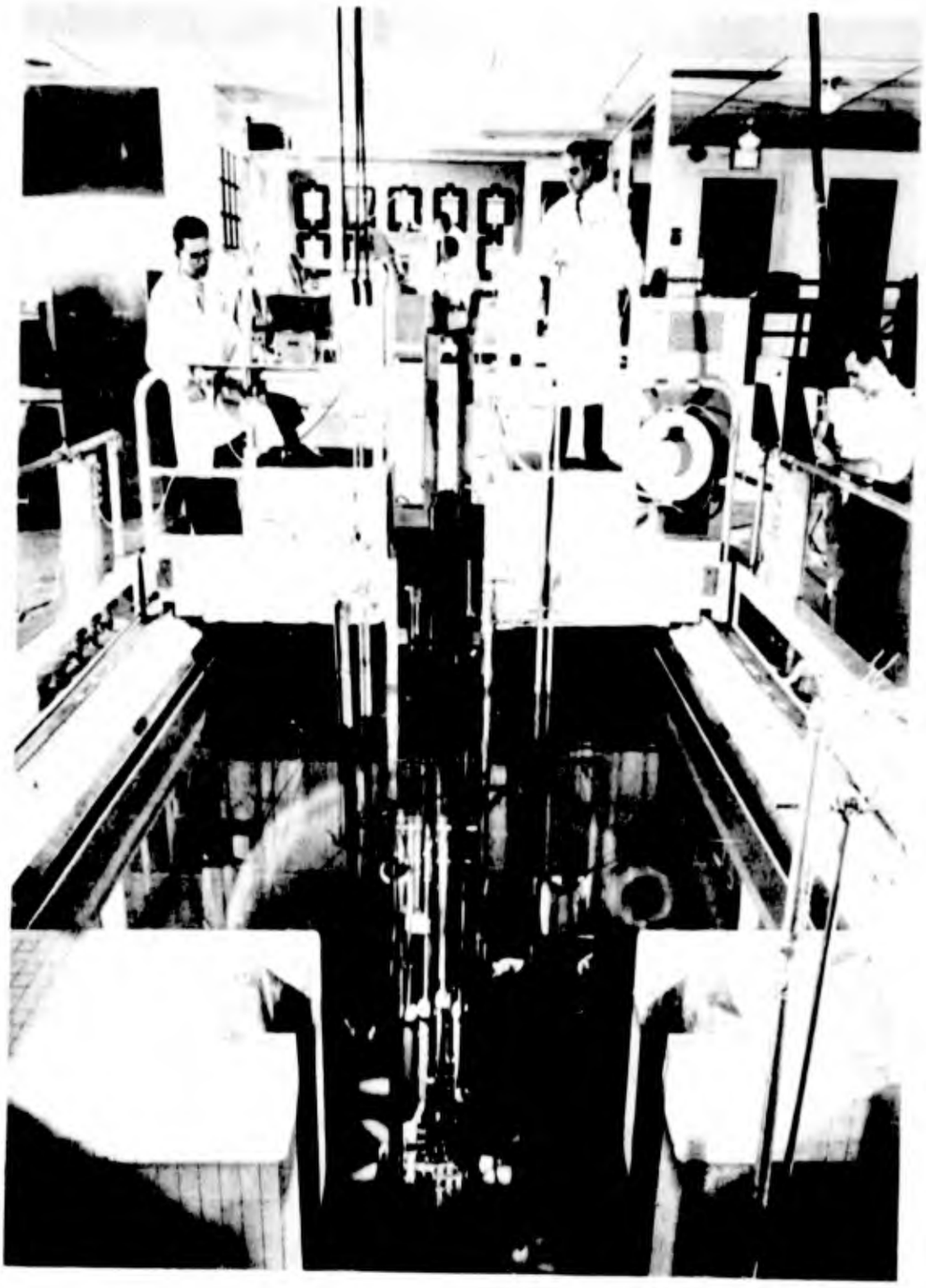

Figure 2
Reactor Test Installation

Figure 3
Diode I Cathode Temperatures - vs - Reactor Power

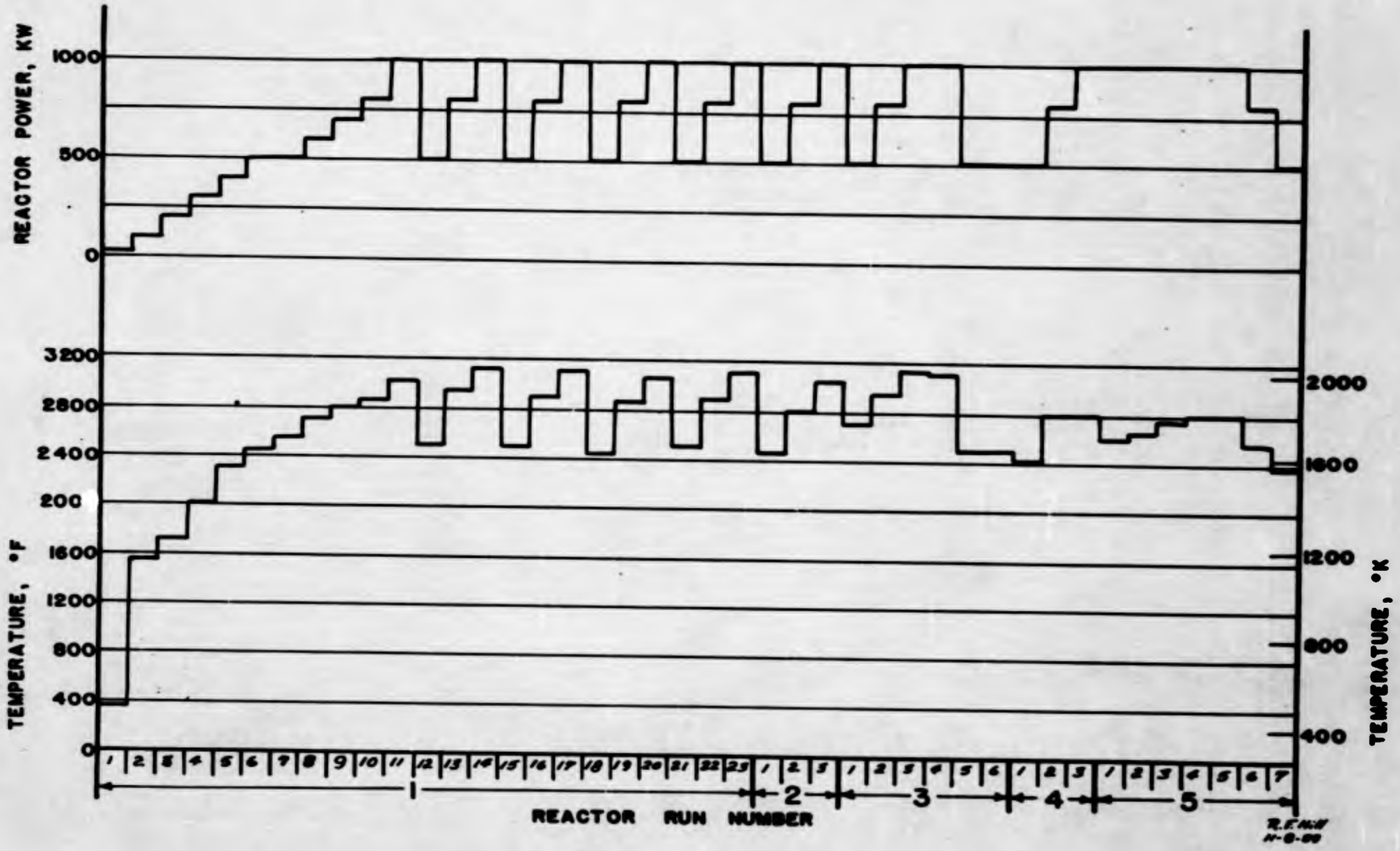

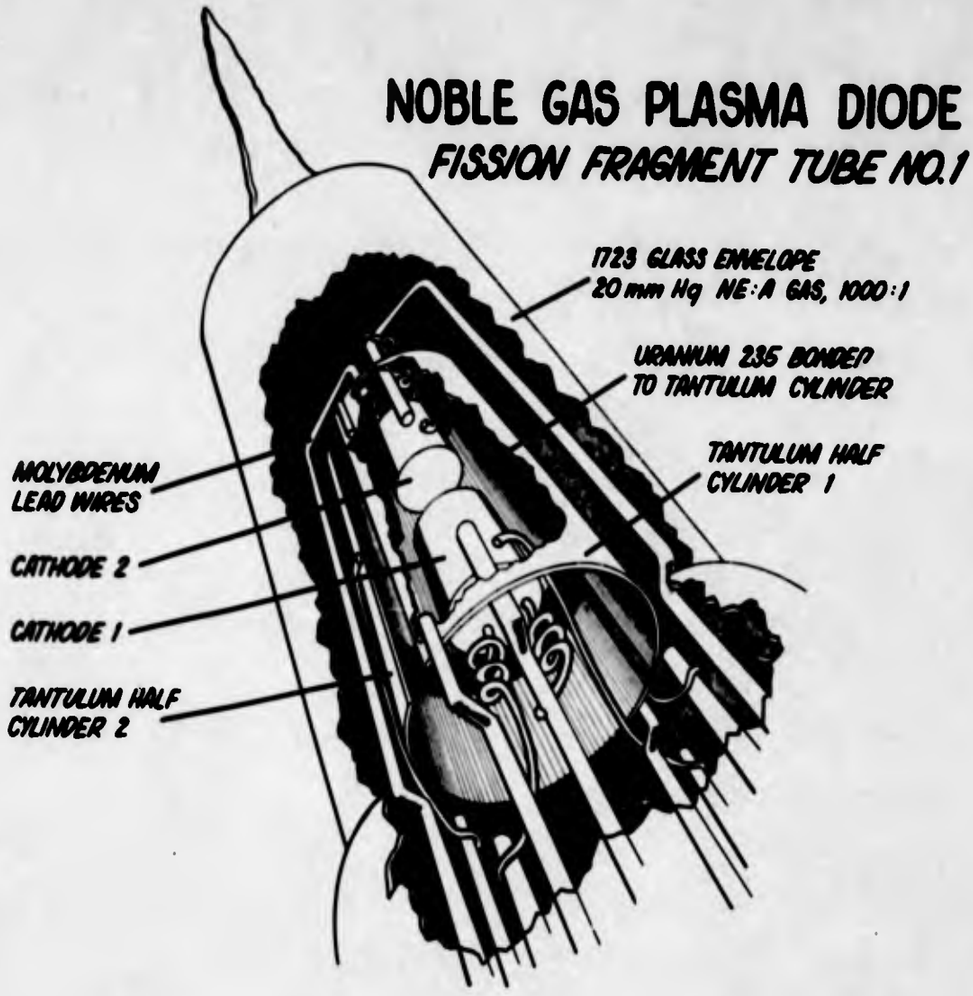

Figure 4
Diode II Perspective Sketch

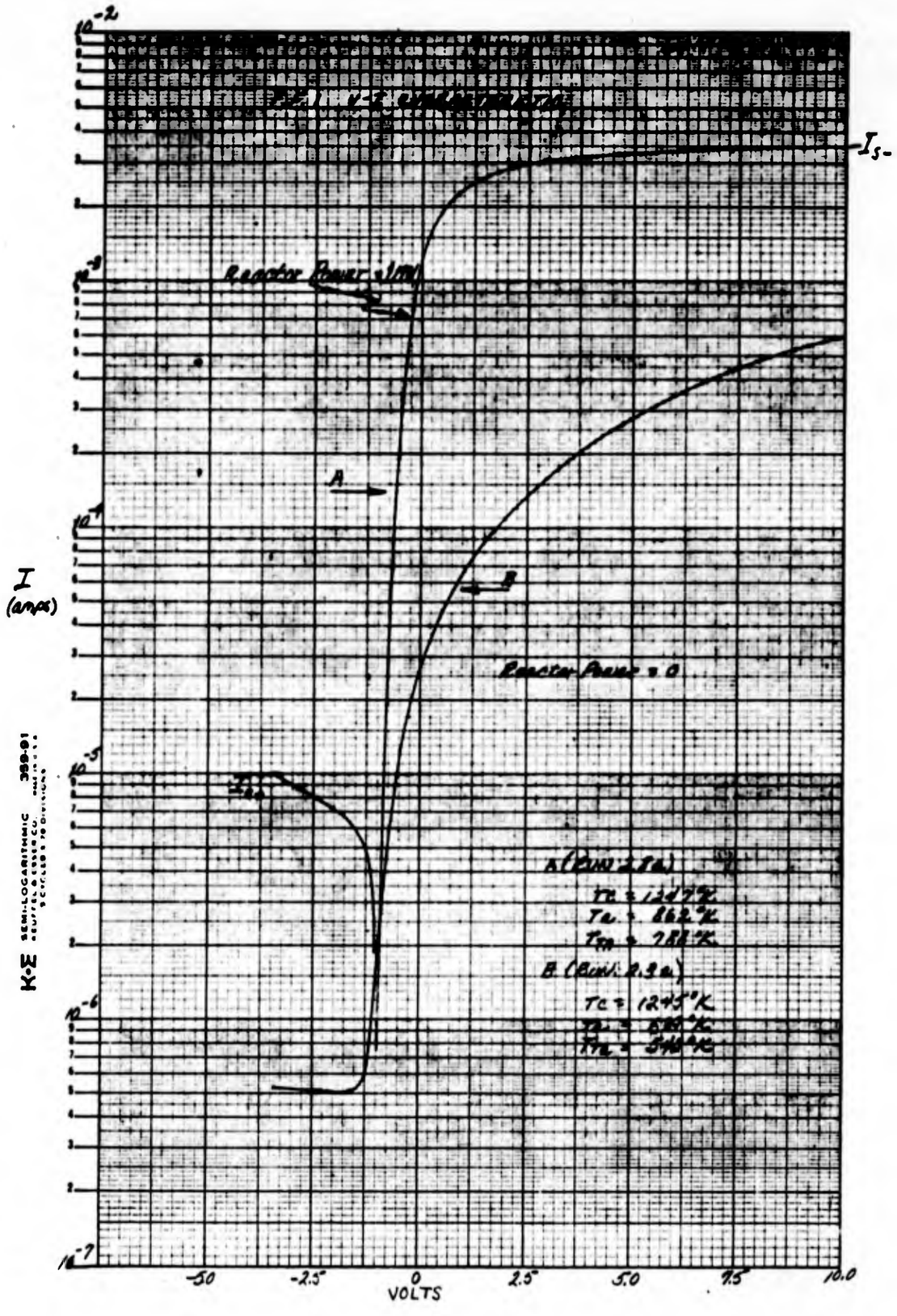

Figure 5
Diode II V-I Curves

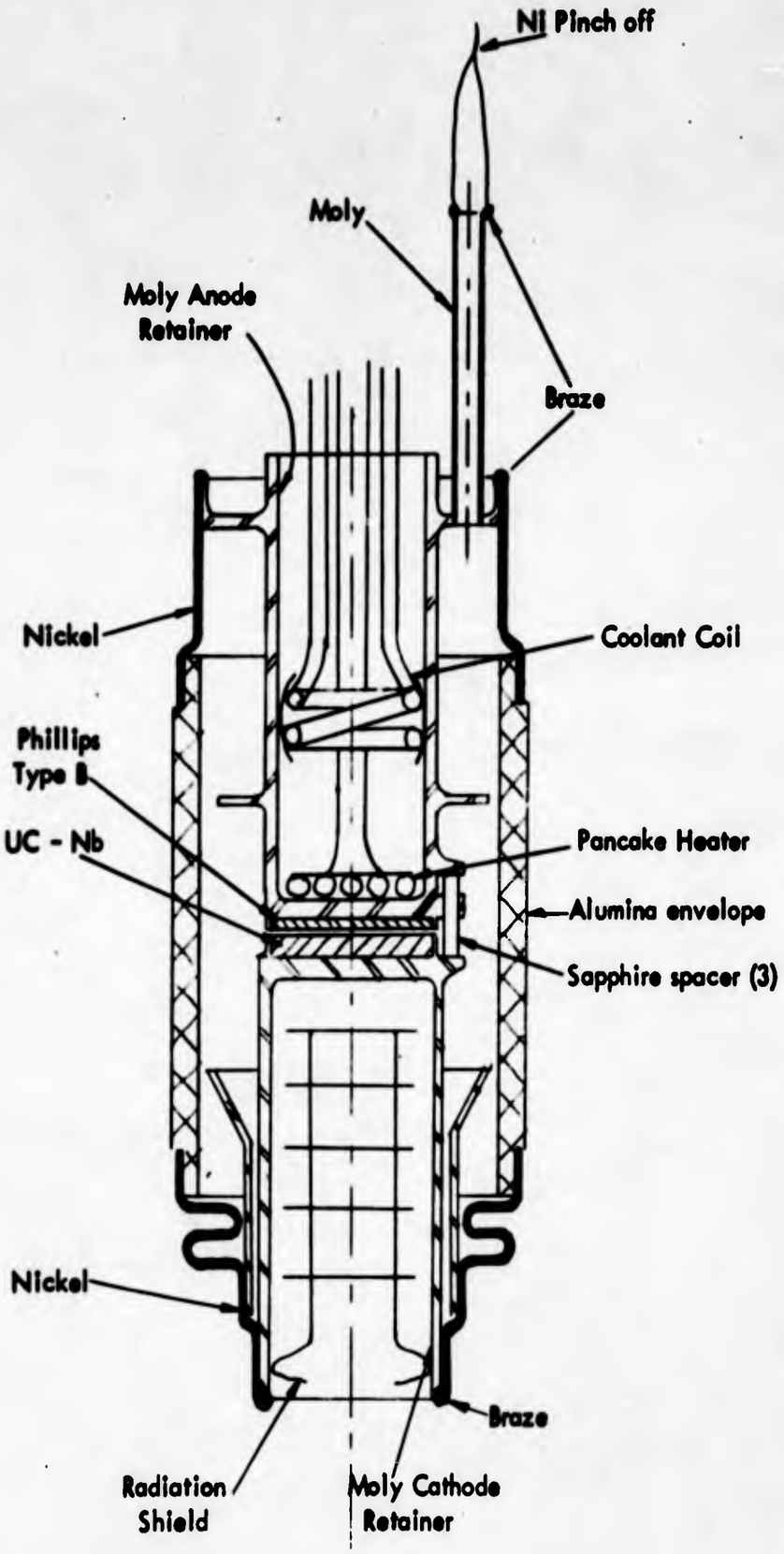

Figure 6
Ceramic Diode - NGPD Configuration

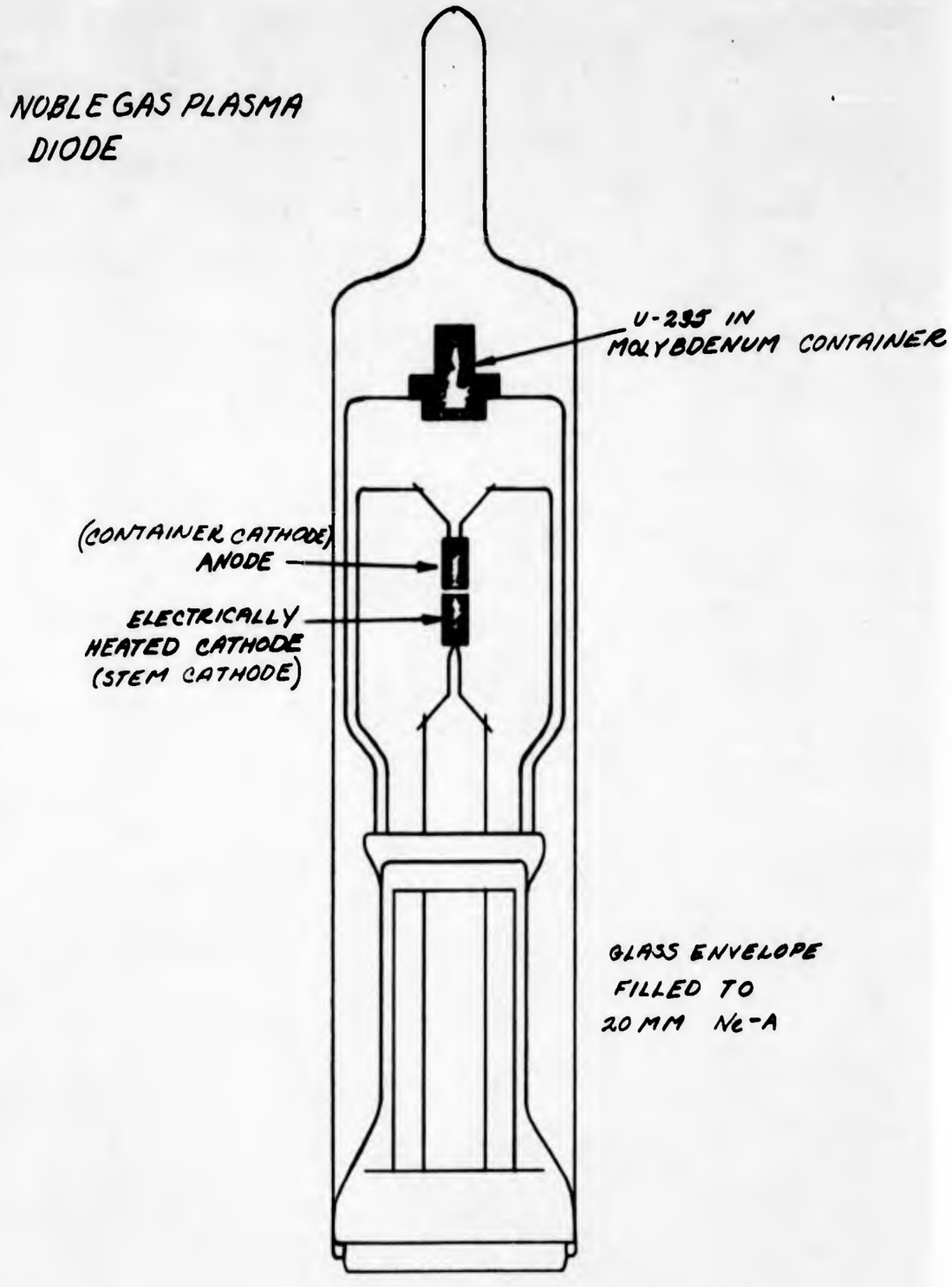

Figure 7
Diode III Sketch

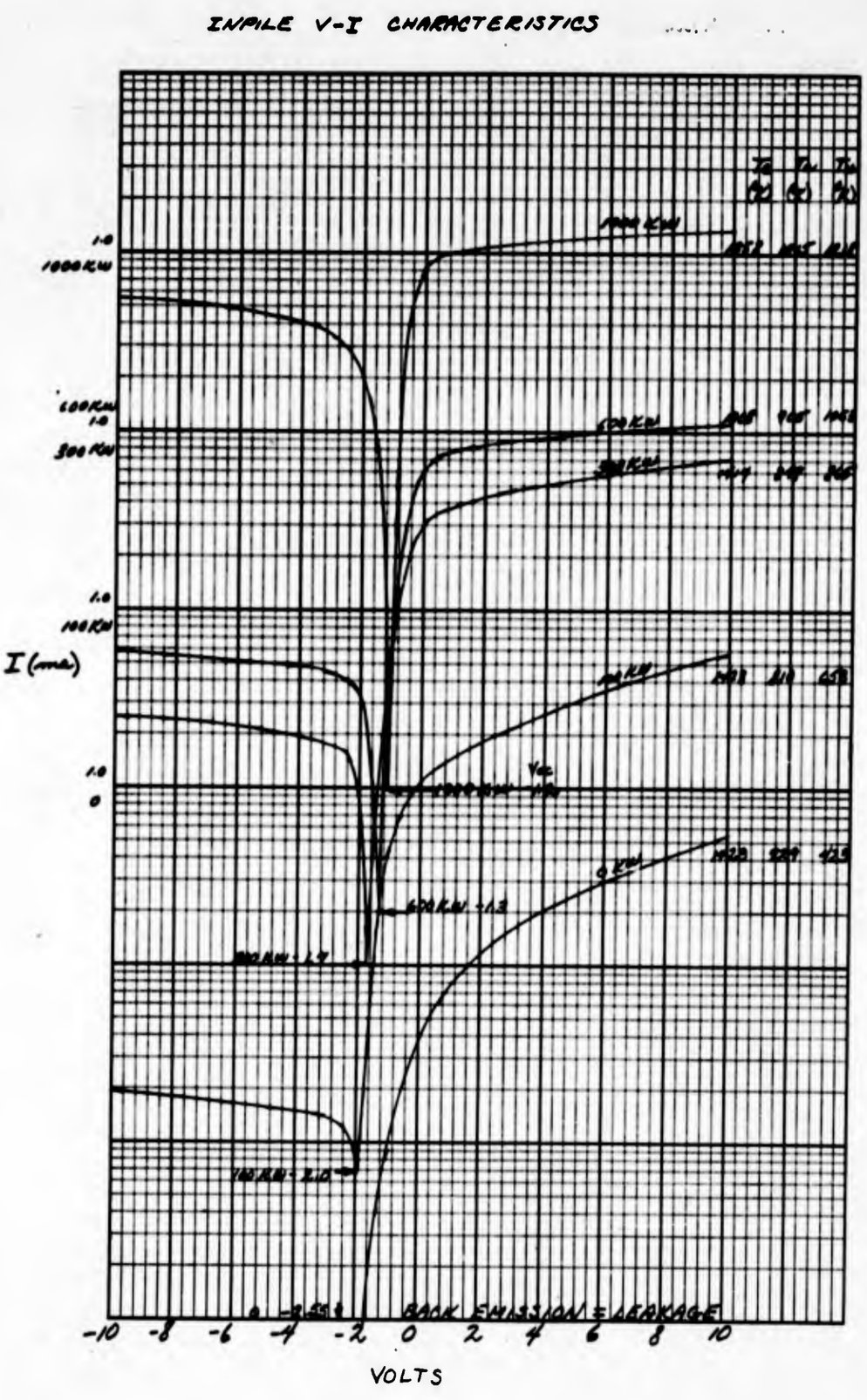

Figure 8
Diode III. Inpile V-I Curves

Figure 9
Figure III. Forward & Back Emission Curves

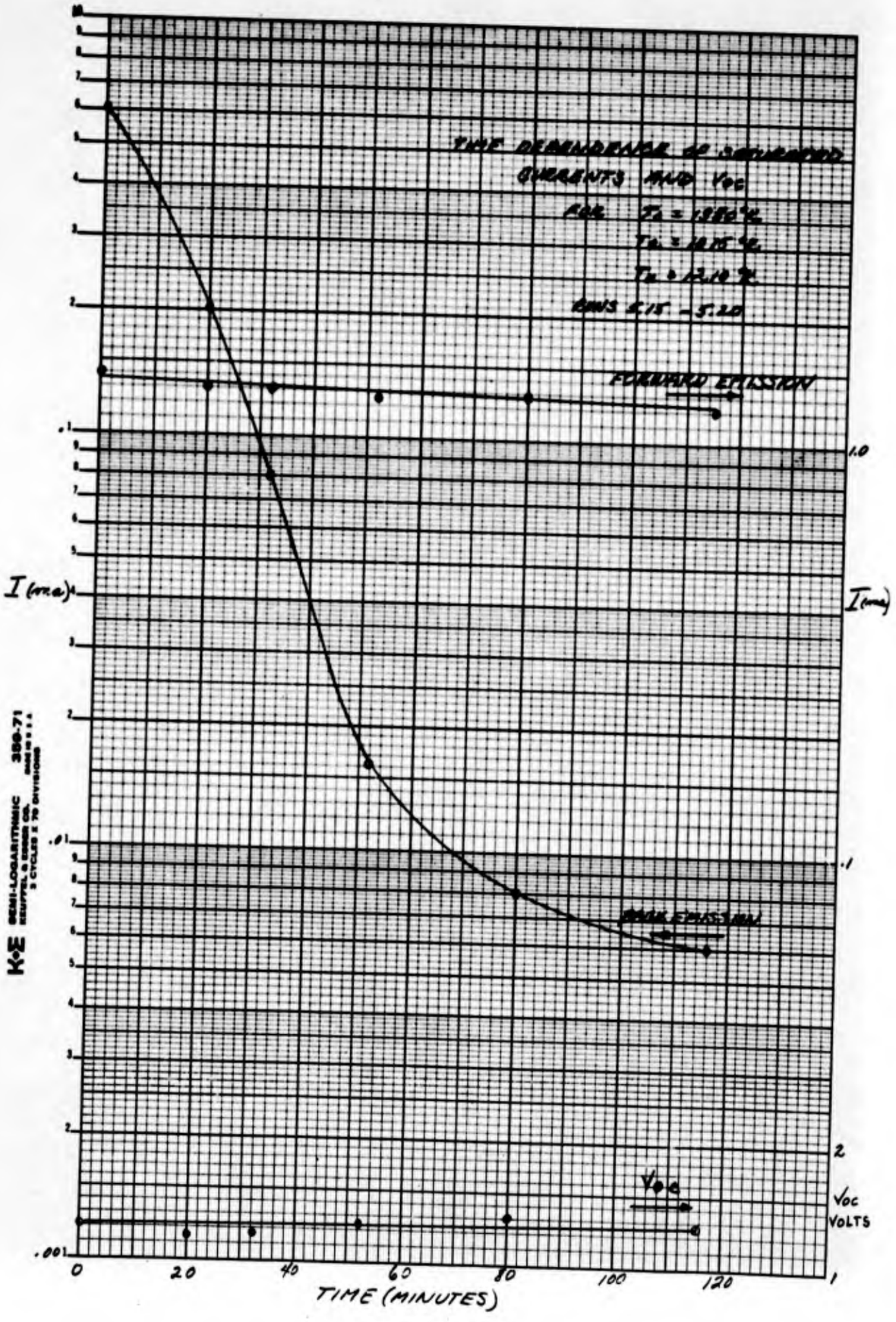

Figure 10

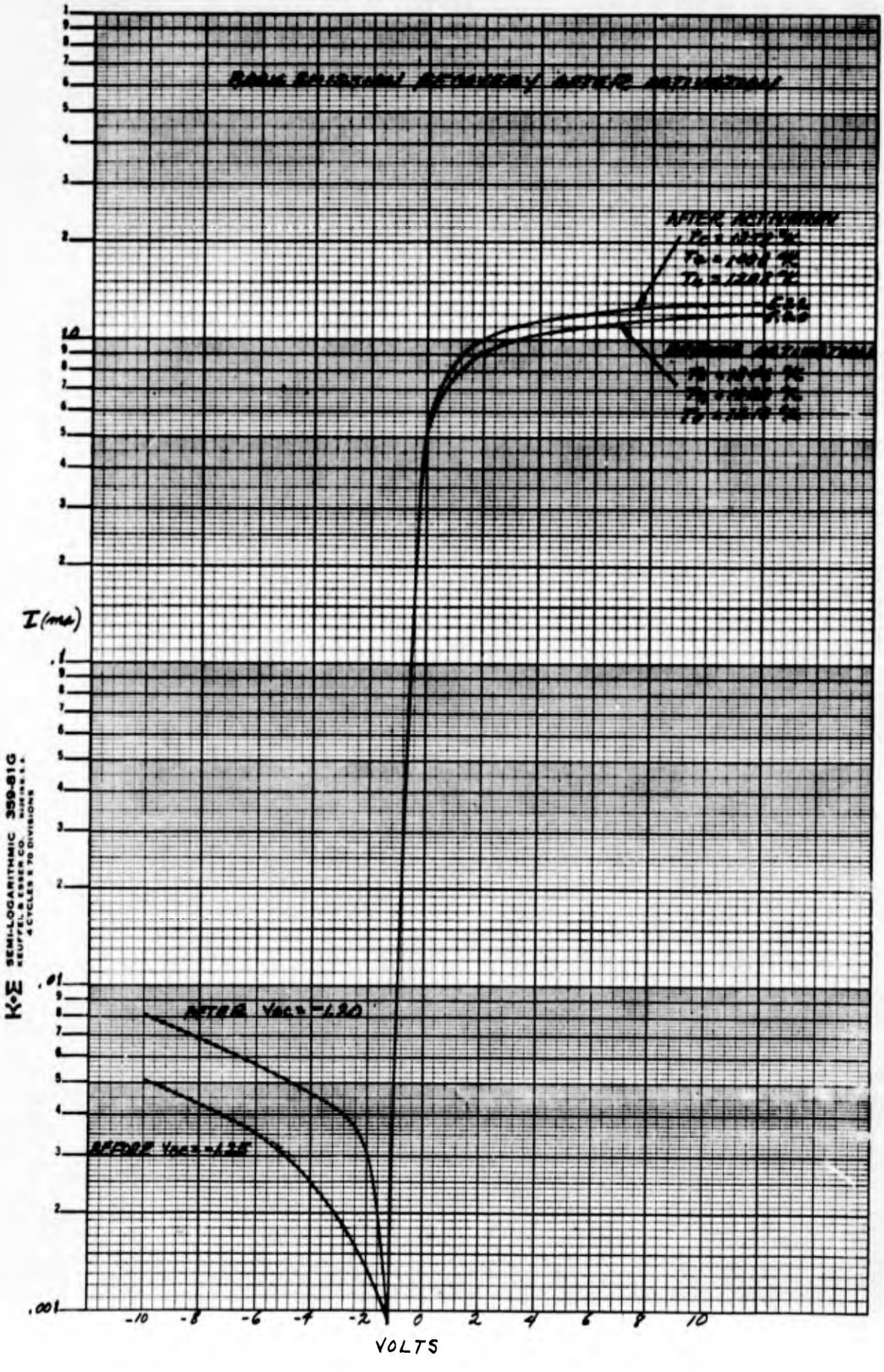
I(ma)
VOLTS
-10
-8
-6
-4
-2
0
2
4
6
8
10
1
.1
.01
.001
AFTER Vac=-4.2V
BEFORE Vac=-4.2V
K&E SEMI-LOGARITHMIC 359-81G
KEUFFEL & ESSER CO.
4 CYCLES X 70 DIVISIONS

Figure 11
Diode III. Open Circuit Voltage & Emission-Time Curves

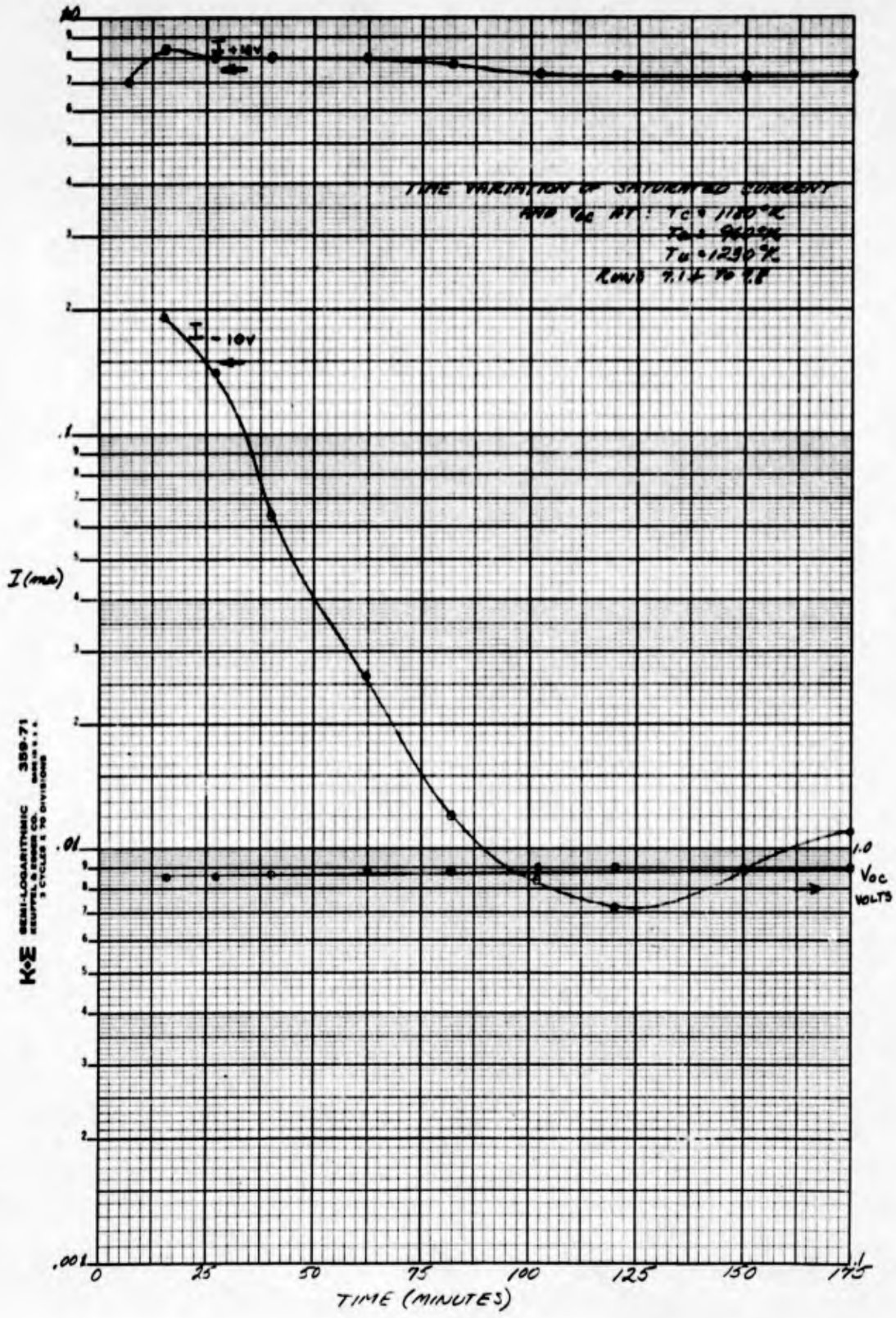

Figure 12

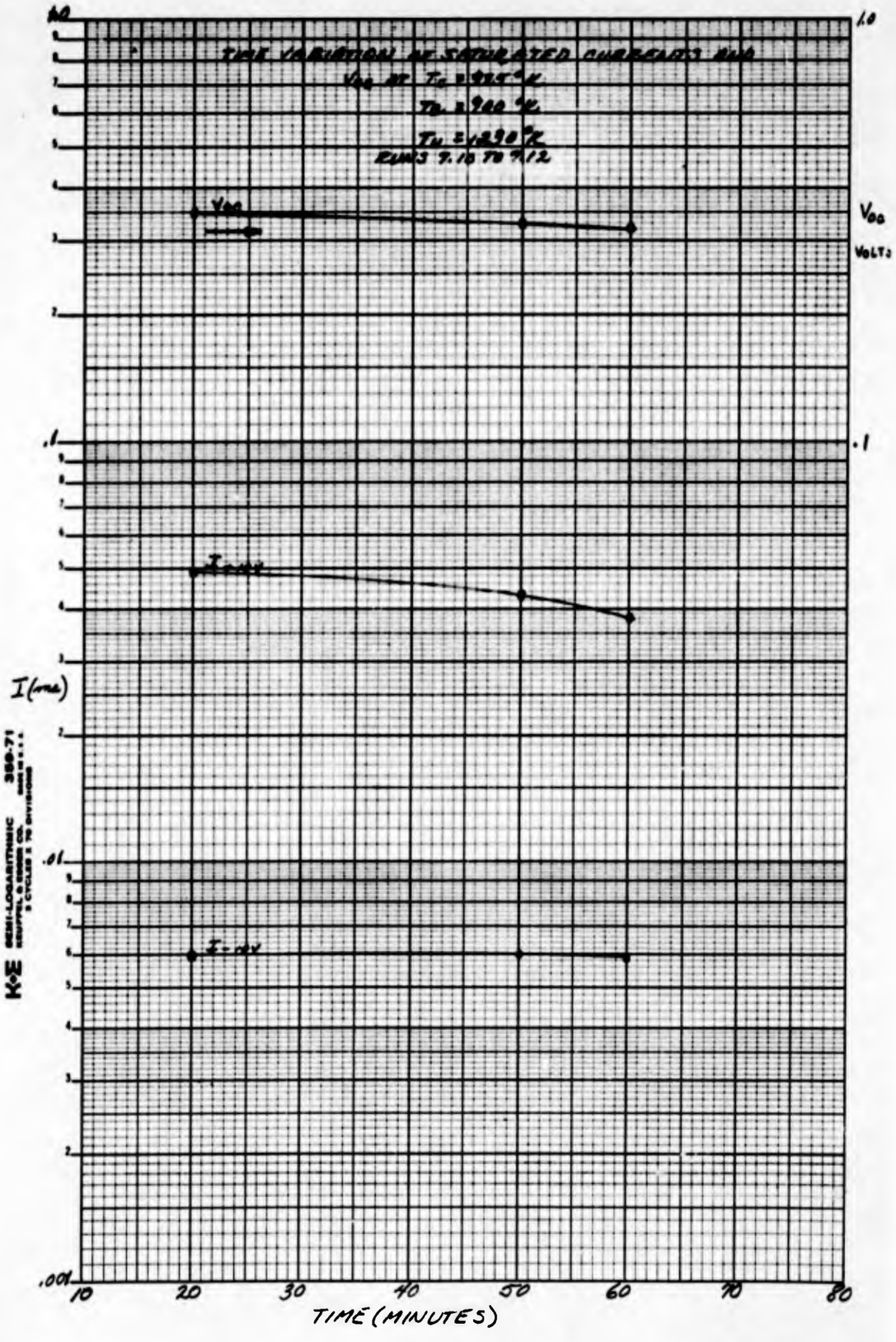
TIME VARIATION OF SATURATED CURRENTS AND
V_{GG} AT T_C = 925 °K
T_D = 900 °K
T_H = 1290 °K
RUNS 9.10 TO 9.12
V_{GG}
I_{sat}
I_{-sat}
V_{GG} VOLTS
I (amps)
TIME (MINUTES)
10
20
30
40
50
60
70
80
1.0
.1
.01
.001

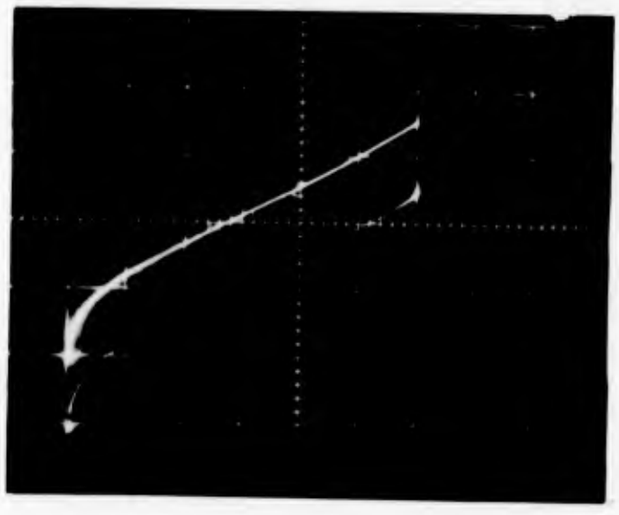

UC-Nb Current-Voltage Traces, T = 1455° K

Voltage: 500 V/division

Current: 2×10^{-5} amp/division

Figure 13
UC-Nb Cathode Emission Current Oscillogram

Figure 14

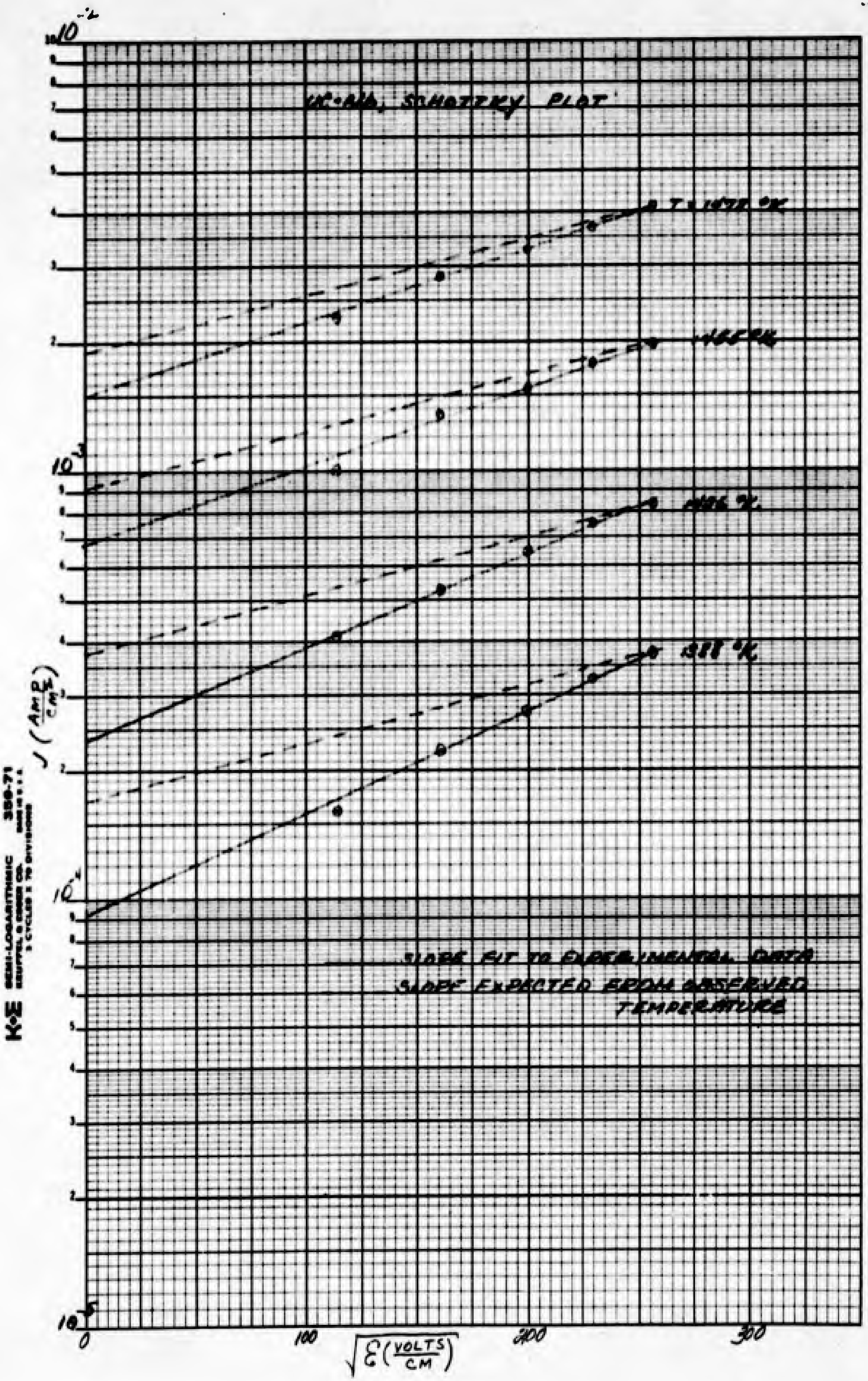
SCHOTTKY PLOT
SLOPE FIT TO EXPERIMENTAL DATA
SLOPE EXPECTED FROM OBSERVED
TEMPERATURE
0
100
200
300
K+E SEMI-LOGARITHMIC 359-71

Figure 15

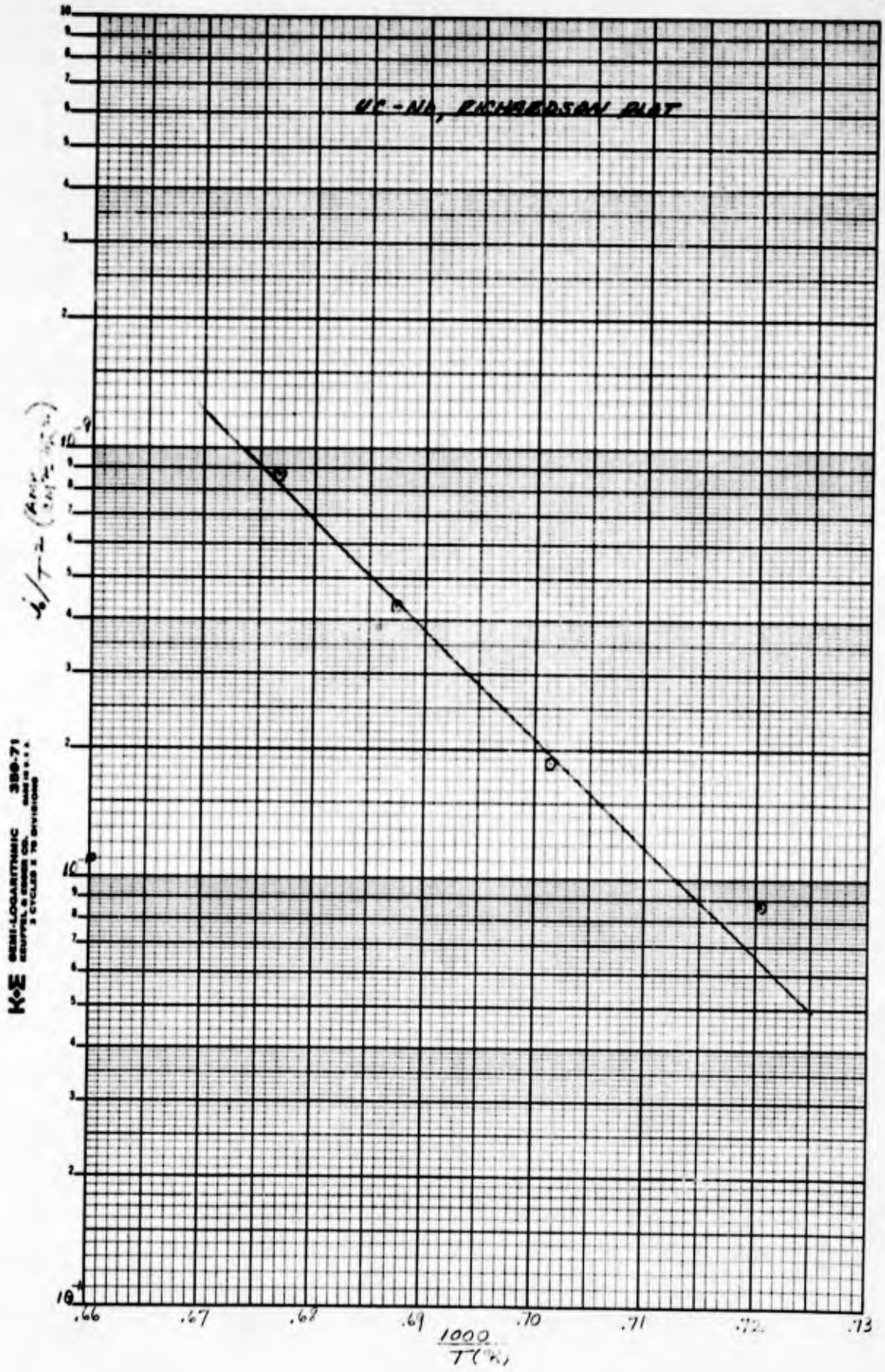

Figure 16
UC-Nb Cathode - vs - UC Cathode Emission Data

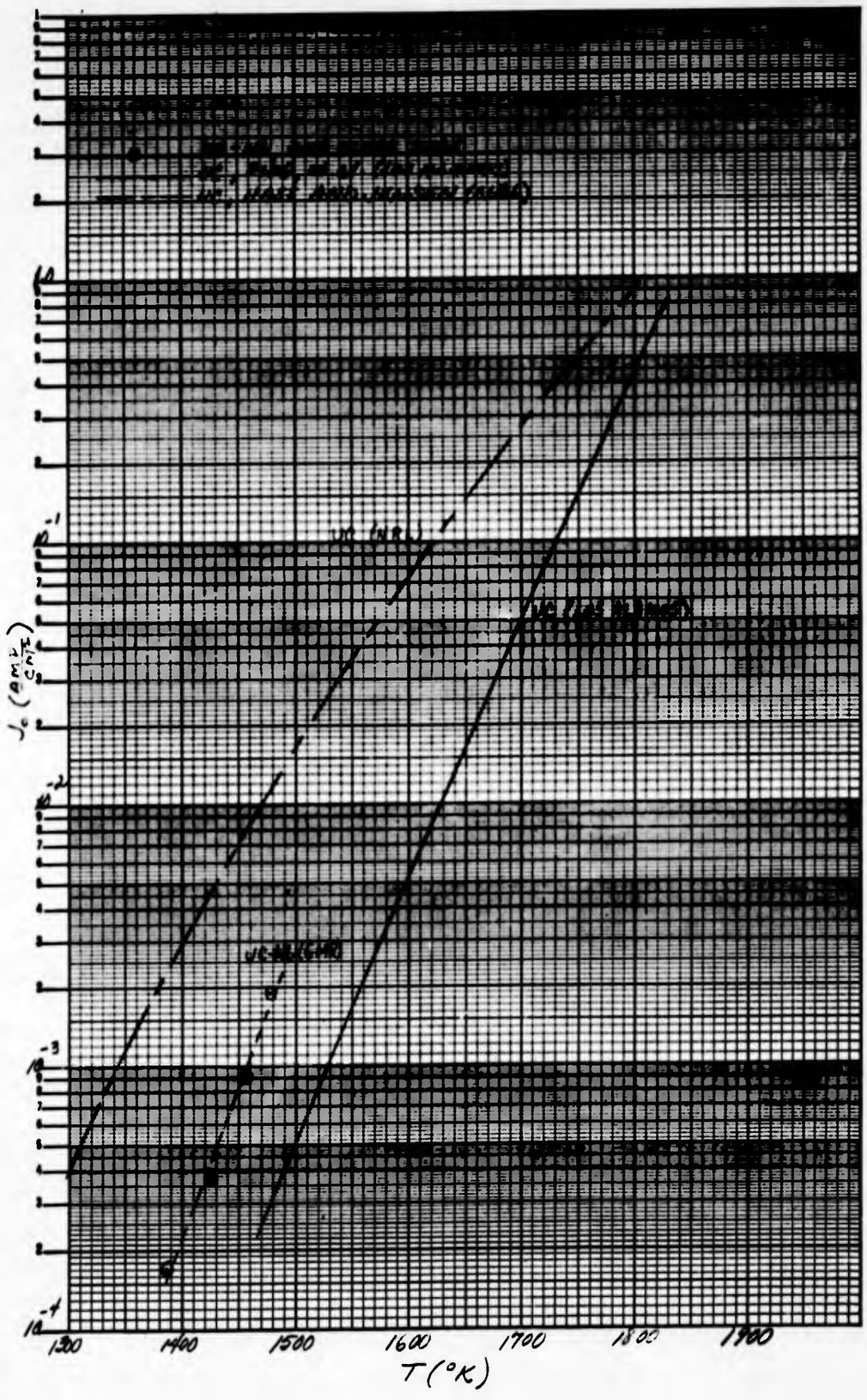

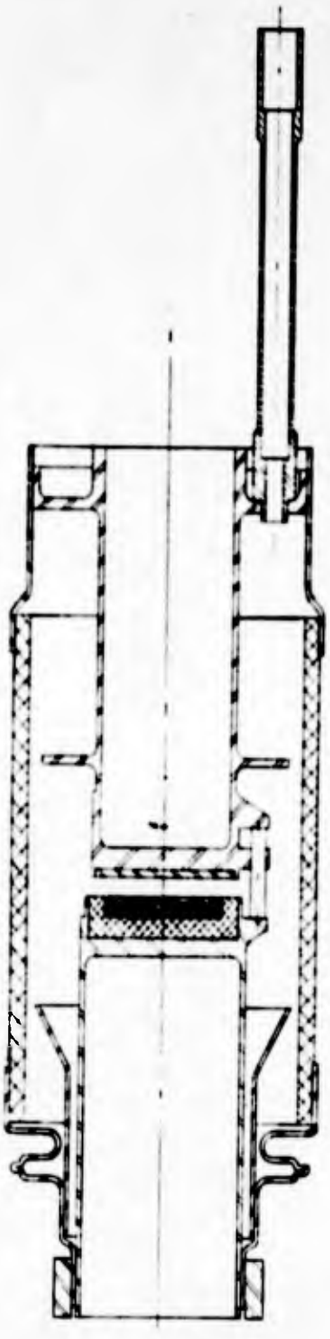

Figure 17
Present Design of Ceramic Diode

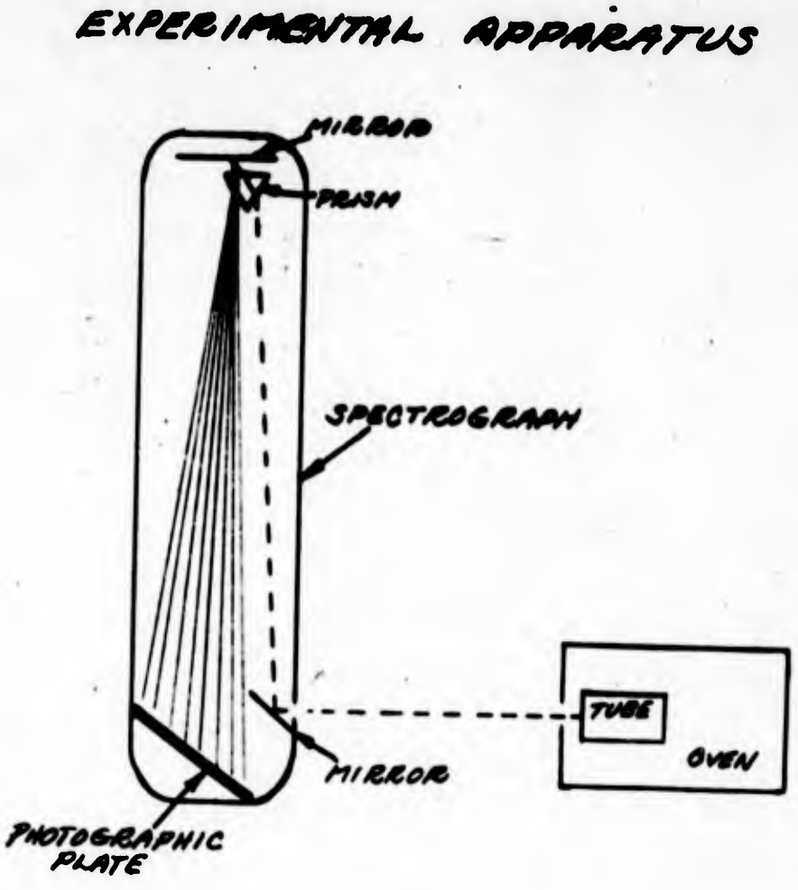

Figure 18
Spectrographic Apparatus Arrangement for Cesium Plasma Studies

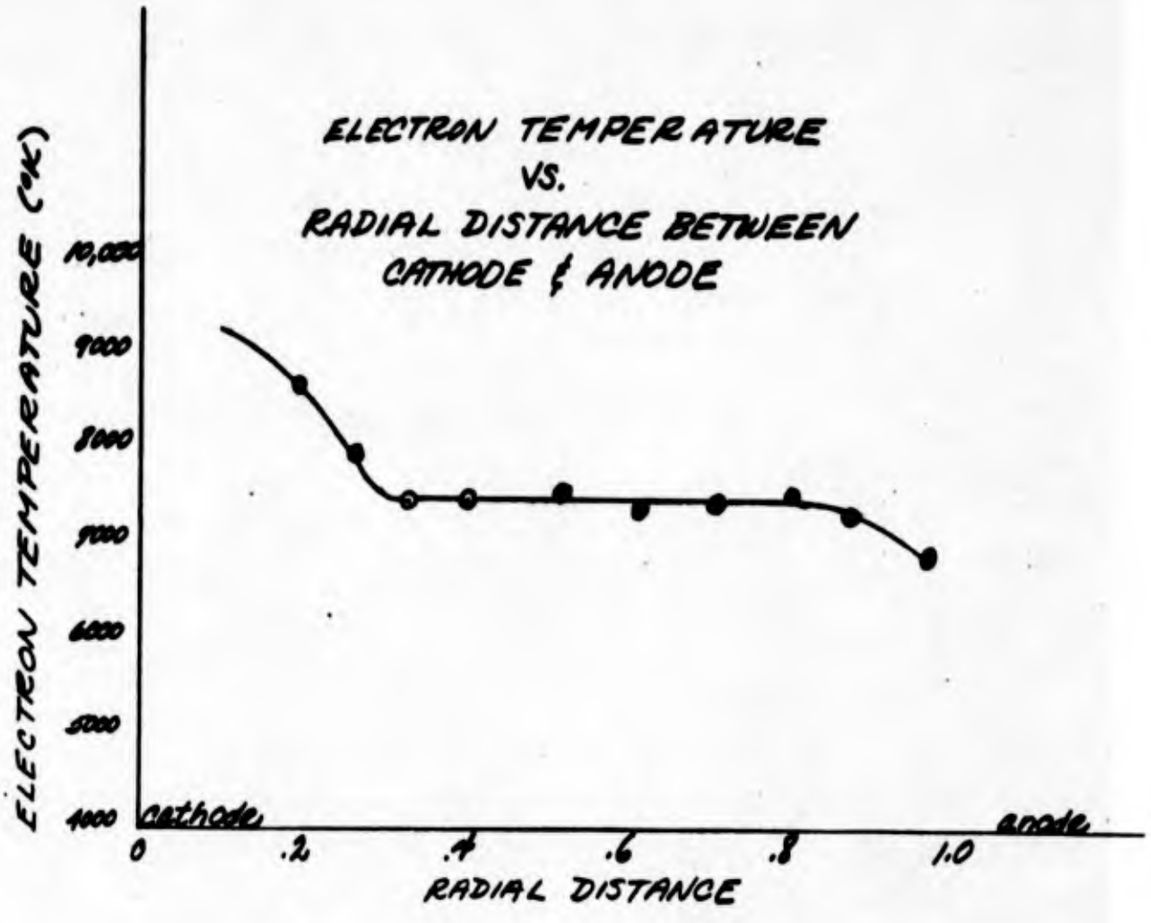

Figure 19
Electron Temperature - vs - Cathode Anode Position

Appendix I. Noble Gas Fission Fragment Diode Theory

Electron Number Density in the Plasma

The first problem is to compute the energy remaining in a fission fragment after it emerges out of the cathode. It is assumed that energy is lost linearly with distance in the cathode and that fission fragments are generated uniformly through a unit range depth of the cathode.

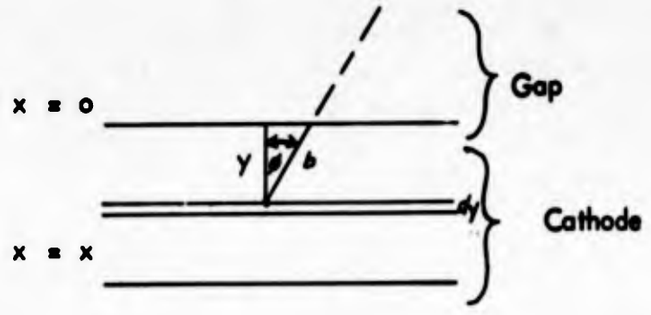

R = range of fission fragment in cathode N_o = number fragments produced/vol in the cathode

$b = y/\cos \phi$ E = kinetic energy of fission fragment

For a fragment moving at an angle ϕ with respect to the normal, its remaining range in the cathode-anode gap is $r - b = \Delta R$ or $\Delta R = R - y/\cos \phi$. Since

$$\Delta E = E \frac{R}{R} \text{ and let } x \equiv y/R \text{ then}$$

$$\frac{\Delta E}{E} = 1 - x/\cos \phi$$

so that x is measured in range units $x_{max} = 1$ and $\Delta E/E$ = fraction of energy remaining after escape into the gap.

The energy escaping into the gap at an angle ϕ from a volume element dV is:

dE = (Total Energy Produced in dV)(Fraction Energy Escaping)(Fraction Geometrically Escaping)

$$dE = (E_f N_o dV) \int_o^{\phi_{max}} (1 - x/\cos \phi) \frac{2\pi \sin \phi d\phi}{4\pi}$$

$$\frac{dE}{dV} = \frac{E_f N_o}{2} \int_o^{\cos^{-1} x} (1 - x/\cos \phi) \sin \phi \, d\phi$$

$$\text{or } \frac{dE}{dV} = \frac{E_f N_o}{2} (1 - x + x \ln x) \qquad (1)$$

where x still denotes y/R and E_f is initial fission fragment energy.

Now $dV = A\,dy = A\,R\,dx$ where A is cathode area.

The total energy escaping per unit area is then:

$$\frac{E}{A} = \frac{R\,E_f\,N_o}{2} \int_o^x (1 - x + x \ln x)\,dx$$

$$\text{or } E/A = \frac{R\,E_f\,N_o}{2} \left[x - 3/4\,x^2 + \frac{x^2}{2} \ln x \right] \qquad (2)$$

Since $R\,E_f\,N_o$ = energy/area initially generated assuming a flat flux distribution, then the fractional energy escaping/area into the gap is given by:

$$F = 1/2 \left[x - 3/4\,x^2 + x^2/2 \ln x \right] \qquad (3)$$

Table 1 shows how F varies as a function of thickness in units of the range R in the uranium film.

Table 1

Film Thickness (units of range in cathode)	F (fraction of total energy emitted from film)
1	.125
1/2	.225
1/4	.32
1/10	.406

Now if the cathode-anode gap was as big as the range of the fission fragment in the gas, then the above value of F = .125 would be the fraction of the fragment energy dissipated in ionizing the gas.

The problem is to now calculate the fractional amount of energy lost when the fission fragment strikes the anode. The difference between this quantity and F above gives the fractional energy left in the gas to produce ionization.

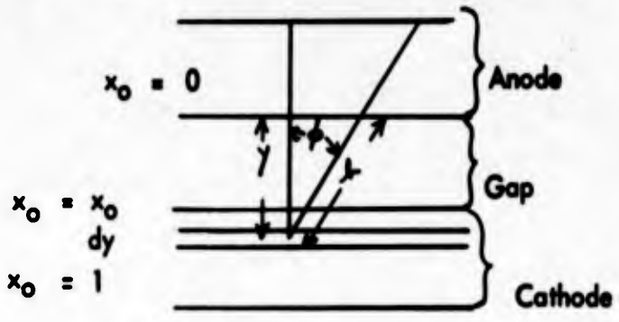

where $x_o = y/R_o$ and R_o = range of fission fragment in gas.

Proceeding as before, we first calculate a dE/dV identically as equation (1) which gives the energy reaching the anode per volume at distance x_o in the film.

$$\frac{dE}{dV} = \frac{E_f N_o}{2} (1 - x_o + x_o \ln x_o) \qquad (4)$$

In this case, to get the total energy

$$dV = A\, dy = AR_o\, dx_o$$

The total energy per area hitting the anode is then:

$$E/A = \frac{E_f N_o R_o}{2} \int_{x_o}^{1} (1 - x_o + x_o \ln x_o)\, dx_o$$

$$E/A = \frac{E_f N_o R_o}{2} \left[1/4 - x_o + \frac{3 x_o^2}{4} - \frac{x_o^2}{2} \ln x_o \right] \qquad (5)$$

The total energy/area created in the cathode of thickness $(1 - x_o)$ is given by $E_f N_o (1 - x_o) R_o$.

Thus the fraction of the total energy per area created that goes into the anode is given by:

$$F_A = \frac{E/A}{E_f N_o (1 - x_o) R_o} = \frac{1}{2(1 - x_o)} \left[1/4 - x_o + \frac{3x_o^2}{4} - \frac{x_o^2}{2} \ln x_o \right] \quad (6)$$

where x_o is the cathode-anode gap in units of the range for the fission fragment in the gas. Table 2 lists some values of F_A.

Table 2

Cathode-Anode Gap (Units of range in gas)	F_A (fraction of energy created that is lost to anode)
0.0	0.125
0.1	0.094
0.2	0.07
0.3	0.051
0.4	0.036
0.5	0.024
0.6	0.015
0.7	0.0078
0.8	0.0042
0.9	0.0

The above values of F_A are for the case where the cathode film thickness in units of R is 1 as can be noted for the 0 gap case where $F_A = F$. For cathode film thicknesses less than one range unit, the values of F_A would be higher. We are concerned only with the former case.

The ion production rate is given by:

$$\frac{dN}{dt} = \frac{\text{energy lost by F.F.}}{\text{sec cm}^3} \times \frac{1}{\text{ev/ion pair}} \quad (7)$$

$$\text{(a)} \qquad \times \qquad \text{(b)}$$

Now we define

$$a = (\Sigma_f \phi E_f R)\ (F - F_A)\frac{1}{g} \qquad (8)$$

where $(\Sigma_f \phi E_f R)$ = energy produced/cm^2 in one F.F.(fission fragment) range in cathode

ϕ = neutron flux; Σ_f = macroscopic fission cross section

g = cathode-anode gap; E_f = fission fragment energy

Substituting for F and F_A into (8), then:

$$\frac{dN}{dt} = \frac{(\Sigma_f \phi E_f R)}{gI}\left[0.125 - \frac{1}{2(1-x_o)}\left(\frac{1}{4} - x_o + \frac{3x_o^2}{4} - \frac{x_o^2}{2}\ln x_o\right)\right] \qquad (9)$$

where $x_o = \frac{g}{R_o}$, I = ev/ion pair, R_o = range of F.F. in gas, and R = range of F.F. in cathode.

The ion production rate is computed for both fission fragments and then averaged. The range of fission fragments in uranium carbide is taken as 0.72×10^{-3} cm and 0.94×10^{-3} cm for the heavy and light fragment respectively. The range of the fragments in the gas at temperature T and pressure p with molecular weight A is obtained from:

$$R_o = R_{air}\sqrt{\frac{A_{air}}{A}}\ \frac{760}{273}\ \frac{T}{p} \qquad (10)$$

Equations (9) and (10) are used to compute some values of $\frac{dN}{dt}$ for neon, argon, and xenon, and are shown in Fig. 1 for the parameters shown. The variation of $\frac{dN}{dt}$ with gap is small except at the higher pressure. Additional computations indicate $\frac{dN}{dt}$ varies linearly with temperature.

The electron number density for our case of loss by recombination alone is obtained from:

$$\frac{dN}{dt} = \alpha N^2 \qquad (11)$$

where α is the recombination coefficient at the pressure of interest. These coefficients are given in Table 3.

Table 3
Recombination Coefficients *

Gas	α (cm^3/sec)	T (°K)	p (mm Hg)
	Radiative		
H	10^{-11}		
A	2×10^{-10}	3100	0.8
Cs	3.4×10^{-10}	2000	0.01-0.03
Ne:A (10^3:1)	$< 10^{-9}$	300	1-30
	Dissociative		
He	1.7×10^{-8}	300	1-30
Ne	2.1×10^{-7}	300	1-30
A	3×10^{-7}	300	1-30
Kr	6×10^{-7}	300	0.5-25
Xe	2×10^{-6}	300	0.5-25

The early probe data are listed as radiative recombination corresponding to $A^+ + e^- \rightarrow A + h\upsilon$ where A^+ is an ionized atom. The dissociative recombination data are given from microwave data where the reaction goes: $A + A^+ \rightarrow (AA)^+ + e^- \rightarrow A + A$. This particular recombination process is said to occur in the presence of very weak electric fields ($< 10^{-2}$ v/cm) since $(AA)^+$ is a rather weakly bound system. It is felt that early probe data conditions were different from this, so those data are called radiative recombinations. The pressures and temperatures at which the measurements were made are given also. For the case of the Ne:A (10^3:1) mixture, the Penning effect leads to a value of recombination given as a lower limit only. * In this case the measurements gave an ambipolar diffusion coefficient which, when converted to a recombination coefficient, is the value shown in Table 3.

* S. C. Brown, Basic Data of Plasma Physics, John Wiley & Sons, 1959

Assuming that radiative recombination is the dominant loss mechanism for pure gases, then the number density is calculated from Equation (11) with the appropriate choice of α. The question of what happens to the recombination coefficient of the noble gas when it also contains fission product gases evolved from the hot cathode is a difficult one to answer. Presently it is assumed not to be affected on the basis that the Los Alamos cesium diode reactor experiment continued to operate after containing an estimated one mm. Hg pressure fission product gas in the diode * .

The fractional ionization in the gas is defined by $f = N/N_n$ or:

$$f = \frac{TN}{9.6 \times 10^{18} p} \qquad (12)$$

Values of f are shown in Fig. 2 as a function of pressure for argon, neon and xenon.

Diode Resistivity

The diode resistivity ρ is assumed to be principally associated with the plasma rather than electrode sheaths. The calculation can be made in two ways. One is a semi-classical argument that leads to a value of ρ as a function of electron-neutral atom collision cross section σ_{en} divided by fractional ionization. Such a calculation assumes that electrons and neutral gas atoms are at thermal equilibrium. The collision probability for argon and xenon exhibits a Ramsauer resonance in the vicinity of 10 ev, and has a minimum at 1 ev. Below this value of energy the collision probability begins to increase again. Consequently, due to the lack of good low energy data and the rapidly varying character of P_c at electron energies corresponding to those in this diode, this analysis gives a value of ρ which is probably good to within only a factor of two or three of reality. The problem is that the collision probability is not well behaved at the energies of interest, and does not lend itself to a very precise analysis. The development of ρ by this method follows:

Consider a parallel plate diode with electrons having random velocity $\bar{v}$, a mean free path d and drift velocity v_d given by:

$$v_d = \frac{eE}{m} \frac{d}{\bar{v}} \qquad (13)$$

* R. W. Pidd, Private Communication

where eE/m is the acceleration acquired in the field direction E between collisions. The current flow is:

$$I = env_d A \tag{14}$$

where A = area and n = electron number density. Thus the resistivity is:

$$\rho = R\frac{A}{d} = \frac{E}{I}A = \frac{mv}{e^2 nd} \tag{15}$$

Since $d = 1/N\sigma_{en}$ where N = number density of neutrals and σ_{en} = electron-neutral elastic scattering cross section, then:

$$\rho = \frac{m\bar{v}}{e^2}\frac{\sigma_{en}}{f} \tag{16}$$

The cross section is related to the collision probability by:

$$P_c = 3.54 \times 10^{-16}\sigma_{en}$$

where P_c has units of cm^{-1} mm Hg^{-1}.

Figure 3 shows the resistivity plotted as a function of gas pressure where P_c is estimated from available data* . In this case, it is evident that the lower the pressure, the lower the resistivity down to the limit of where recombination theory is no longer applicable.

One of the best behaved collision probabilities is that of neon. It exhibits a very broad Ramsauer type resonance at 25 ev and at less than 1 ev P_c is decreasing as $\sqrt{V}$ where V is electron energy in volts. In this case it is contended that a more exact calculation can be made by taking account of the Boltzmann electron distribution in the calculation of the mobility. The conductivity ($\sigma = \rho^{-1}$) is given by $Ne\mu$ where μ is the electron mobility.

* S. C. Brown, Basic Data of Plasma Physics, John Wiley & Sons, 1959

The collision probability for neon is given as:

$$P_c = av = a\sqrt{\frac{2e}{m}V} \qquad (17)$$

From experimental data *, $P_c = 10\sqrt{V}$ so that $a = 10\sqrt{m/2e} = 1/6 \times 10^6$ sec/cm^2 mm Hg where v is random velocity. Now the collision frequency ν_c is given by $\nu_c = av^2$ for electrons < 2 ev in neon.

From Boltzmann theory, the electron mobility is given for the case of a direct current and in the absence of an external magnetic field by: #

$$\mu = \frac{e}{Nm}\,\frac{4\pi}{3}\int_0^{\infty} v^3/\nu_c\,\frac{\partial f}{\partial v}\,dv \qquad (18)$$

where f is the Boltzmann distribution function:

$$f = Ae^{-mv^2/2kT} \qquad (19)$$

$$\text{and } A = \left(\frac{m}{2\pi kT}\right)^{3/2} N$$

Now $\nu_c = v p_o P_c$ by definition where $p_o = \frac{p}{T}273$ with p and T the actual system pressure and temperature. The quantity P_c is generally given for a gas at 1 mm Hg and 273° K, and p_o is called the "reduced pressure". Now since $P_c = av$ then $\nu_c = a\,p_o v^2$. Using this for the collision frequency in Equation (18) leads to:

$$\mu = \frac{e}{3kT_o}\,\frac{1}{ap} \qquad (20)$$

or $$\mu = \frac{8500}{p(\text{mm Hg})} \quad \text{m}^2/\text{sec volt}$$

* S. C. Brown, ibid

\# W. P. Allis, et al, Notes on Plasma Dynamics, MIT 1959

Now the conductivity σ is related to mobility by $N_e \mu$ and since resistivity $\rho = 1/\sigma$ then:

$$\rho = 7.3 \times 10^{-3} \frac{p}{N'} \text{ ohm-cm} \qquad (21)$$

where p is in mm Hg and N' is in units of 10^{13} ions/cm^3. For example, at a pressure of 10 mm Hg and N' = 0.1 (corresponding to a neutron flux of 5×10^{13} and using $\alpha = 10^{-9}$ cm^3/sec for Ne-A), the resistivity $\rho = 0.7$ ohm-cm (the high pressure cesium diode had a resistivity of 0.16 ohm-cm)*. Values of ρ versus p are plotted in Fig. 4, assuming the recombination coefficient for the Ne-A mixture.

Voltage Current Characteristic

In this section, an initial attempt is made at a description of the diode characteristic. In our case the potentials associated with the cathode and anode sheaths, as well as the plasma potential, have to be considered. Also some distinction needs to be made between the random currents in the plasma and the cathode emission current. If random current is greater than emission current, then the system is defined as being emission-limited and if this ratio is less than one the system is defined as being plasma-limited. The cases considered below are for the cathode work function (ϕ_C) greater than the anode work function (ϕ_A).

The plasma potential is taken to increase from cathode to anode, i.e. the electrons lose potential energy in going from cathode to anode. This description is consistent with the plasma potential direction given for the low pressure cesium diode though in our case there may be conditions for which this may not be true.

The ions and electrons produced by fission fragment ionization are assumed to be in thermal equilibrium with the gas molecules, though a temperature gradient exists between cathode and anode. Random current densities at the electrodes are then calculated from velocities determined by the gas temperature near the cathode and anode. This is taken approximately as the temperature of the cathode and anode respectively for the present.

The currents to be considered in the diode analysis are defined as:

* Grover, Roehling, Salmi & Pidd, J.Appl. Phys. 29, 1611, 1958.

J_c and J_a = random electron current near cathode and anode respectively

J_{sc} and J_{sa} = electron emission current from the cathode and anode respectively

J_o = electron current in the anode that eventually does useful work in an external load

J^+_c and J^+_a = random ion current near cathode and anode respectively

where:

$$J_{sc} = A T_c^2 e^{-\phi_c/T_c} \qquad J_{sa} = A T_a^2 e^{-\phi_a/T_a} \tag{22}$$

$$J_c^{(+)} = \frac{N e v_c^{(+)}}{4} \qquad J_a^{(+)} = \frac{N e v_a^{(+)}}{4} \tag{23}$$

and N is number density of ions or electrons since they are equal in the plasma and the density is assumed uniform between cathode and anode. The A and ϕ are Richardson constants and T in the exponential is in units of ev.

The voltages in the circuit are defined as:

$\phi_c - \phi_a = \Delta\phi$ = difference of cathode and anode single valued work functions (neglecting patch effects for the present)

V_c and V_a = cathode and anode sheath potentials

V_p = ohmic potential drop in the plasma

(a) Plasma limited operation

In this case emission current is greater than random current so that a negative space charge is built up at the cathode and the potential diagram is given in Fig. 5. The random ion current is generally

10^3 smaller than the random electron current, but it is carried in the analysis for completeness.

The current balance equation is:

$$J_{sc} e^{-V_c/T_c} + J_c^+ e^{-V_c/T_c} - J_c = J_a e^{-V_a/T_a} - J_{sa} - J_a^+ \tag{24}$$

where

$$J_o = J_a e^{-V_a/T_a} \tag{25}$$

The voltage balance equation is:

$$V_o = \Delta\phi + V_c + V_a - V_p \tag{26}$$

Now take

$$V_p = J_o R_p \tag{27}$$

where R_p is the plasma resistance.

The voltage-current characteristic is derived considering Equations (24), (25) and (26). Solving Equation (25) for V_a and Equation (24) for V_c leads to the following expression for V_o as a function of J_o with J_{sc} as a parameter.

$$V_o = \Delta\phi + T_a \ln \frac{J_a}{J_o + J_{sa} + J_a^+} + T_c \ln \frac{J_{sc} + J_c^+}{J_c + J_o - J_{sa} - J_a^+} - J_o \rho_p g. \tag{28}$$

Several cases of J_o vs V_o are plotted in Fig. 6. These are plotted for the assumed parameters shown. These V-J characteristics exhibit a power maximum in the neighborhood of two volts. The influence of the plasma potential term ($J_o \rho_p g$) is evident. The product $\rho_p g$ should be made as small as possible.

(b) Emission limited operation

In this case, emission current is taken to be less than random current so that a positive space charge can build up at the cathode as well as the anode. The potential diagram is shown in Fig. 7.

The current balance equation is:

$$J_{sc} - J_c e^{-V_c/T_c} + J_c^+ = J_o - J_{sa} - J_a^+ \qquad (29)$$

From the potential balance:

$$V_o = \Delta\phi - V_c + V_a - V_p \qquad (30)$$

The voltage-current characteristic is found, combining Equations (29) and (30), to be:

$$V_o = \Delta\phi + T_a \ln \frac{J_a}{J_o + J_{sa} + J_a^+} - T_c \ln \frac{J_c - J_{sa} - J_a^+}{J_{sc} - J_o + J_c^+} - J_o \rho_p g \qquad (31)$$

A plot of Equation (31) is shown in Fig. 8 for the parameters selected. As seen in Fig. 8 this limits itself to $J \leq J_{sc} + J_c^+$ mathematically. The cathode sheath corresponds to a barrier for random electron flow into the cathode, but allows full saturated emission to be drawn out of the cathode. Thus if plasma density were high enough to make random current greater than emission current, the diode would limit at the saturation value as exhibited in Fig. 8.

Conclusions

Calculation indicates that even though fractional ionization is rather low (10^{-5}), reasonably low values of resistivity can be obtained in this low density plasma. The resistivity calculated from scattering cross section (Eq. 16) for neon:argon does not agree very well with that calculated from mobility considerations (Fig. 3 and 4). The former value has the highest degree of uncertainty so that subsequent calculations used the values derived from mobility which are based on reliable measurements of recombination coefficient and mobility itself. Even though larger ionization rates are available in a gas like xenon, the recombination coefficients measured so far for this gas indicate an unfavorable resistivity.

A number of calculations were made for assumed parameters which are representative of reality for a uranium carbide emitter and a neon-argon plasma. The voltage current characteristic for the plasma limited case (Fig. 6) indicates that current is limited by random plasma current. In the emission limited case (Fig. 8) the output current approaches the saturated value when S_g is small and the neutron flux large enough. Even though saturated emission is not predicted theoretically. from the value of neutron flux (5×10^{12} n/sec cm^2) available at the U. of Michigan reactor, a comparison of experimental voltage-current characteristic with theory should lead, it is anticipated, to definite conclusions on the operating characteristic of the noble gas plasma diode.

In summary, then, a description of the noble gas plasma diode incorporating cathode and anode sheaths with an intervening plasma of finite resistivity leads to a voltage-current characteristic that is reasonable from the standpoint of being able to deliter power of order several watts/cm^2. Pressures of order 10 mm. Hg in neon:argon and cathode-anode gaps of order 1 mm. or less are indicative of some of the parameters which make the S_g term small.

The analysis is to be further extended by considering in detail the following: (1) details of electron temperature in the vicinity of cathode and anode, (2) inclusion of patch work functions, (3) lower limit of pressure for which volume recombination holds, (4) heat transfer losses such as radiation and conduction through the gas leading to some estimates of system efficiency.

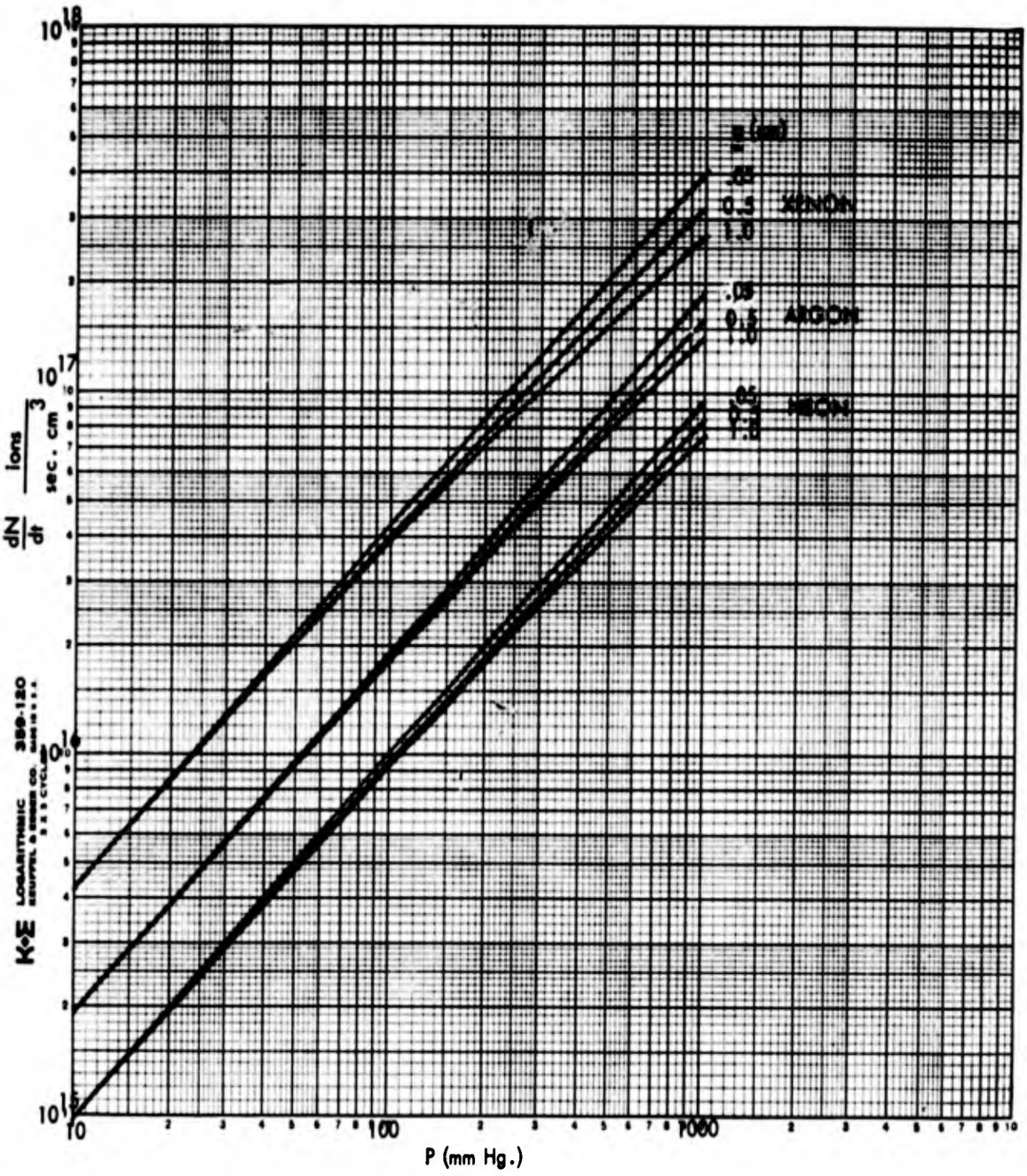

Fig 1. Ion production rate vs gas pressure for a neutron flux of $5 \times 10^{13}/cm^2$ sec on UC with a gas T = 1000 °K.

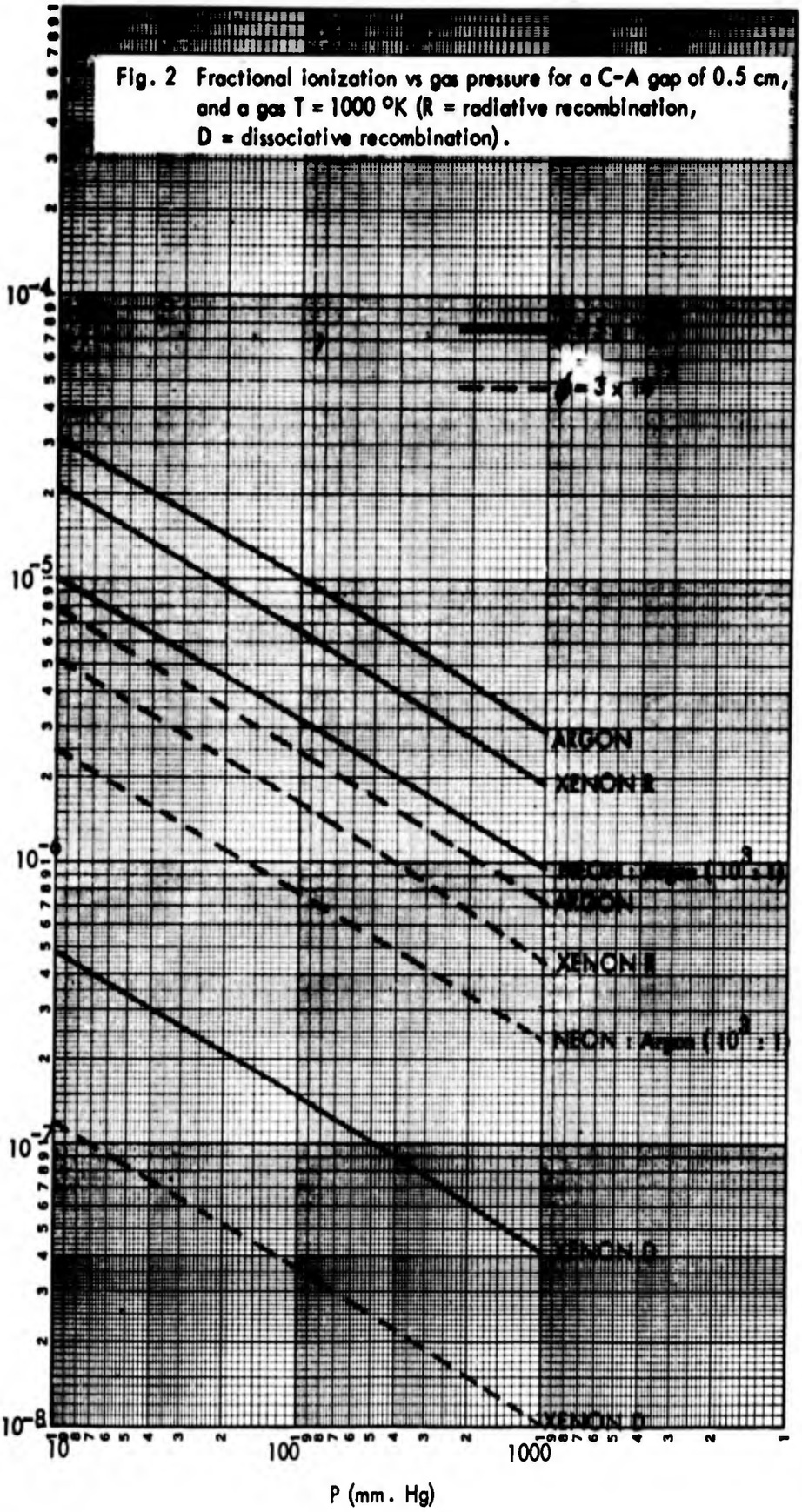

Fig. 2 Fractional ionization vs gas pressure for a C-A gap of 0.5 cm, and a gas T = 1000 °K (R = radiative recombination, D = dissociative recombination).

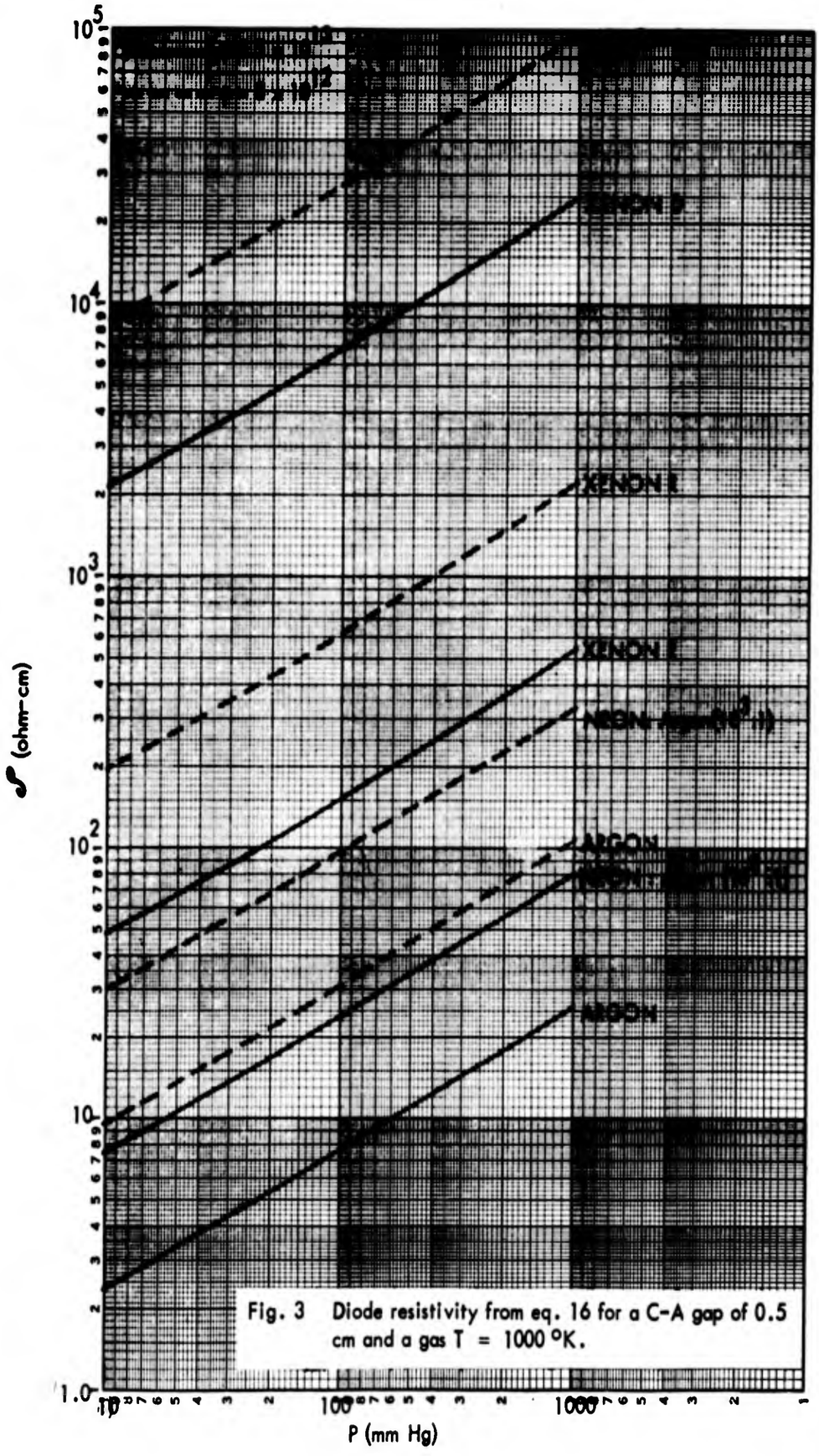

Fig. 3 Diode resistivity from eq. 16 for a C-A gap of 0.5 cm and a gas T = 1000 °K.

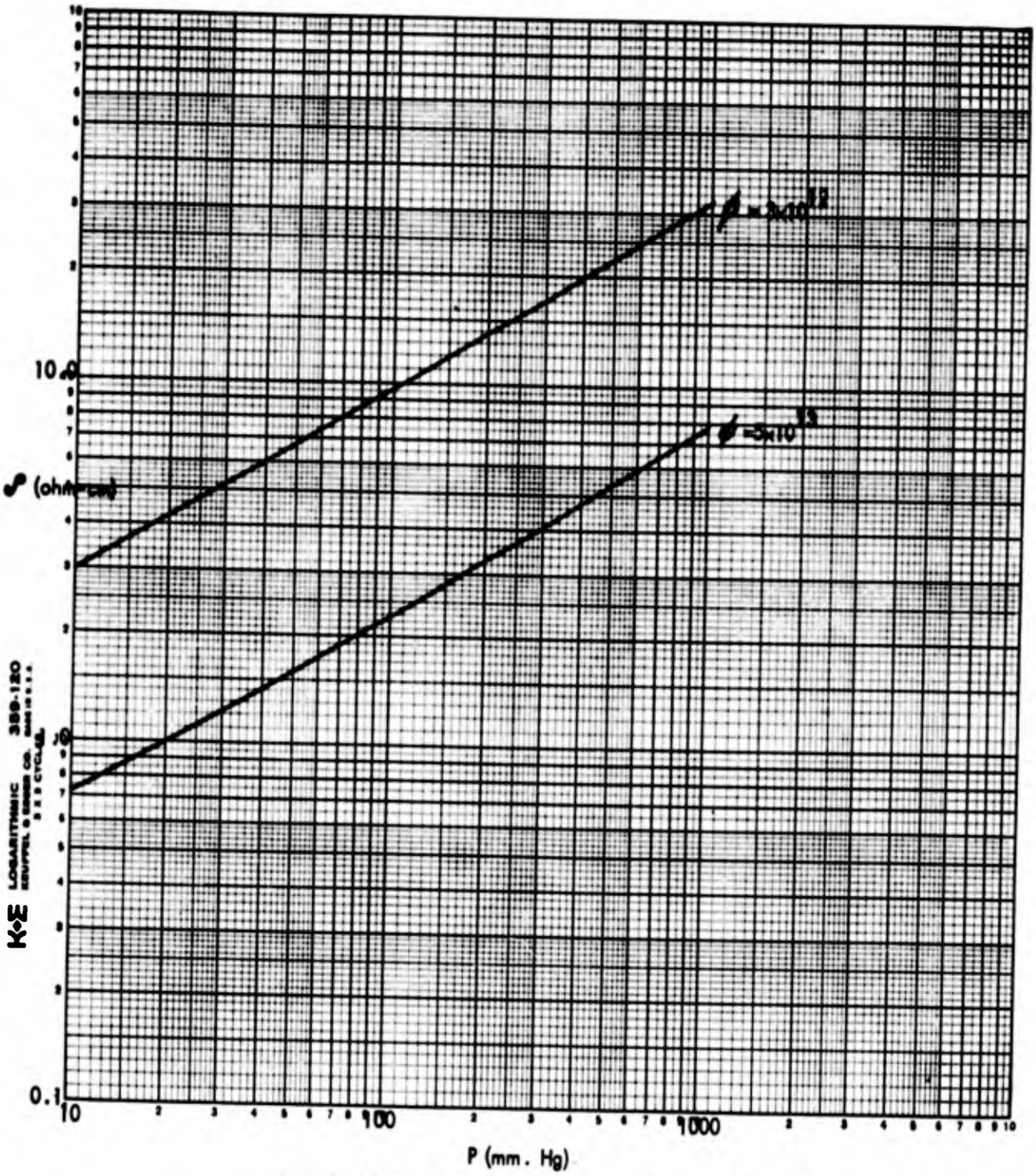

Fig. 4. Diode resistivity calculated from mobility for neon: argon (10^3:1) with g = 0.5 cm and gas T = 1000 °K.

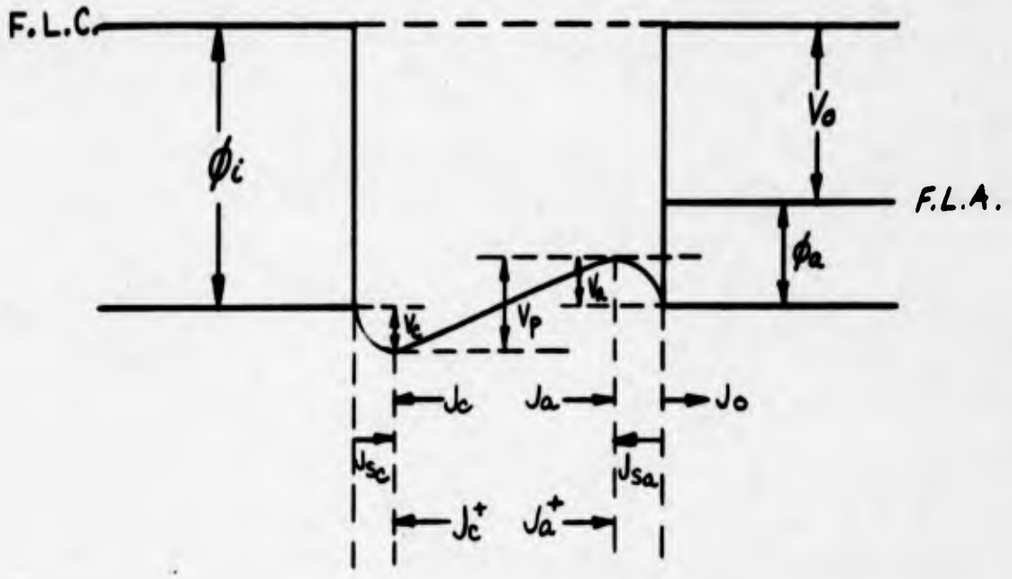

Fig. 5. Plasma limited potential energy diagram

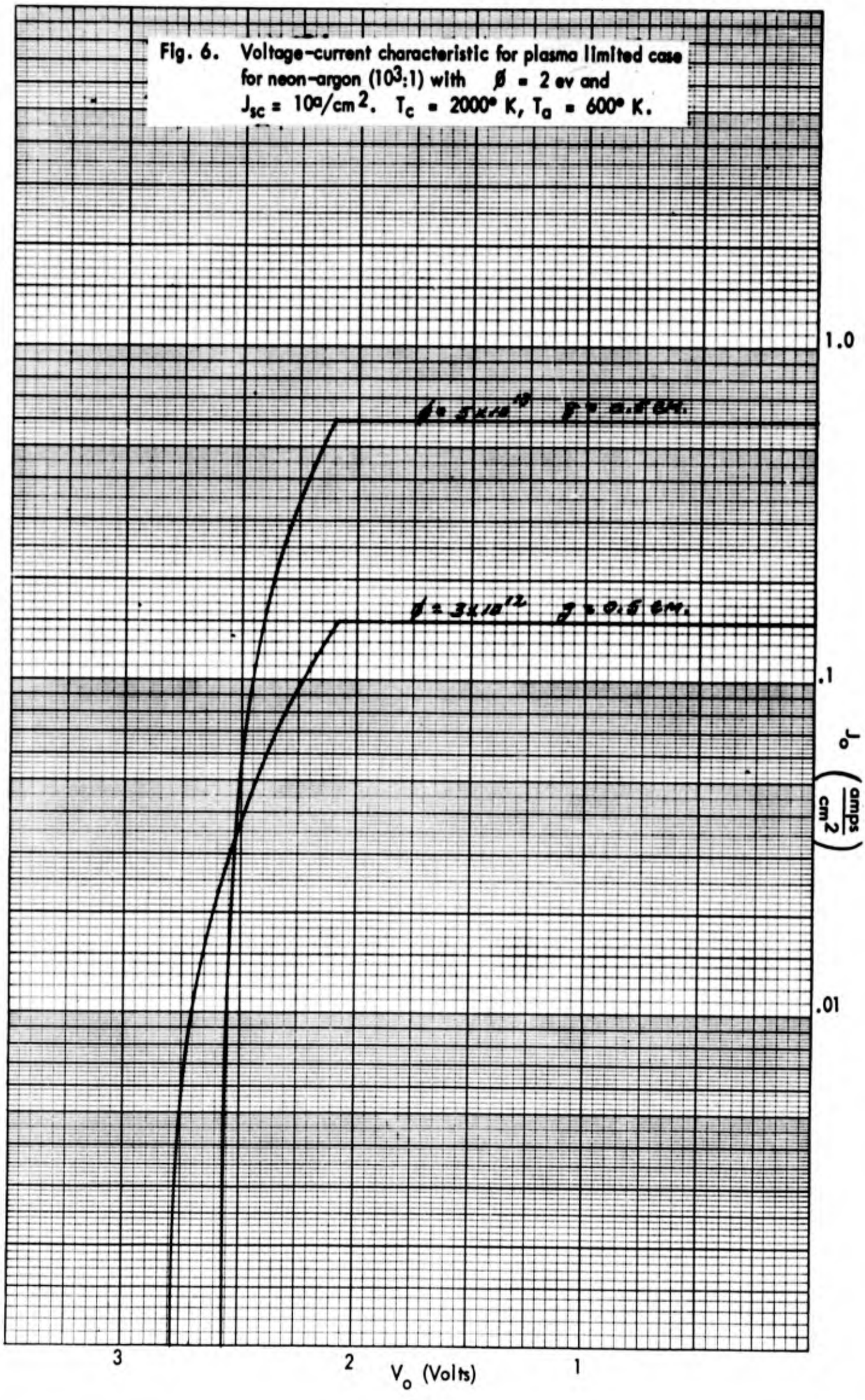

Fig. 6. Voltage-current characteristic for plasma limited case for neon-argon (10^3:1) with β = 2 ev and J_{sc} = $10^a/cm^2$. T_c = 2000° K, T_a = 600° K.

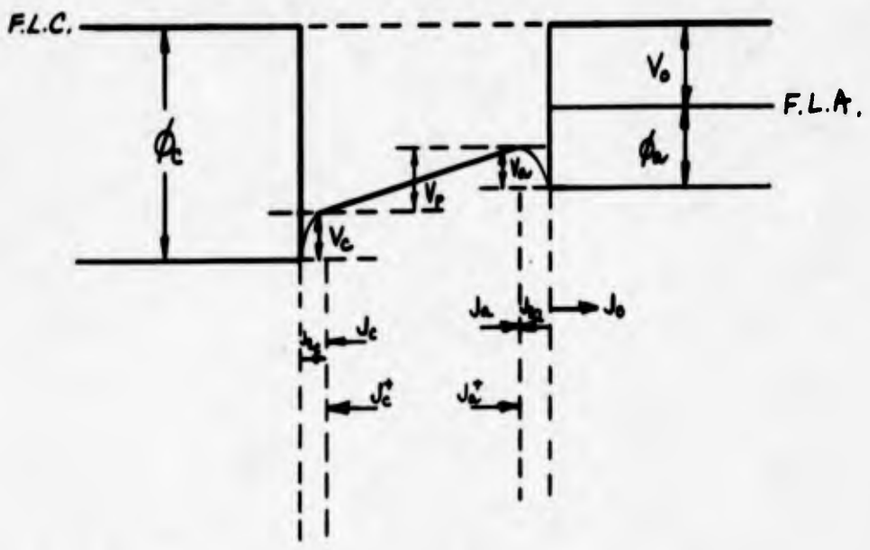

Fig. 7. Emission limited potential energy diagram.

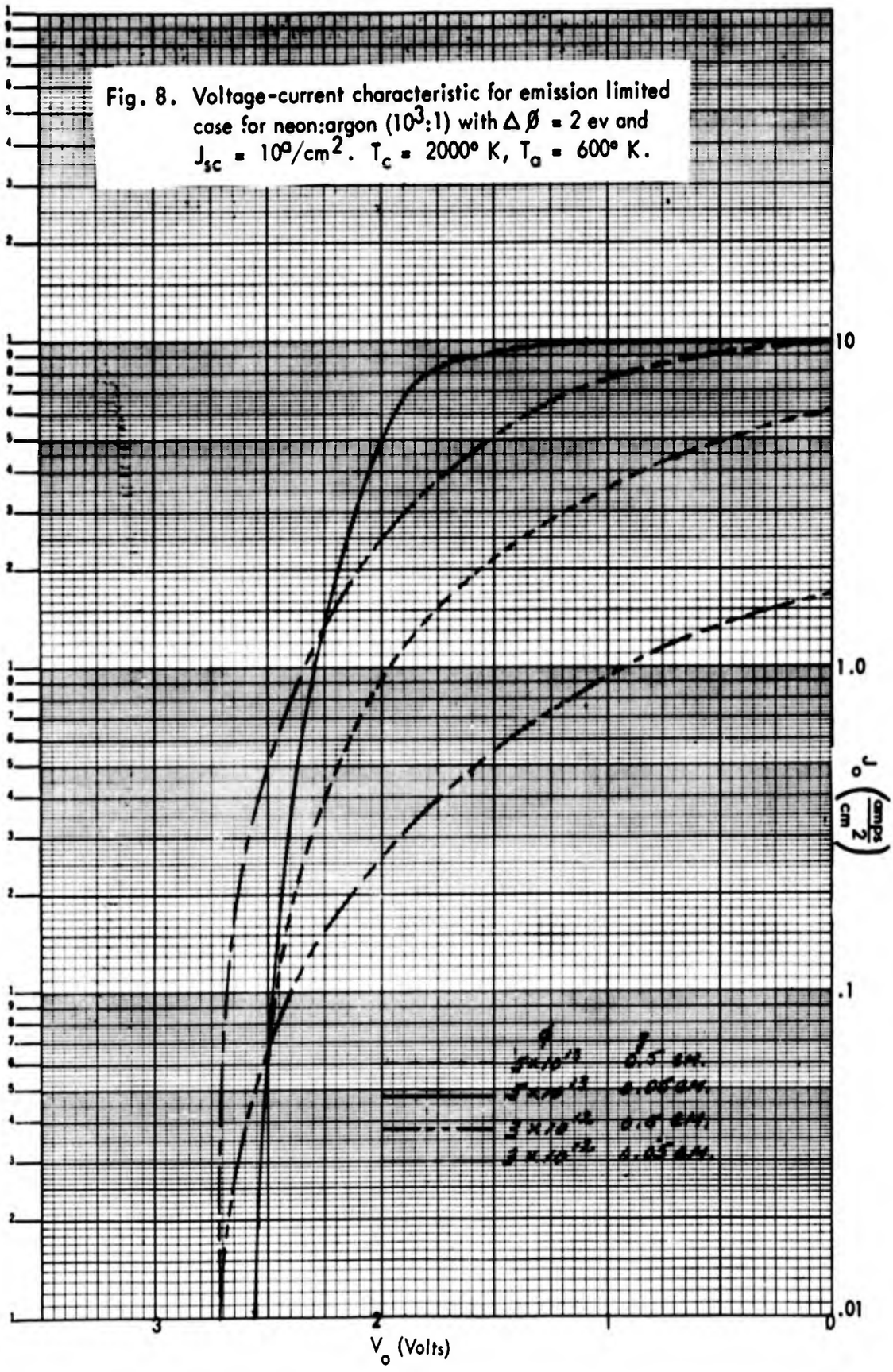

Fig. 8. Voltage-current characteristic for emission limited case for neon:argon (10^3:1) with $\Delta\phi$ = 2 ev and J_{sc} = $10^0/cm^2$. T_c = 2000° K, T_a = 600° K.

Appendix II

The problem is to develop the potential distribution in sheaths under a variety of conditions including "free falling" ions and electrons as well as a Boltzmann distribution of particles. Sheath analyses at cathode and anode are combined to yield a voltage-current characteristic for the noble gas plasma diode thermionic converter. Several possible modes of operation are developed. With a reasonable set of diode parameters, power densities of order 5 watts/cm^2 are calculated which is in the range of practical interest.

General Charge Density Relations

Defining terms:

$\rho = N_q$ where N is particle density and q is electronic charge

ρ_+ and ρ_- = charge density of ions and electrons

j_+ and j_- = current density of ions and electrons

v_+ and v_- = average velocity of ions and electrons

V = potential in volts

T_+ and T_- = temperature of ions and electrons in volts

ρ_o and v_o are constants of charge density and velocity not necessarily the same for both particles

M and m = ion and electron mass

For particles in a Boltzmann distribution (local thermal equilibrium):

$$\rho_+ = \rho_o e^{-V/T_+} \qquad (1)$$

$$\rho_- = \rho_o e^{V/T_-} \qquad (2)$$

For particles in "free fall":

$$\rho_+ = j_+/v_+ \tag{3}$$

$$\rho_- = j_-/v_- \tag{4}$$

Considering V to be the potential change over some distance where initial particle velocity was v_o, at V = 0, the energy balance is:

$$1/2\, M v_+^2 = 1/2\, M v_o^2 - qV \tag{5}$$

$$1/2\, m v_-^2 = 1/2\, m v_o^2 + qV \tag{6}$$

At any position of potential V the net charge density is:

$$\rho = \rho_+(V) - \rho_-(V) \tag{7}$$

From Poisson's equation:

$$\nabla^2 V = -\rho/\epsilon_o \tag{8}$$

since $\nabla^2 V = -\frac{\partial E}{\partial x} = E\frac{\partial E}{\partial V} = \frac{1}{2} d\frac{(E^2)}{dV}$ then:

$$E^2 = -\frac{2}{\epsilon_o}\int \rho\, dV \tag{9}$$

which in defining a "Debye" length

$$l_d = \left(\frac{\epsilon_o T}{2\rho_o}\right)^{1/2} \tag{10}$$

with $l_d = \sqrt{2\pi}\, l_d'$ where l_d' is the usual Debye length definition. Thus rewriting (9):

$$E^2 = -\frac{T^2}{l_d^2}\int \frac{\rho}{\rho_o}\frac{dV}{T} \qquad (11)$$

where $\rho = f(V/T)$.

The potential as a function of distance is obtained by using E from (11) in

$$x = -\int \frac{dV}{E} \qquad (12)$$

Equations (11) and (12) are now to be utilized along with combinations of (1), (2), (3) and (4) to obtain the sheath potential distribution.

1. Equilibrium Sheath

Consider ions and electrons at the same temperature T with their distributions given by (1) and (2). At $V = 0$, $\rho_+ = \rho_-$ so that the ρ_o's are taken equal. Thus from (11) and (7):

$$E^2 = \frac{T^2}{l_d^2}\int \left(e^{V/T} - e^{-V/T}\right)\frac{dV}{T}$$

or

$$E^2 = \frac{2T^2}{l_d^2}\int \sinh V/T \,\frac{dV}{T}$$

$$E^2 = \frac{2T^2}{l_d^2} \cosh V/T + C$$

Relating cosh to sinh gives:

$$E^2 = \frac{4T^2}{l_d^2} \sinh^2 V/2T + E_o^2 \qquad (13)$$

where E_o is the field when $V = 0$.

The case $E_o = 0$ corresponds to zero current and gives the potential distribution in an emitting cavity with volume ion source. From (12) and (13) then:

$$x/l_d = (\ln \tanh V/4T) \qquad (14)$$

This is illustrated below:

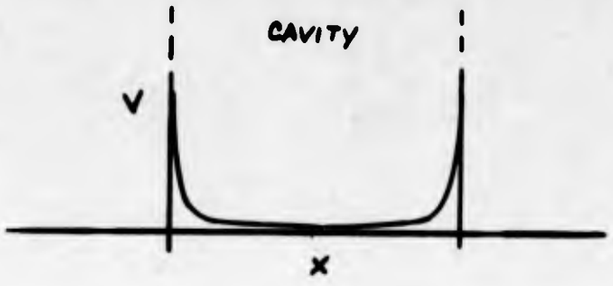

Fig. 1

II. Probe Sheaths

The plasma adjoining a probe is divided into two areas, a pre-sheath in which ion and electron densities are approximately equal, and a sheath in which densities are not equal. Electrons are described by a Boltzmann distribution, whereas ion density is determined from the current. The potential and charge distribution is illustrated below.

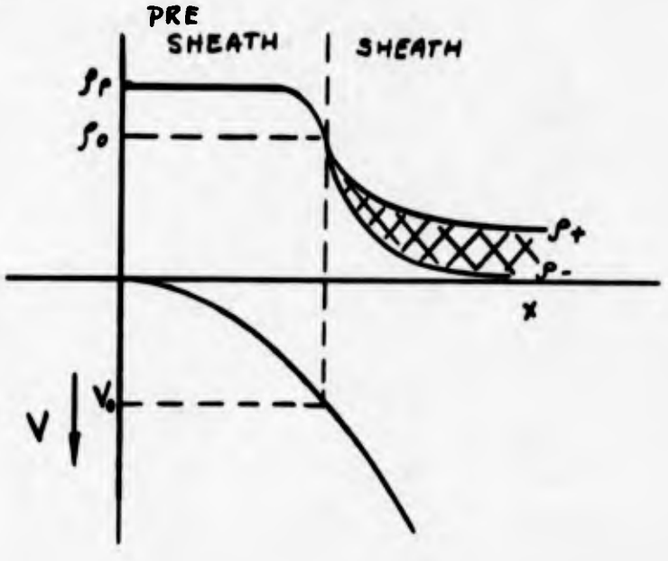

Fig. 2

In the pre-sheath, the charge densities are equal to the plasma density ρ_p:

$$\rho_+ \approx \rho_- \equiv \rho_p \tag{15}$$

$$\rho_- = \rho_p e^{-V/T_-} \tag{16}$$

$$\rho_+ = i_+/v_+ \tag{17}$$

$$1/2\, M v_+^2 = -qV \tag{18}$$

Equation (18) implies that initial ion velocity is zero at $x = 0$, i.e. the probe. Thus, from (7)

$$\rho = i_+ \sqrt{\frac{-M}{2qV}} - \rho_p e^{V/T_-} \tag{19}$$

At $V = V_o$; $\rho = 0$ and $\partial\rho/\partial V = 0$. These boundary conditions applied to (19) yield the following:

$$V_o = -T_-/2 \tag{20}$$

and

$$\rho_o = -\rho_p/\sqrt{e} \tag{21}$$

That is, the pre-sheath charge density is smaller by $1/\sqrt{e}$ at the boundary between the sheath and pre-sheath.

In the sheath (making use of the boundary values at $V = V_o$, i.e. $i_+ = \rho_+ v_+ = \rho_o v_o$ and $\rho_- = \rho_o$ at $V = V_o$) then:

$$\rho_- = \rho_o e^{(V - V_o)/T_-}$$

$$\rho_+ = \rho_o v_o/v_+ \tag{23}$$

So that, using (18) and (20) to substitute for V and V_o then:

$$\rho = \rho_o \left[v_o/v_+ - e^{(v_+^2/v_o^2 - 1)/2} \right] \tag{24}$$

Now since from (18) and (20):

$$\frac{dV}{T_-} = - \frac{v_+ \, dv_+}{v_o^2} \qquad (25)$$

then from (24), (25) and (11):

$$E^2 = \frac{T^2}{l_d^2} \left[\frac{v_+}{v_o} - e^{(v_+^2/v_o^2 - 1)/2} + K \right] \qquad (26)$$

The constant of integration is calculated for given boundary conditions. Equation (26) with (12) has been integrated numerically by Langmuir * where K is determined by setting $E = 0$ at $V = 0$.

Results of the previous analysis are used to explain probe curves. Ion velocities are determined by their potential drop across the pre-sheath, i.e. $v_+ = \sqrt{\frac{-2qV_o}{M}}$. Making use of (20) and (21) then the saturated ion current is:

$$i_{+sat} = S_p \sqrt{\frac{qT_-}{eM}} \qquad (27)$$

where "e" is the base of natural logs.

Near the probe boundary the electron current is given by $i_- = \frac{S_- \bar{v}}{4}$ where $\bar{v}$ is average velocity. This yields:

$$i_- = S_p \sqrt{\frac{qT_-}{2\pi m}} \, e^{V/T} \quad V_f < V < V_p \qquad (28)$$

where V_f is the floating potential, V_p is the plasma potential.

Now saturated electron current is given by:

$$i_{-sat} = S_p \sqrt{\frac{qT_-}{2\pi m}} \quad V > V_p \qquad (29)$$

Thus both electron and ion current are a function of electron temperature. The probe characteristic is illustrated below:

* D. Langmuir. Phy.Rev. 33, 954, 1929

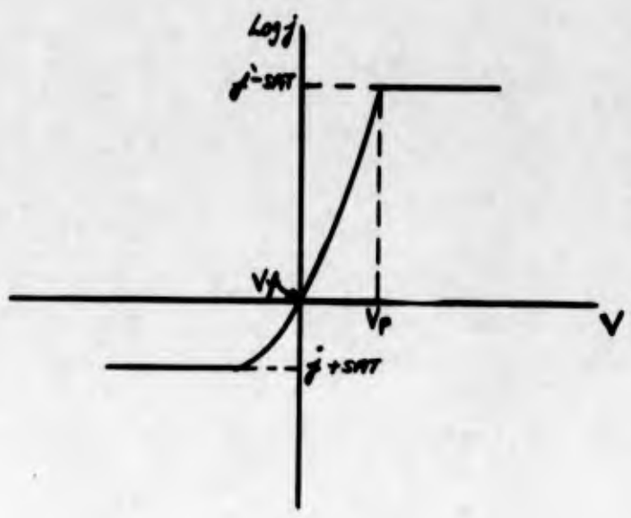

Fig. 3

The floating potential V_f is defined for $j_+ = j_-$ and the plasma potential is V_p. Thus from (27) and (28):

$$V_p - V_f = T_- \ln \sqrt{\frac{2\pi m}{eM}} \tag{30}$$

The ratio of saturated currents is independent of temperature:

$$\frac{j_{-sat}}{j_{+sat}} = \sqrt{\frac{eM}{2\pi m}} \tag{31}$$

III. Effect of Ions on Space Charge Currents

Consider a parallel plate cathode-anode geometry with electrons being emitted with zero initial velocity from the cathode. The problem is to compute the potential distribution when ions are generated uniformly in the cathode-anode space with zero initial velocity. It is assumed there are no collisions so that from (3), (4), (5), (6) and (7):

$$\rho = j_+ \sqrt{\frac{M}{2q(V_a - V)}} - j_- \sqrt{\frac{m}{2qV}} \tag{32}$$

where the potential V_a is anode potential.

Defining

$$\alpha = \frac{i+}{i-}\sqrt{\frac{M}{m}} \tag{33}$$

then from (9) and (32); and the boundary condition that E = 0 at the cathode, i.e. V = 0;

$$E^2 = \frac{i-}{\epsilon_o}\sqrt{\frac{8m}{q}}\left[\sqrt{V} + \alpha\sqrt{V_a - V} - \alpha\sqrt{V_a}\right] \tag{34}$$

The potential distribution derivable from (34) is given by Langmuir* for various values of α considering ions formed at a particular plane. Figure 4 indicates the shape of the potential for several limiting values of α. The value $\alpha = 0$ corresponds to the Child-Langmuir law, i.e. no ions. The value $\alpha = 1$ corresponds to zero potential gradient at both cathode and anode. The value $\alpha = \infty$ corresponds to a uniform plasma over the space except for a cathode sheath.

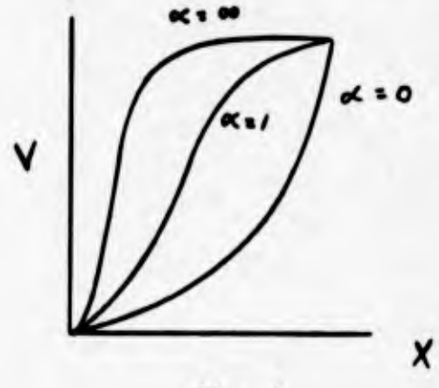

Fig. 4

For the case of ions emitted from the anode Langmuir(1) finds that the electron current is increased to 1.8605 x I_o where I_o is the space charge limited current in the absence of space charge. A calculation for the planar position between cathode and anode for ion generation that leads to the greatest increase in electron current flow indicates that this is a point 4/9 of the distance from the cathode to anode.

An extension of Langmuir's work is found in a paper by Auer et al# in which the cathode sheath potential distribution is calculated considering space charge resulting from primary electrons from the cathode and from ions generated in the cathode sheath. This corresponds to a low density gas discharge in which the analysis indicates how, with increasing gas pressure and voltage, the cathode sheath and positive column in the discharge are formed.

* D. Langmuir, Phy Rev. 33, 954, 1929

\# P.L. Auer, et al, Phy Rev. 111, 1017, 1958

IV. Space Charge Neutralization by Positive Ions in Diodes

The problem of computing the potential distribution in a diode in which ions are in thermal equilibrium at cathode temperature has been developed by Auer et al # and is outlined here in the notation used previously. The starting point is the solution to the electron density distribution for the case of space charge limitation where electrons are emitted from the cathode with a Maxwellian distribution. The earliest treatment by Fry * had some errors as indicated by Langmuir /. Auer begins with Langmuir's results. The potential distribution in the absence of ions is shown.

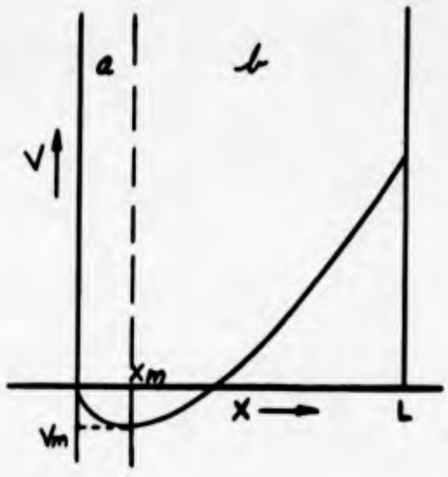

Fig. 5

Electrons flow in a double stream in region (a) since some electrons are reflected back by the potential barrier where a single stream flows in region (b). The cathode is at temperature T, and electrons and ions are assumed to have the same T.

The electron density is defined in terms of the current and the average velocity of the emitted electrons at the space charge minimum.

$$\rho_{-0} = \frac{j_-}{v_0} \tag{35}$$

$$v_0 = \left(\frac{2kT}{\pi m}\right)^{1/2} \tag{36}$$

P. L. Auer et al, J.Appl.Phys. 30, 161, 1959
* T.C.Fry, Phy Rev. 17, 441, 1921
/ D. Langmuir, Phys.Rev. 21, 419, 1923

The solution for ρ_- as a function of position is given by Langmuir as:

$$\rho_-(x) = \rho_{-o} e^{V/T} \left[1 \pm \operatorname{erf}\sqrt{\frac{V}{T}}\right] \begin{matrix} +\text{for } x < x_m \\ -\text{for } x > x_m \end{matrix} \tag{37}$$

where the potential V is taken with respect to V_m.

Now assuming ions at the same temperature as the cathode, then Auer writes:

$$\rho_+ = \rho_{+o} e^{-V/T} = \alpha \rho_{-o} e^{-V/T} \tag{38}$$

$$\rho_{+o} = \alpha \rho_{-o} \tag{39}$$

Thus

$$\rho_+ (V = 0) = \alpha \rho_{-o} \tag{40}$$

The quantity α is an arbitrary parameter relating ion to electron densities. The total charge density is then from (37) and (38).

$$\rho = \rho_{-o} \left[\alpha e^{-V/T} - e^{V/T} (1 \pm \operatorname{erf} \sqrt{V/T})\right] \tag{41}$$

Thus from (11) and (41):

$$E^2 = \frac{T^2}{l_d^2} \int \left[e^{V/T} \left(1 \pm \operatorname{erf}\sqrt{V/T}\right) - \alpha e^{-V/T}\right] \frac{dV}{T} \tag{42}$$

This integrates to:

$$E^2 = \frac{T^2}{l_d^2} \left[e^{V/T} - 1 + \alpha (e^{-V/T} - 1) \mp \left(e^{V/T} \operatorname{erf}\sqrt{V/T} - \frac{2}{\sqrt{\pi}} \sqrt{V/T}\right)\right] + E_\mp^2 \tag{43}$$

$$- \text{for } x > x_m \qquad + \text{for } x < x_m$$

The quantity $E_{\mp} = 0$ if the potential minimum occurs between the electrodes. The potential is obtained from (12) and (43) with $E_d = 0$. Auer computes this numerically and several cases of interest are reproduced.

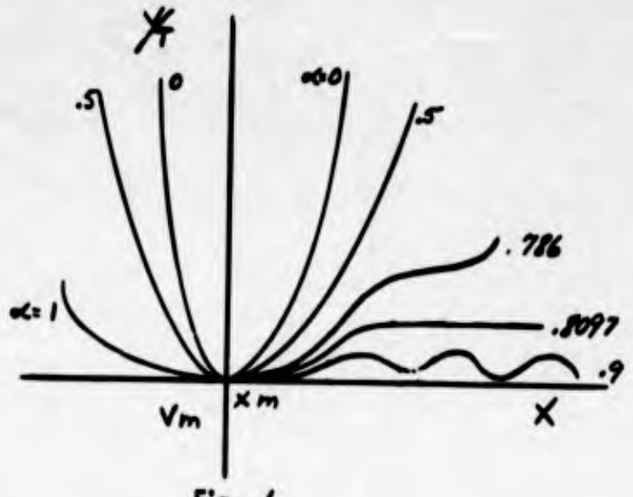

Fig. 6

For $\alpha = .8097 = \alpha_{CR}$, V/T approaches a limiting value whereas for $\alpha = .786$, V/T has a pronounced inflection. Above the limiting value α_{CR} the potential has the appearance of standing waves. These curves are all based on the assumed boundary condition that minimum in the potential appears between cathode and anode. That is, even if ion density approaches electron density ($\alpha = 1$) a minimum is still observed and $V/T \sim x^4$.

The constant $E_{\mp}$ in (43) not equal to zero corresponds to the case of no potential minimum due to insufficient cathode emission, i.e. potential is more positive at the cathode and anode boundaries. This case is treated qualitatively by Auer[3]

V. Application to the Noble Gas Plasma Diode

The problem is to calculate the current voltage characteristic for a cathode sheath and anode sheath and then to join the two solutions to get the diode characteristic. Consider anode emission small relative to random electron current at the anode so that the anode sheath consists of a single sheath with excess positive charge. The cathode sheath potential distribution is dependent on cathode emission and consequently several modes of operation can be discussed. These are first described with the following notation used to differentiate between the various quantities.

T_+ and T_- = temperature of ions and electrons in volts ($\pm$ c and $\pm$ a refer to temperature near cathode and anode)

J_{ec} and J_{ea} = saturated electron emission from cathode and anode at temperatures T_c and T_a

J_{-rc} and J_{-ra} = random electron current in the plasma near cathode and anode (+ rc and + ra refer to ion current)

J = net electron current flowing in the plasma between cathode and anode and into external circuit

V_p = plasma potential taken arbitrarily as the reference for sheath potentials

V_c and V_a = cathode and anode potential relative to plasma potential

V_m = potential of space charge minimum relative to plasma potential

A. Anode Sheath

For an anode area comparable or greater than the cathode area, the electron current to the anode is generally smaller than the random current in the plasma. This is caused by a retarding field for plasma electrons at the anode and is considered here. If anode area is smaller than the cathode area, an electron sheath develops corresponding to a positive sheath drop and in some discharges leads to a "ball of fire" mode wherein ionization takes place in the region of sheath potential greater than ionization potential *. Figure 7 shows the potential diagram for the plasma electron retarding field case.

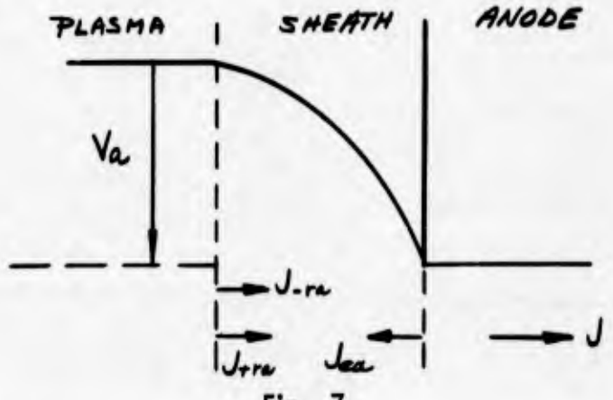

Fig. 7

* L. Malter, et al, RCA Review, 415, 1951

In this case random ion current is not neglected. It is related to J_{-ra} by Eq. (31) so that:

$$\frac{J_{+ra}}{J_{-ra}} = \sqrt{\frac{2\pi m}{e M}} \tag{44}$$

Current balance at the anode gives; where V_a is a negative quantity:

$$J = J_{-ra}\, e^{V_a/T_{-a}} - J_{ea} - J_{+ra} \tag{45}$$

Combining (44) and (45)

$$V_a = T_{-a} \ln\left[\sqrt{\frac{2\pi m}{e M}} + \frac{J + J_{ea}}{J_{-ra}}\right] \tag{46}$$

$$\text{For } V_a = 0 \quad J = J_{-ra}\left(1 - \sqrt{\frac{2\pi m}{e M}}\right) - J_{ea} \tag{47}$$

$$\text{For } J = 0 \quad V_a(J=0) = T_{-a} \ln\left[\sqrt{\frac{2\pi m}{e M}} + \frac{J_{ea}}{J_{-ra}}\right] \tag{48}$$

From (47) it is evident that maximum electron current drawn from the diode is J_{-ra} considering anode emission small. Now since $J_{-ra} = \frac{Nqv}{4}$ then both N and v (i.e. electron temperature) want to be kept large. Figure 8 shows, for example, values of J_{-r} vs gas pressure for the noble gases studied in TM 40-98[7] where electron and gas temperatures were both taken as 1000° K.

The characteristic given by (46) will be combined with subsequent cathode sheath characteristics.

2/2/60

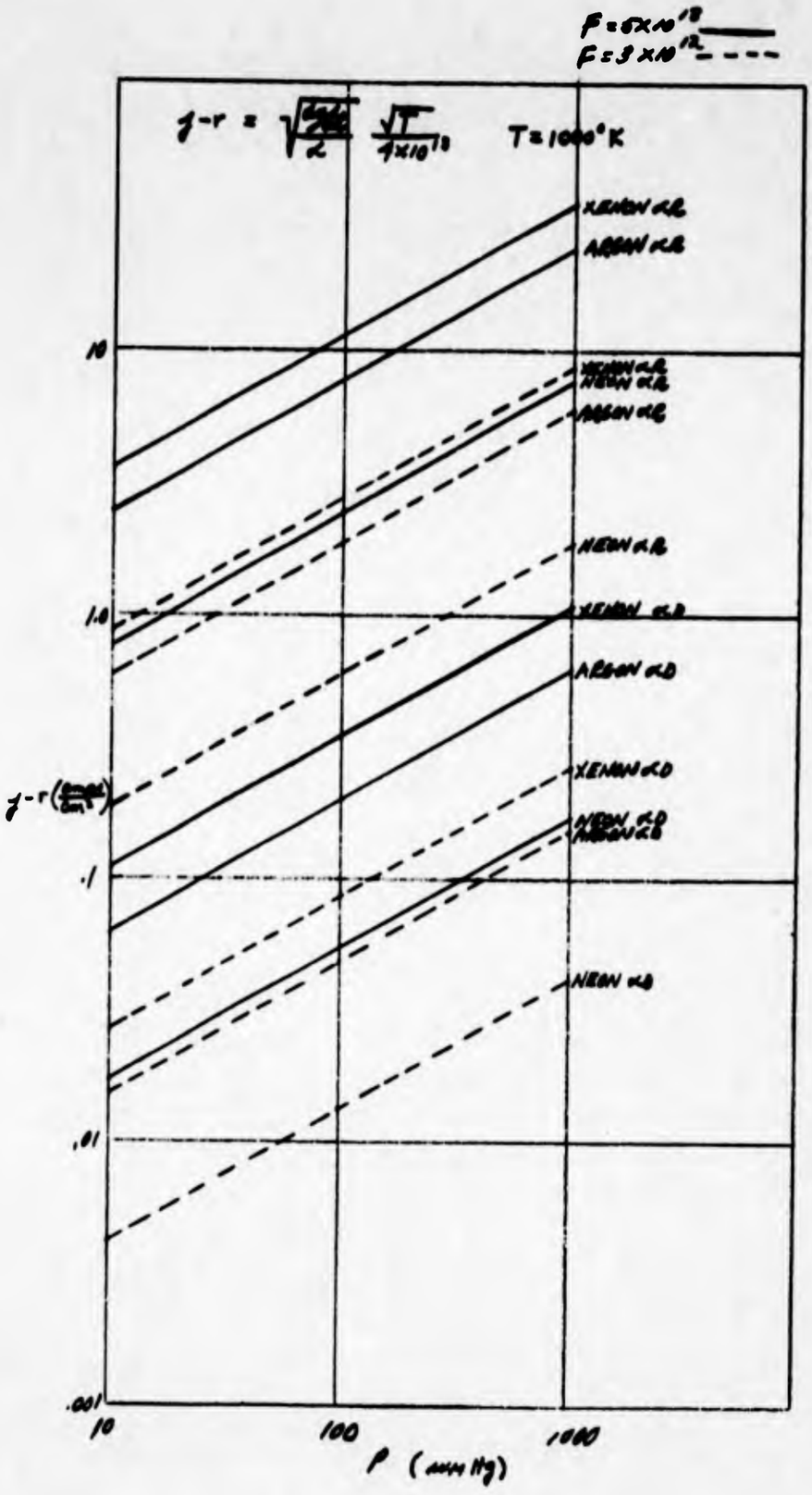
F = 6X10^12
F = 3X10^12
T = 1000°K
XENON cm
ARGON cm
NEON cm
XENON cm
NEON cm
ARGON cm
NEON cm
XENON cm
ARGON cm
XENON cm
NEON cm
ARGON cm
NEON cm
10
1.0
.1
.01
.001
10
100
1000
P (mm Hg)

Fig. 8

B. Cathode Single Sheath (Strong Emitter Solution)

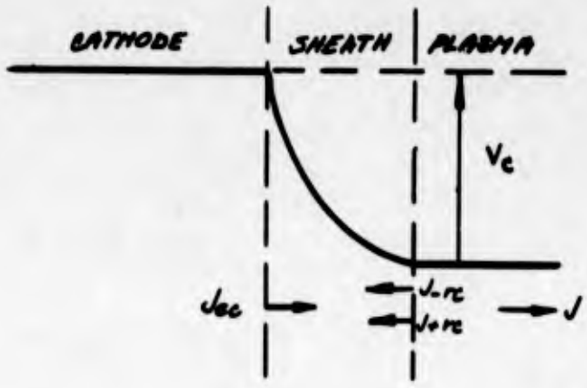

Fig. 9

The current balance is:

$$J = J_{ec}\, e^{-V_c/T_c} - J_{-rc} + J_{+rc}\, e^{-V_c/T_{+c}} \tag{49}$$

For $V_c = 0$ $\quad J = J_{ec} - J_{-rc} + J_{+rc}$ (50)

The sheath potential as determined from (49) for $J_{+rc}\, e^{-V_c/T_{+c}}$ small is:

$$V_c = T_c \ln \frac{J_{ec}}{J + J_{-rc}} \tag{51}$$

For $J = 0$ $\quad V_c(J=0) = T_c \ln \dfrac{J_{ec}}{J_{-rc}}$ (52)

Now using Richardson's equation $J_{ec} = AT_c^2\, e^{-\phi_c/T_c}$ where ϕ_c = cathode work function then:

$$V_c(J=0) = T_c \ln \frac{AT_c^2}{J_{-rc}} - \phi_c \tag{52a}$$

Defining $\lambda_c = \ln \frac{AT_c^2}{J_{-rc}}$ then the open circuit voltage becomes:

$$V_c\,(J = 0) \equiv \lambda_c T_c - \phi_c \tag{53}$$

The sheath potential will be positive relative to the plasma when:

$$J_{ec} > J + J_{-rc} \tag{54}$$

Now since the maximum $J = J_{-ra}$ then:

$$J_{ec} > J_{-ra} + J_{-rc} \tag{55}$$

If electron temperature near anode and cathode is the same then the cathode sheath potential is always positive when approximately:

$$J_{ec} \geq 2\, J_{-rc} \tag{56}$$

C. Cathode Single Sheath (Weak Emitter Solution)

For a weak emitter, it is possible for the cathode sheath potential to become negative with respect to the plasma. This is true if in (51):

$$J_{ec} < J + J_{-rc} \tag{57}$$

which similar to the argument derived for (56) then

$$J_{ec} < 2\, J_{-rc} \tag{58}$$

is the condition for a negative cathode sheath potential.

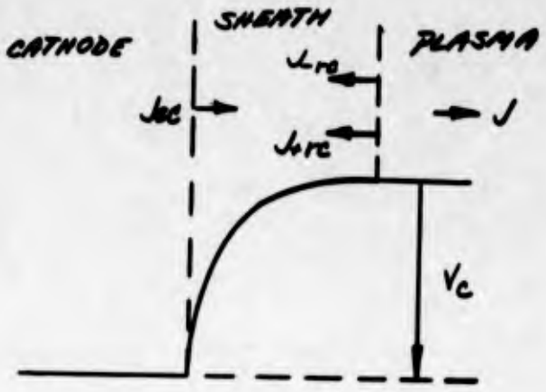

Fig. 10

The current balance is:

$$J = J_{ec} - J_{-rc}\, e^{-V_c/T_{-c}} + J_{+rc} \tag{59}$$

Thus,

$$V_c = T_{-c} \ln \frac{J_{-rc}}{J_{ec} + J_{+rc} - J} \tag{60}$$

For $J = 0$ $\qquad V_c\,(J = 0) = T_{-c} \ln \dfrac{J_{-rc}}{J_{ec} + J_{+rc}}$ (61)

D. Cathode Couble Sheath (Auer Solution)

In this case, use is made of the condition found by Auer * for V_m. The sheath potential is positive relative to the plasma as shown in Fig. 11.

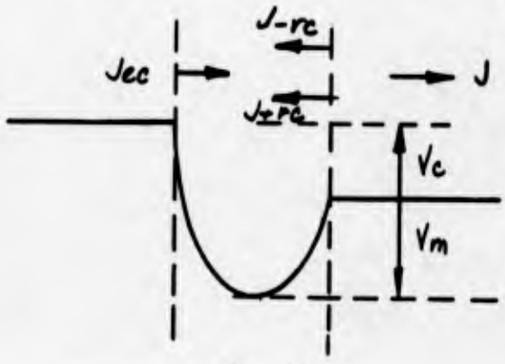

Fig. 11

* P.Auer et al, J.Appl.Phys. 30, 161,1959

The current balance is:

$$J = J_{ec}\, e^{(V_m - V_c)/T_c} - J_{-rc}\, e^{V_m/T_{-c}} + J_{+rc}\, e^{-V_c/T_{+c}} \qquad (62)$$

For small ion current and for $J = 0$, this reduces to eq. (52) for V_c, noting that $V_m \neq -\infty$. Now Auer[3] calculates that for cathode, electrons and ions all at the same temperature, the value of V_m which provides V_p = constant in x (i.e. assuming no potential gradient in the plasma) is $V_m = -0.344\, T_c$.

Now since $J_{+rc}\, e^{-V_c/T_{+c}}$ is small and $T_c \approx T_{-c}$ then (62) becomes:

$$J = (J_{ec}\, e^{-V_c/T_c} - J_{-rc})\, e^{-0.344} \qquad (63)$$

For $V_c = 0$ $\qquad J = (J_{ec} - J_{-rc})\, e^{-0.344} \qquad (64)$

For $J = 0$, V_c from (63) has the same form as (52) for the single sheath strong emitter solution and the cathode sheath would be a single sheath at this value unless $\alpha = 0.8097$ in which case the sheath potential would appear as in Fig. 11 with plasma potential at cathode potential.

E. Cathode Double Sheath (Langmuir Solution)

Langmuir* treats the case of a double sheath in which the cathode is negative with respect to the plasma. The ratio of electron current to ion current, when cathode emission is raised to the point of current limitation by space charge, is given by the ratio of masses $(M/m)^{1/2}$. This holds when initial velocities are ignored and is good for large cathode sheath potential drop (V_c). For small sheath drops the ratio is calculated by Langmuir including initial velocities. This tends to decrease the ratio J/J_{-rc} at the double sheath.

The Langmuir double sheath is shown in Fig. 12 and is treated here in the same way as previous cases with initial particle velocities neglected.

* D.Langmuir, Phy.Rev. 33, 954, 1929

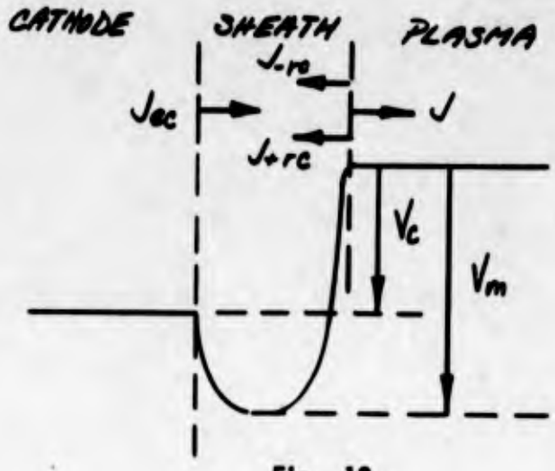

Fig. 12

Current balance gives

$$J = J_{ec}\, e^{(V_m - V_c)/T_c} - J_{-rc}\, e^{V_m/T_{-c}} + J_{+rc} \tag{66}$$

For a double sheath the saturated electron current (neglecting random current) is $J_{ec}\, e^{(V_m - V_c)/T_c}$ and the saturated ion current is J_{+rc}. Thus from (31) then

$$J_{ec}\, e^{(V_m - V_c)/T_c} = J_{+rc} \sqrt{\frac{eM}{2\pi m}} = J_{-rc} \tag{67}$$

Thus from (31), (66) and (67) and since the right side of (67) is just J_{-rc}

$$J = J_{-rc} \left[1 + \sqrt{\frac{2\pi m}{eM}} - e^{V_m/T_{-c}} \right]$$

Also from (67) after raising both sides to the T_c/T_{-c} power;

$$e^{V_m/T_{-c}} = \left(\frac{J_{-rc}}{J_{ec}} \right)^{T_c/T_{-c}} e^{V_c/T_{-c}} \tag{68}$$

and thus:

$$J = J_{-rc}\left[1+\sqrt{\frac{2\pi m}{eM}}-\left(\frac{J_{-rc}}{J_{ec}}\right)T_c/T_{-c}\ e^{V_c/T_{-c}}\right] \tag{69}$$

For $V_c = 0$, $T_c \approx T_{-c}$ and neglecting $\sqrt{\frac{2\pi m}{eM}}$:

$$J(V_c = 0) = \frac{J_{-rc}}{J_{ec}}\left[J_{ec} - J_{-rc}\right] \tag{70}$$

Equations (64) and (70) describe the same conditions for a double sheath ($V_c = 0$); however they are equivalent only at one particular value of $\frac{J_{-rc}}{J_{ec}} = e^{-0.344}$. This anomalous behavior indicates that the assumption of ignoring initial ion and electron velocities in the Langmuir double sheath case may be in considerable error. Additional calculations are in progress on the double sheath mode of diode operation to check this point.

VI. Computation of Diode Characteristic for Single Cathode Sheath

The strong emitter solution of the single cathode sheath is joined to the anode sheath solution to give the voltage current characteristic. This case yields the highest power output for the noble gas plasma diode, whereas the weak emitter solution would be operative when $J_{-rc} > J_{ec}$ which is the case for a cesium diode where ion densities of $10^{14}/cm^3$ provide random currents of order 100 amps/cm^2.

The potential diagram of the diode for the single sheath case including plasma drop ΔV_p is shown in Figure 13.

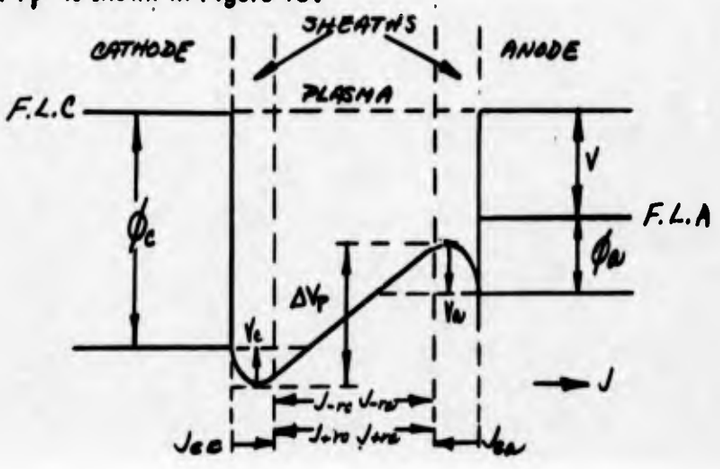

Fig. 13

The voltage balance, where V, V_c and V_a are positive quantities, is then:

$$V = \phi_c - \phi_a + V_c + V_a - \Delta V_p \qquad (71)$$

That is, for the diode characteristic, V is calculated to be a positive quantity which corresponds to the cathode being positive with respect to the anode.

Equations (51) and (46) are applied to (71) with the $\sqrt{\frac{2\pi m}{eM}}$ term neglected in (46) and remembering that V_a was a negative quantity in (46) and is now taken as positive by inverting the quantities in the ln term:

$$V = \phi_c - \phi_a + T_c \ln \frac{J_{ec}}{J + J_{-rc}} + T_{-a} \ln \frac{J_{-ra}}{J + J_{ea}} - JRg \qquad (72)$$

where R is plasma resistivity and g is cathode-anode gap. Using Richardson's law for $J_{ec} = AT_c^2 e^{-\phi_c/T_c}$ then:

$$V = T_c \ln \frac{AT_c^2}{J + J_{-rc}} + T_{-a} \ln \frac{J_{-ra}}{J + J_{ea}} - JRg - \phi_a \qquad (73)$$

Equations (72) and (73) are valid for $J_{ec} > J_{-rc}$ and $J \leq J_{-ra}$. From (73) it is evident that Rg and ϕ_a want to be made small consistent with a small back emission from the anode J_{ea}.

Figures 14 and 15 show the voltage-current characteristics calculated for several values of gas pressure. These were obtained using the following data: Cathode: UC at 2000° K with A = 33 ϕ_c = 3.14 ev ; anode - BaO/SrO at 900° K with ϕ_a = 1.0 ev; neutron flux of 5×10^{13} and an average Ne:A gas temperature of 1450° K. Electron temperatures at cathode and anode are taken as equal to cathode and anode temperature. Power densities of order 5 watts/cm^2 are seen to be computed which is in the range of practical interest when extended system lifetime is considered.

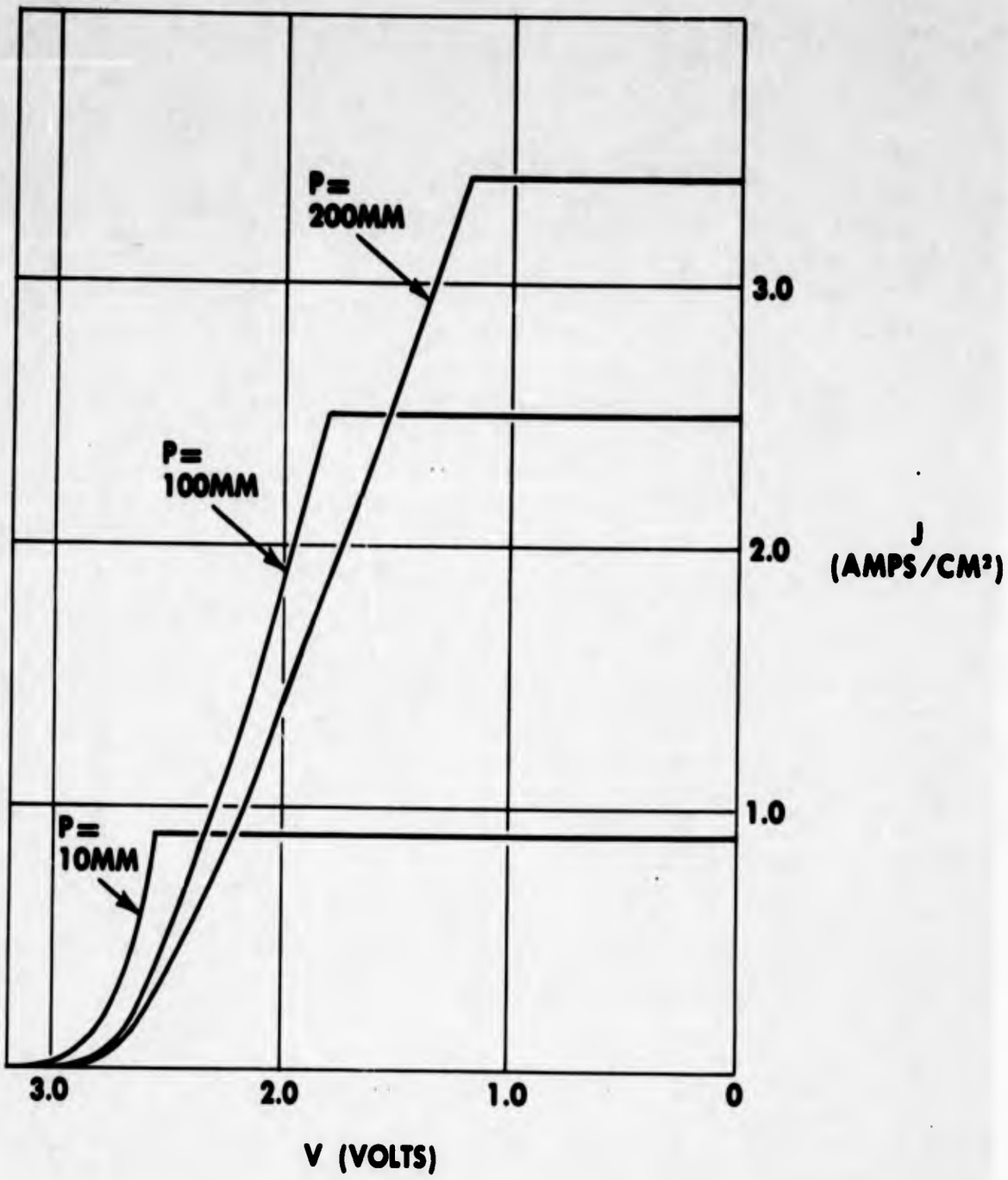

Fig. 14. Voltage-Current Characteristic Calculated for a UC Cathode: T_c = 2000° K, T_a = 900° K, $\Delta\phi$ = 2.14 ev, Ne:A (10^3:1), Neutron Flux = 5×10^{13} n/sec cm^2

Fig. 14

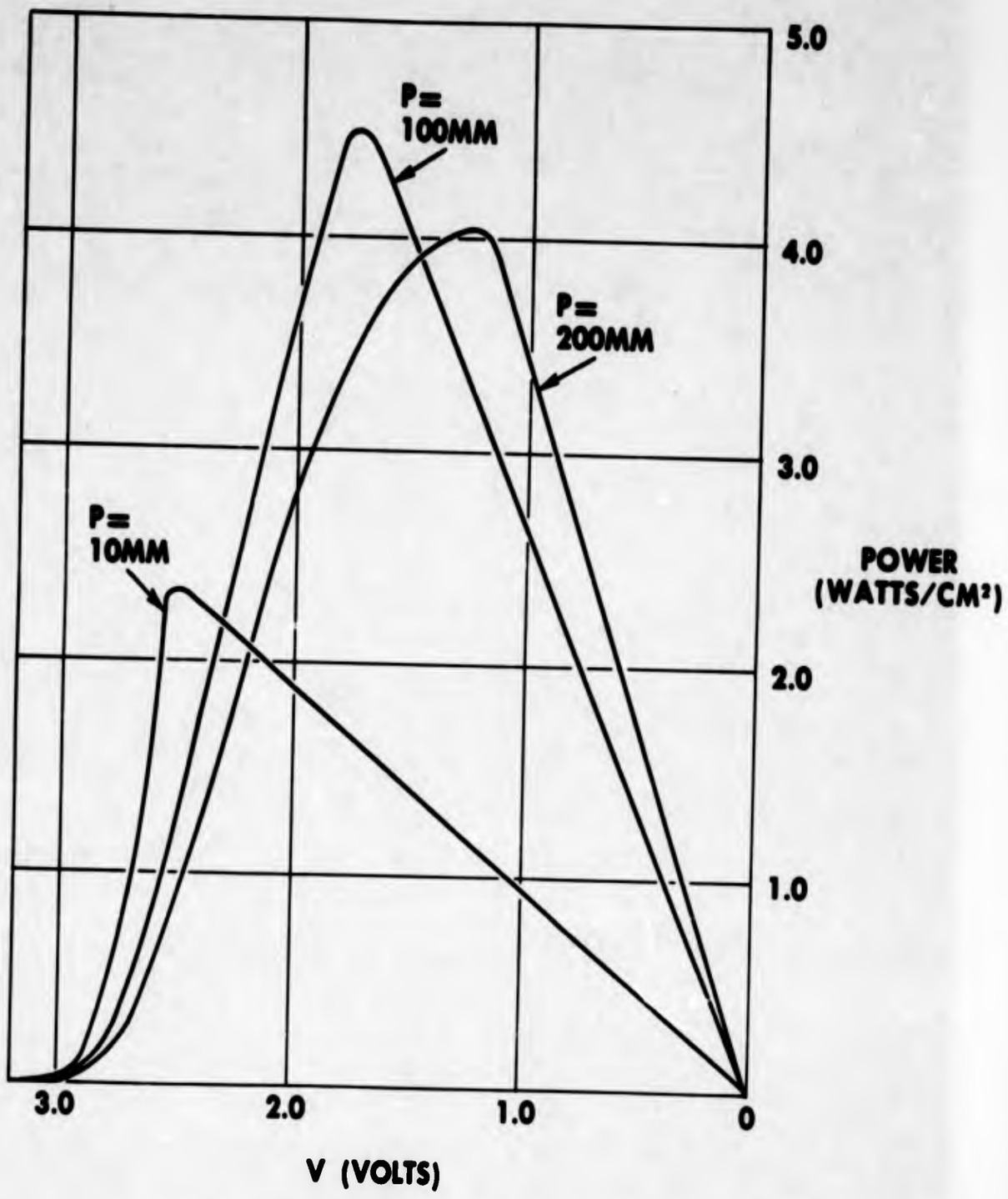

Fig.15. Power Characteristic Calculated for a UC Cathode: T_c = 2000° K, T_a = 900° K, $\Delta\phi$ = 2.14 ev, Ne:A (10^3:1), Neutron Flux = 5×10^{13} n/sec cm^2

Fig. 15

VII. Conclusions

Single sheaths and double sheaths can exist at the cathode, whereas a single sheath exists at the anode in the NGPD. The combination of the cathode single sheath and anode sheath are shown in Fig. 16 for both weak and strong emitter solutions. In this case, the plasma potential drop is neglected. This illustrates how the cathode sheath changes with current drawn from the diode. Figure 17 shows how the introduction of the plasma potential drop (assuming resistivity is a constant) changes the combined sheath characteristic. Conditions for which the double sheath mode of operation exists are not yet well enough understood to be reported.

Current drawn from the NGPD is limited to the random electron current at the anode. Now since $J_{-ra} \propto N \sqrt{T_{-a}}$, then large ion density and a high electron temperature are desired. The density is limited by available fission fragment flux and electron temperature is determined from heat balance considerations in the plasma. The latter is presently being investigated.

Utilizing parameters calculated in Appendix I, the calculated diode characteristic for a NGPD yields power densities of order 5 watts/cm^2. System efficiency depends on what input energy is assumed to maintain the system at the desired temperatures. It is evident that if better material parameters are selected or a higher neutron flux assumed, the power output density could be proportionately increased.

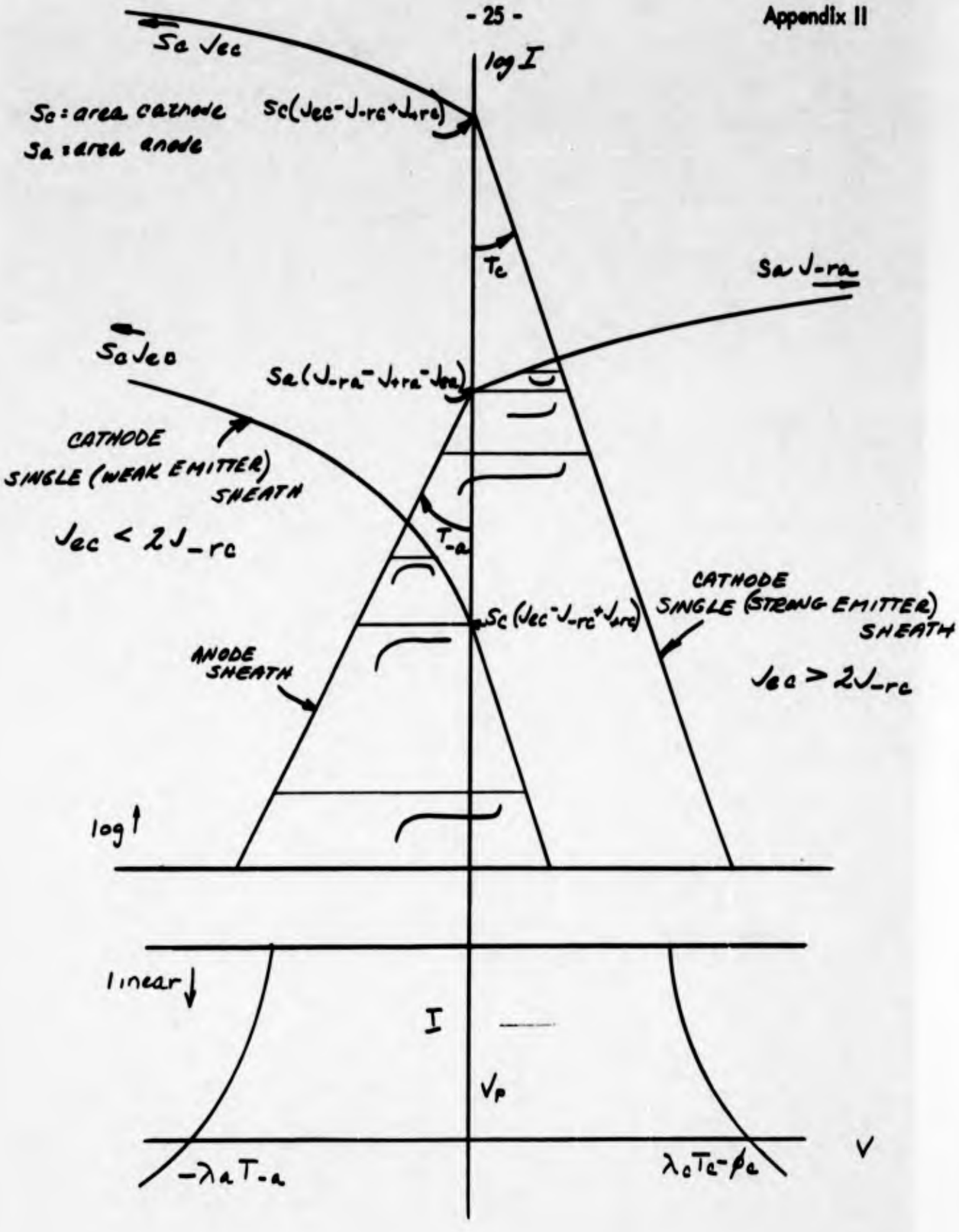

Fig. 16

NGPD Sheath Characteristics for Single Cathode Sheaths

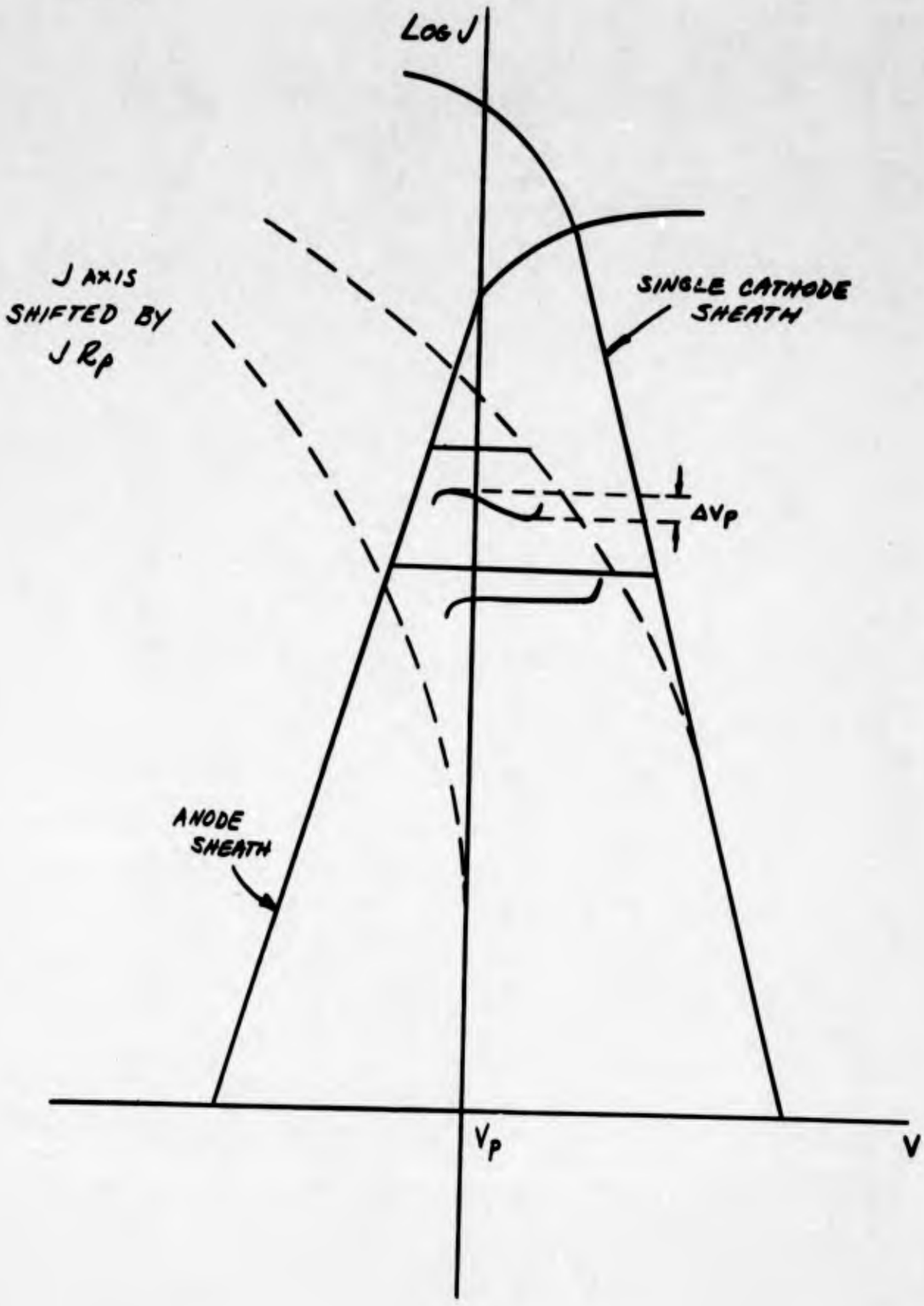

Fig. 17
NGPD Single Cathode Sheath Characteristic Including Plasma Potential Drop ΔV_p

Appendix III

In-pile operation of reactor experiment II yielded characteristic curves as shown in Fig. 1. (The I_{s+} curve is drawn by the logarithmic amplifier of the X-Y recorder in a reverse direction to its true sign.) At 1 megawatt reactor power (neutron flux of 5×10^{12} n/sec cm^2) a short circuit current increase of about 50 fold over the case of zero neutron flux is observed and the curve is relatively flat at a positive bias greater than 2.5 volts. This saturated current is defined as I_{s-} and the reversed current (back emission plus ion) is defined as I_{s+}. Fig. 2 shows how I_{s-} varies with cathode temperature for fixed reactor power. As plasma limited current this corresponds to a number density varying from 3.8×10^{10} to 1.8×10^{11} ions/cc.

The saturation current I_{s-} yields the most information. As it is so much lower than I_e it must be caused by plasma saturation. I_e = cathode saturated emission current density.

$$I_{s-} = ne\sqrt{eT/2\pi m} \qquad (1)$$

However, it increases by a factor 5 as the emitter temperature changes from 1164 to 1467° K so that n must change by almost that factor.

In order to explain the low saturation current, it is expected that the emission is held back by a negative potential

$$\frac{\Delta V}{T_e} = \ln \frac{I_{s-}}{I_e} \qquad (2)$$

If it is assumed that the space around the electrodes, where the fission fragments are densest and most of the ionization is taking place, is at cathode potential, or at a constant difference from cathode potential, then the voltage ΔV will pull ions into the interelectrode space and may cause the observed increase in I_{s-}. The objective of the following calculations is to obtain a qualitative picture of how this may occur.

The flow of ions in the plasma is given by

$$\Gamma_+ = -\nabla D_+ n + \mu_+ En = -D_+ (\nabla n - En/T_+) \qquad (3)$$

and the plasma balance equation is

$$\frac{dn}{dt} = S - \alpha n^2 + D_+ (\nabla^2 n - \nabla . nE/T_+) = 0 \qquad (4)$$

The increase in I_s with reactor power indicates that the bulk of the plasma is recombination controlled. Hence it will be assumed that the plasma density n_r in the space around the electrodes is given by

$$\alpha n_r^2 = S \tag{5}$$

In the space between the electrodes recombination is negligible, and let us consider first the situation defined by $I_e = I_{s-} = I_o$ when $E = 0$. Then

$$S + D\nabla^2 n_o = 0 \tag{6}$$

We shall assume semi-infinite parallel planes instead of cylindrical geometry. Then the solution of (6) is

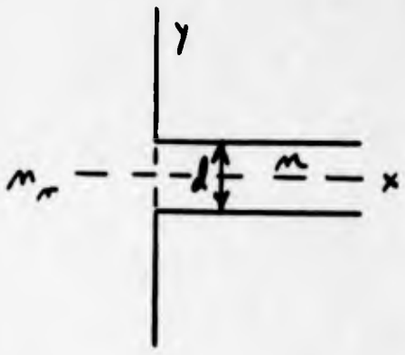

$$\begin{aligned} n_o &= n_1 + n_2 \\ n_1 &= \frac{S}{2D}\left(\frac{d^2}{4} - y^2\right) \\ n_2 &= \left(n_r - \frac{S}{2D}\frac{d^2}{4}\right)\cos\frac{\pi y}{d}\, e^{-\gamma_o x} \\ \gamma_o^2 &- (\pi/d)^2 = 0 \end{aligned} \tag{7}$$

Now when $I_e > I_o$ the solution of (4) with $\alpha n^2 = 0$ $\vec{E} = \vec{E}_x$, a constant, is

$$n = n_1 + n_3$$

$$n_3 = \left(n_r - \frac{S}{2D}\frac{d^2}{4}\right)\cos\frac{\pi y}{d}\, e^{-\gamma x}$$

$$\gamma 2 - \left(\frac{\pi}{d}\right)^2 + \frac{\gamma E}{T} = 0$$

or

$$\frac{\Delta V}{T_+} = \gamma_x - \frac{(\gamma_o x)^2}{\gamma x} \tag{8}$$

where x is now an average distance of penetration by the plasma.

In (7) $\frac{S}{2D}\frac{d^2}{4} \ll n_r$ because d is so small, and hence could be neglected. Also because random currents are proportional to densities, neglecting the factor $\sqrt{T}$,

$$I_o = I_1 + I_2$$
$$I_2 = (I_r - I_1)\, e^{-\gamma_o x}$$
$$I_{s-} = I_1 + I_3$$
$$I_3 = (I_r - I_1)\, e^{-\gamma x}$$

Therefore

$$\gamma_o x = \ln \frac{I_r - I_1}{I_o - I_1}$$
$$\gamma x = \ln \frac{I_r - I_1}{I_{s-} - I_1} \qquad (9)$$

$$-\frac{V}{T_+} = \frac{T_e}{T_+} \ln \frac{I_e}{I_{s-}} = \frac{\left(\ln \frac{I_r - I_1}{I_o - I_1}\right)^2}{\ln \frac{I_r - I_1}{I_s - I_1}} - \ln \frac{I_r - I_1}{I_{s-} - I_1} \qquad (10)$$

For $I_e/I_{s-} = 0$ $I_{s-} = I_f$; $I_e/I_{s-} = 1$ $I_{s-} = I_b$; $I_e/I_{s-} = \infty$ $I_{s-} = I_r$

where $$I_1 = \frac{\sqrt{T}}{4 \times 10^{13}} \frac{S d^2}{8D} A \qquad (11)$$

(This is the maximum value of I_1); d = C-A gap, D = diffusion coefficient, T = electron temperature and A is taken as planar part of cathode area = 0.07 cm^2.

Also,

$$I_o = \left[I_1 + (I_r - I_1)\, e^{-\frac{\pi x}{d}} \right] \frac{\sqrt{T}}{4 \times 10^{13}} \text{ A} \qquad (3)$$

I_r = current corresponding to recombination controlled ion density in the gap between the Ta shield and C-A electrodes.

To make quantitative comparison of theory and experimentwe need to know I_r, I_1 and I_o. The calculations of Appendix I give an ionization rate of 2×10^{14} ion/cm^3 sec for Ne at p = 20 mm and T = 1000° K. Using the radiative recombination coefficient of $\alpha = 10^{-10}$ gives $I_r = 73 \times 10^{-3}$ a. ($n_r = 1.4 \times 10^{12}$ ions/cc) and a dissociative term $\alpha = 2 \times 10^{-7}$ gives $I_r = 1.6 \times 10^{-3}$ a. ($n_r = 3 \times 10^{10}$). Since values of I_{s-} bigger than the latter value were measured, let us consider the use of $I_r = 73 \times 10^{-3}$ a. for the calculations. This would be the maximum current that could be drawn from the plasma then and corresponds to a current density of 1 a./cm^2.

Now I_1 is calculated using $S = 2 \times 10^{14}$, d = 0.1 cm and $D \simeq \frac{D_a}{2} = 22$ cm^2/sec.

The ion diffusion coefficient is obtained from the ambipolar coefficient measured by Biondi *. This gives:

$$I_1 = \frac{\sqrt{1000}}{4 \times 10^{13}} \frac{2 \times 10^{14} (.1)^2}{8 \times 22} \times .07 = 0.6 \text{ ma.}$$

In computing I_o consider $x = 3/2d$ which is the collector radius. Thus:

$$I_o = \left[0.6 + (73.6)\, e^{-\pi 3/2} \right] \times 10^{-3} = 1.26 \text{ ma.}$$

This value of I_o is somewhat higher than that indicated by the data. From I_1, I_o and I_r, K is computed to be 110.

Fig. 3 is a plot of $\frac{I_{s-} - I_1}{I_r - I_1}$ versus I_e / I_{s-}. In this case, T_e is taken equal to T_+ and $K = \frac{I_r - I_1}{I_o - I_1}$. The theoretical curves are computed for K = 50 and K = 100 and the and the data points use measured values of I_{s-} and $I_1 = 0.6$ ma and $I_r = 73$ ma as computed above. This indicates a rather rough correlation between the theory and experiment.

* M. A. Biondi. Phy.Rev. 83, 1078, 1951

Fig. 4 shows the data of I_{s-} plotted versus (reactor power)$^{1/2}$. This characteristic taken at essentially constant cathode and anode temperatures indicates plasma density is recombination limited ($dn/dt \propto$ reactor power $= \alpha n^2$ since $n \propto I_{s-}$). This is consistent with the model suggested by Prof. Allis since the diffusion into the C-A gap is from a recombination limited source which is indicated by Fig. 4.

With large retarding voltages, the diode current reverses and should correspond to the sum of back emission and positive ion current. Fig. 5 illustrates the possible sheath picture at the anode.

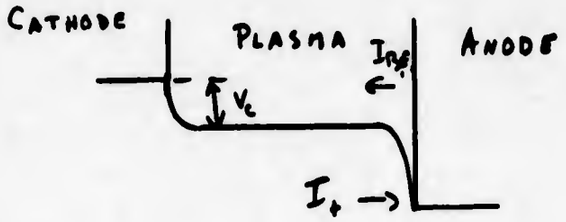

Fig. 5. F.F..1 with Large Retarding Field

The ratio of saturated electron to saturated ion current should be constant and equal to $\sqrt{m\ N_e/m_e}$ which is 200. This is true if the following conditions exist: plasma density is constant with cathode temperature and with change in applied bias, and also if back emission from the anode (I_{BE}) is small.

The measured variation of open circuit voltage, V_{oc}, with temperature is shown in Fig. 6. This can be related to the theory since V_{oc} can be derived from Eq. (72) of Appendix II, neglecting plasma resistance and setting $J = 0$:

$$V_{oc} = \phi_c - \phi_A + \frac{T_{-c}}{11{,}600} \ln \frac{J_{ec}}{J_{-rc}} + \frac{T_{-a}}{11{,}600} \ln \frac{J_{-ra}}{J_{ea} + J_{+ra}} \qquad (13)$$

Substituting the Richardson equation for J_{ec} yields:

$$V_{oc} = \frac{T_c}{11,600} \ln \frac{A_c T_c^2}{J_{-rc}} + \frac{T_{-a}}{11,600} \ln \frac{J_{-ra}}{J_{ea} + J_{+ra}} - \phi_a \qquad (14)$$

where T_c and T_a are cathode and anode temperatures (°K)

T_{-c} and T_{-a} are electron temperatures near the C and A (°K)

A_c is the thermionic A value for the C (120 amps/cm^2°K)

$$J_{-rc} = \frac{n\sqrt{T_{-c}}}{4 \times 10^{13}} \qquad J_{-ra} = J_{-rc}\sqrt{\frac{T_{-a}}{T_{-c}}}$$

$$J_{+ra} = J_{-ra}\sqrt{\frac{m_e}{M_{ion}}}$$

n = ion number density/cm^3

Now using the number density as computed from the measured saturated electron currents and electron temperature equal to T_a the random currents in the V_{oc} equation were calculated as indicated above. Anode work function was computed from published Phillips data,* and electron temperatures were set equal to electrode temperatures to yield the theoretical points shown in Fig. 6.

The measured saturated back current ($J_{ea} + J_{+ra}$) as indicated above should be roughly 1/200th of the saturated forward current. At the higher cathode temperature, this ratio was observed to be a factor of 3 smaller than this value (possibly due to reduced back emission and reduced plasma density in the gap at high negative potential). The effect of this magnitude change in ($J_{ea} + J_{+ra}$) however leads only to a calculated 0.1 volt increase in V_{oc}. This magnitude is within the experimental error so the agreement between theory and experiment indicates the choice of number density (from saturated current) and temperature values is reasonable.

A comparison of the voltage current characteristic as calculated from the emission limited theory (Eq. (72), Appendix II), using a number density obtained from measured saturated current, is shown in Fig. 7 for one of the reactor runs. In this case the calculated back current corresponds to anode back emission plus random ion current. The curvature of the experimental curve could arise from geometrical factors or variation of plasma density at retarding voltages.

Implicit in all the calculations above was that electron temperature was taken equal to emitter temperature. In a probe characteristic the difference between the plasma potential and floating potential yields the electron temperature from:

$$V_p - V_f = T_- \ln \sqrt{\frac{2\pi m}{eM}} \qquad (15)$$

* Levi, R., Phillips Tech.Rev. 19, 186 (1958)

The data at 1267° K indicates a well behaved $\frac{I_{s-}}{I_{s+}}$ ratio so let us calculate T- at this point. Here $V_p \approx 0.1$ volts and $V_f \approx -0.6$ volt. From (6) we obtain $T_- = 0.7 \times 5.28 = 3.7$ v. or 42,500° K electron temperature. This seems rather high indicating that the usual probe theory may not apply here.

The general character of the results so far indicate that plasma density in the C-A gap changed not only with emitter temperature but also with retarding potential.

Again noting from the present experiment that $I_r \gg I_s$, we have from Eq. (10)

$$\frac{T_c}{T_+} \ln \frac{I_e}{I_s} = \frac{\ln^2 \frac{I_r - I_1}{I_o - I_1} - \ln^2 \frac{I_r - I_1}{I_s - I_1}}{\ln \frac{I_r - I_1}{I_s - I_1}}$$

$$= \ln \frac{I_s - I_1}{I_o - I_1} \frac{\ln \frac{(I_r - I_1)^2}{(I_s - I_1)(I_o - I_1)}}{\ln \frac{I_r - I_1}{I_s - I_1}}$$

$$= \ln \left(\frac{I_s - I_1}{I_o - I_1} \right)^2 \left[1 + \frac{1}{2} \frac{\ln \frac{I_s - I_1}{I_o - I_1}}{\ln \frac{I_r - I_1}{I_s - I_1}} \right] \qquad (16)$$

If $$I_r / I_s \gg I_s / I_o \qquad (17)$$

The second term in the square brackets may be neglected. If furthermore we let $T_+ \cong T_c$ this gives

$$\sqrt{\frac{I_e}{I_s}} = \frac{I_s - I_1}{I_o - I_1} \qquad (18)$$

A plot of I_s vs $\sqrt{I_e/I_s}$ is given in Fig. 7. The experimental points are rather scattered, but may be represented, within experimental error, by a straight line through the origin. This corresponds to the constants

$$\begin{aligned} I_r &= \infty \\ I_o &= 1.21 \text{ ma} \\ I_1 &= 0 \end{aligned} \tag{19}$$

The open circuit voltage is correctly given by Eq. (13).

$$V_{oc} = \phi_c - \phi_a + T_c \ln \frac{J_{ec}}{J_{-rc}} + T_{-a} \ln \frac{J_{-ra}}{J_{ea} + J_{+r}} \tag{20}$$

in which it is assumed that $J_{+r} \ll J_{ea}$.

If we substitute

$$\begin{aligned} J_{ec} &= A_c T_c^2 \, e^{-\phi_c/T_c} \\ J_{ea} &= A_a T_a^2 \, e^{-\phi_a/T_a} \end{aligned} \tag{21}$$

we obtain

$$V_{oc} = T_c \ln \frac{A_c T_c^2}{n} \sqrt{\frac{2\pi m}{e T_{-c}}} + T_{-a} \ln \frac{n}{A_a T_a^2} \sqrt{\frac{e T_{-a}}{2\pi m}} + \frac{T_{-a} - T_a}{T_a} \phi_a \tag{22}$$

It is reasonable to assume that the electrons near the cathode are at cathode temperature, $T_{-c} = T_c$, but near the anode the electrons might be above anode temperature, $T_{-a} > T_a$, and then the last term in Eq. (14), which was omitted from Eq. (13), would contribute importantly to V_{oc}.

FIGURE 1

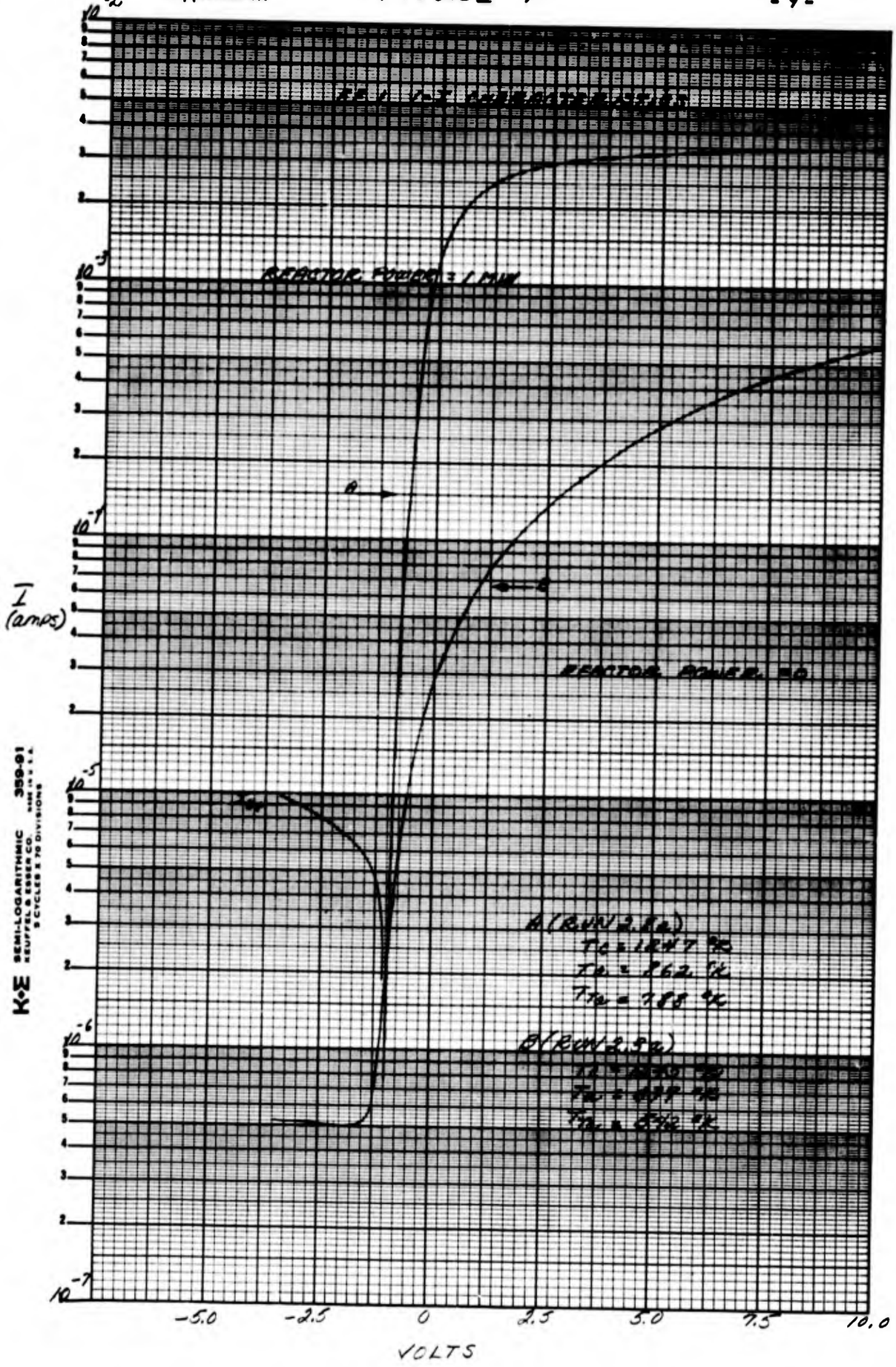
REACTOR POWER = 1 MW
REACTOR POWER = 0
I (amps)
VOLTS
-5.0
-2.5
0
2.5
5.0
7.5
10.0
K&E SEMI-LOGARITHMIC 359-91
KEUFFEL & ESSER CO.
5 CYCLES X 70 DIVISIONS

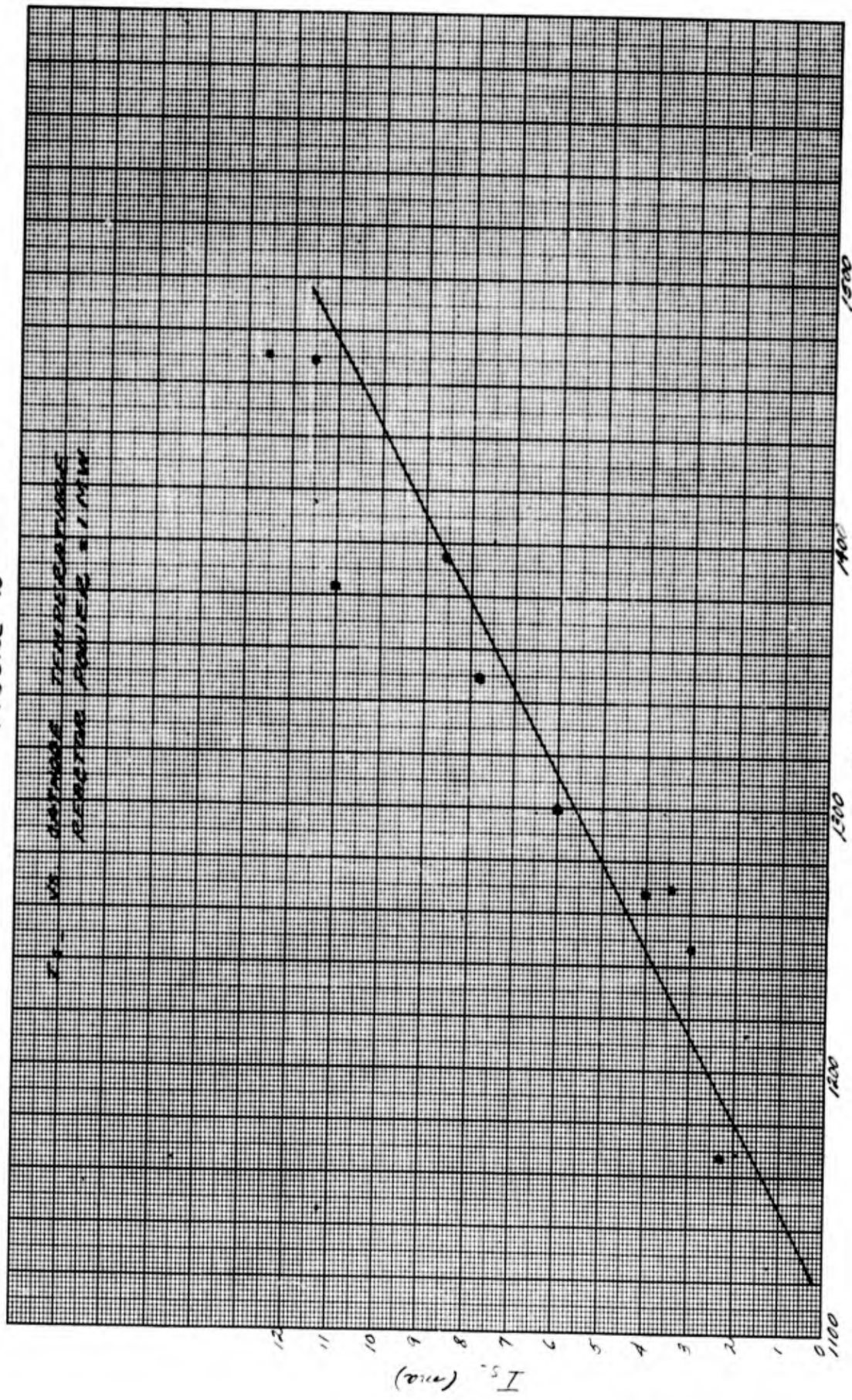

FIGURE 2

T_c vs. maximum persistent power at 1 MW

K•E 10 X 10 TO THE CM. 359-14
KEUFFEL & ESSER CO.

K•Σ LOGARITHMIC 359-125G
KEUFFEL & ESSER CO. MADE IN U.S.A.
3 X 5 CYCLES

Figure 3
COMPARISON OF DATA TO THEORY (EQ.10)

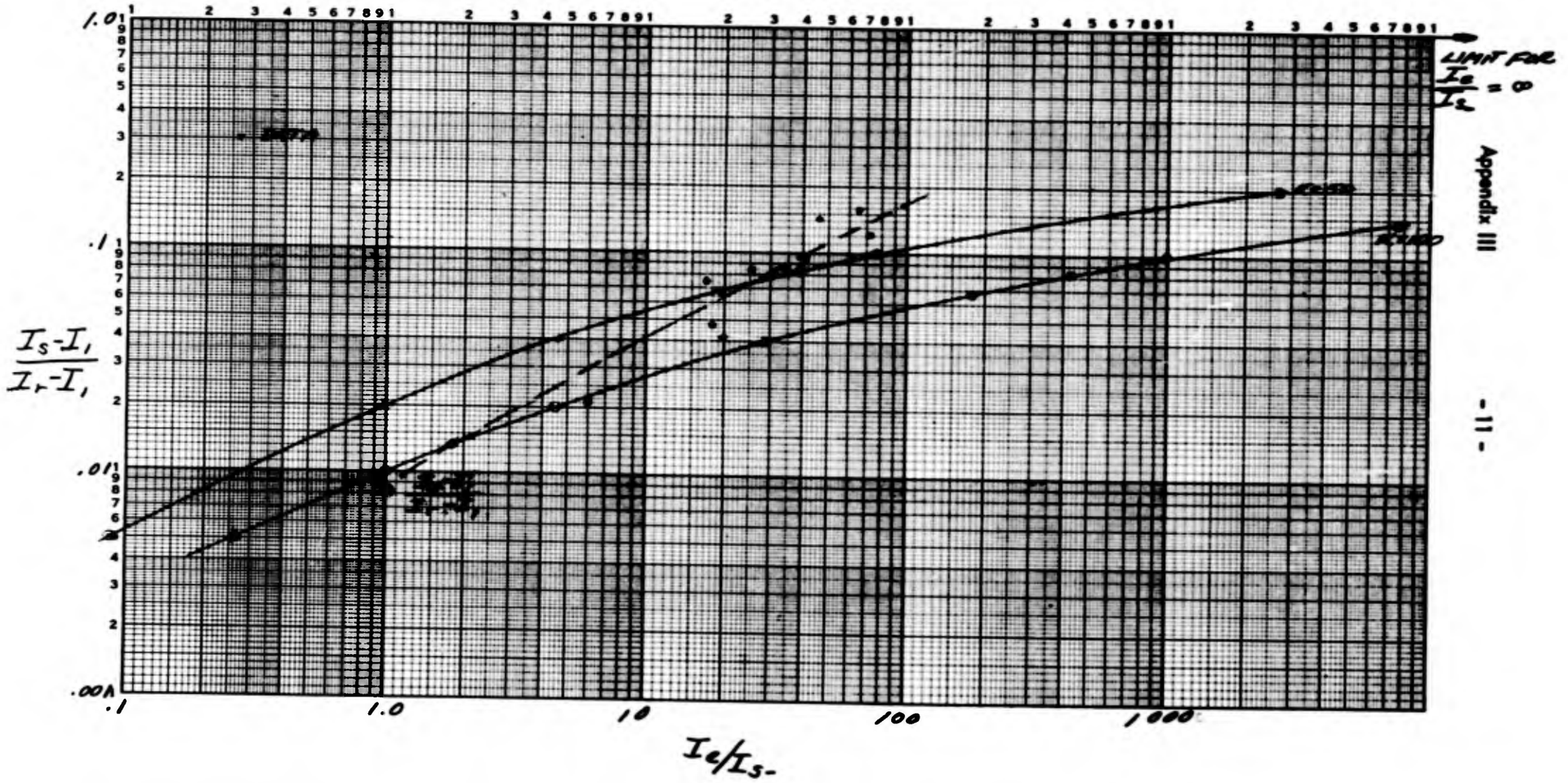

Figure 4

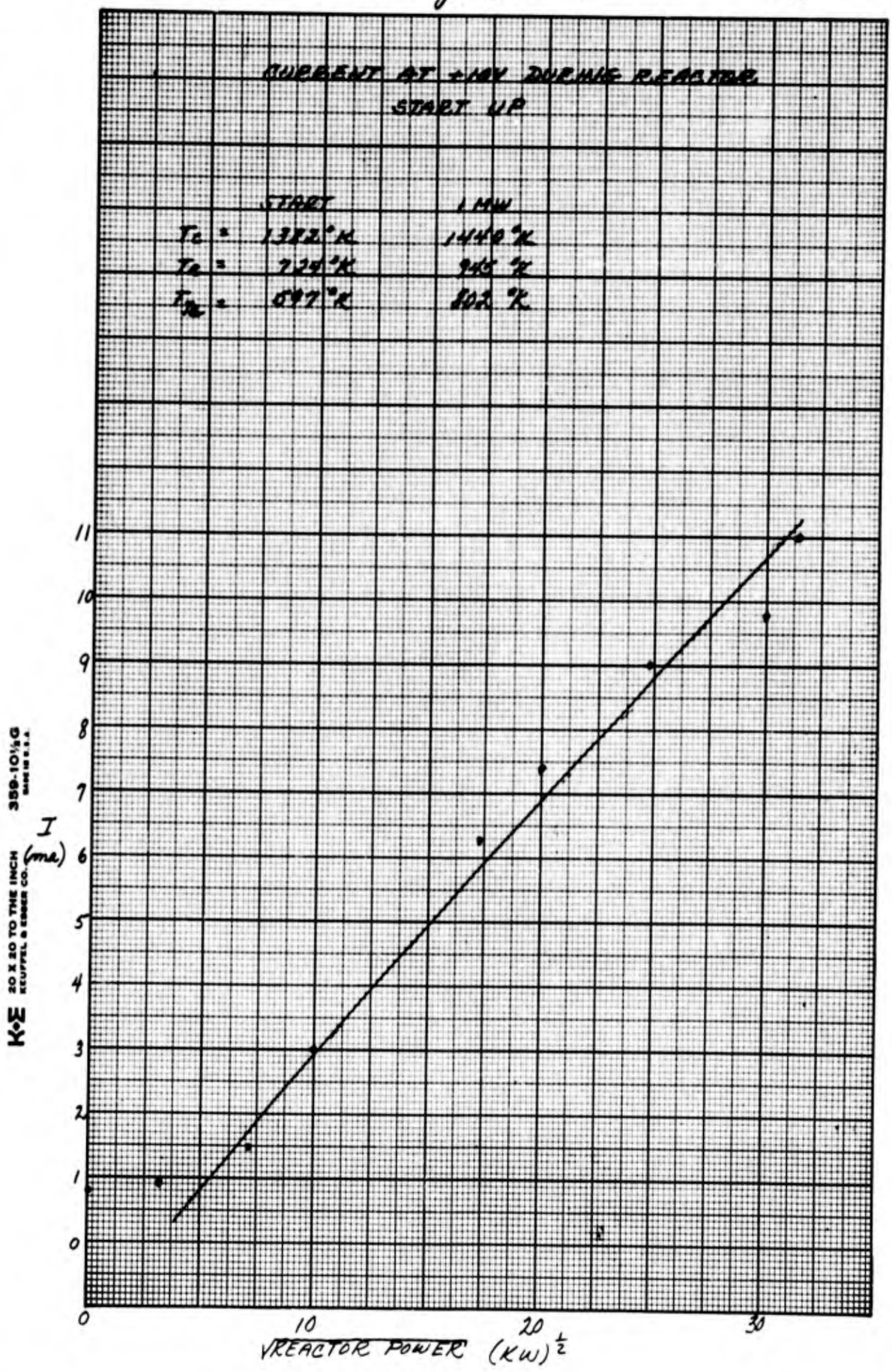
CURRENT AT +10V DURING REACTOR START UP
START
1 MW
T_c = 1382°K 1440°K
T_e = 724°K 745°K
T_{in} = 697°K 802°K
I (ma)
0
1
2
3
4
5
6
7
8
9
10
11
0
10
20
30
√REACTOR POWER (KW)$^{\frac{1}{2}}$
K&E 20 X 20 TO THE INCH KEUFFEL & ESSER CO. 359-10½G

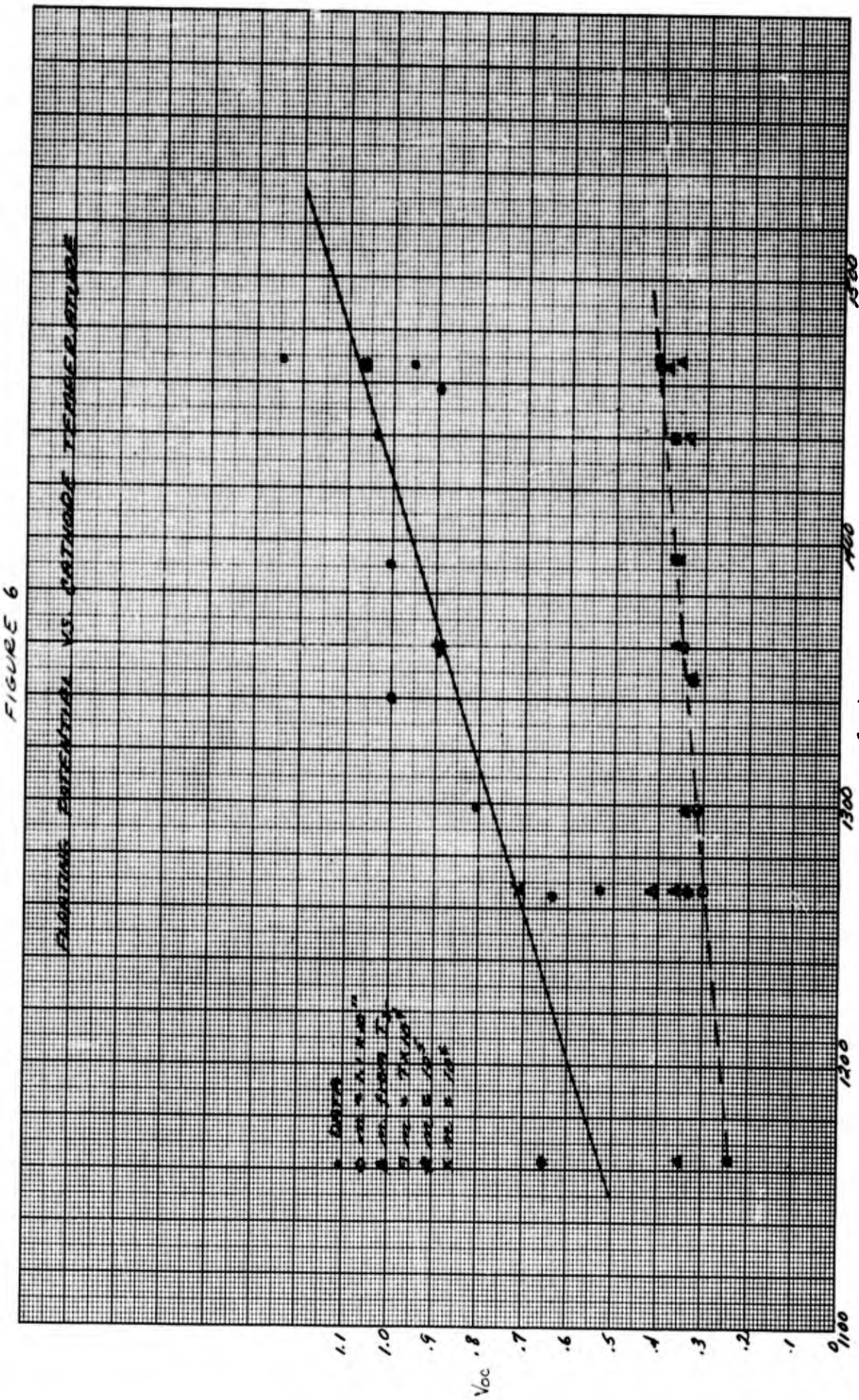
FIGURE 6
FABRITIUS POTENTIAL VS CATHODE TEMPERATURE
Data
1.1
1.0
.9
.8
.7
.6
.5
.4
.3
.2
.1
0
1100
1200
1300
1400
1500
Voc
Tc (°K)

Figure 7

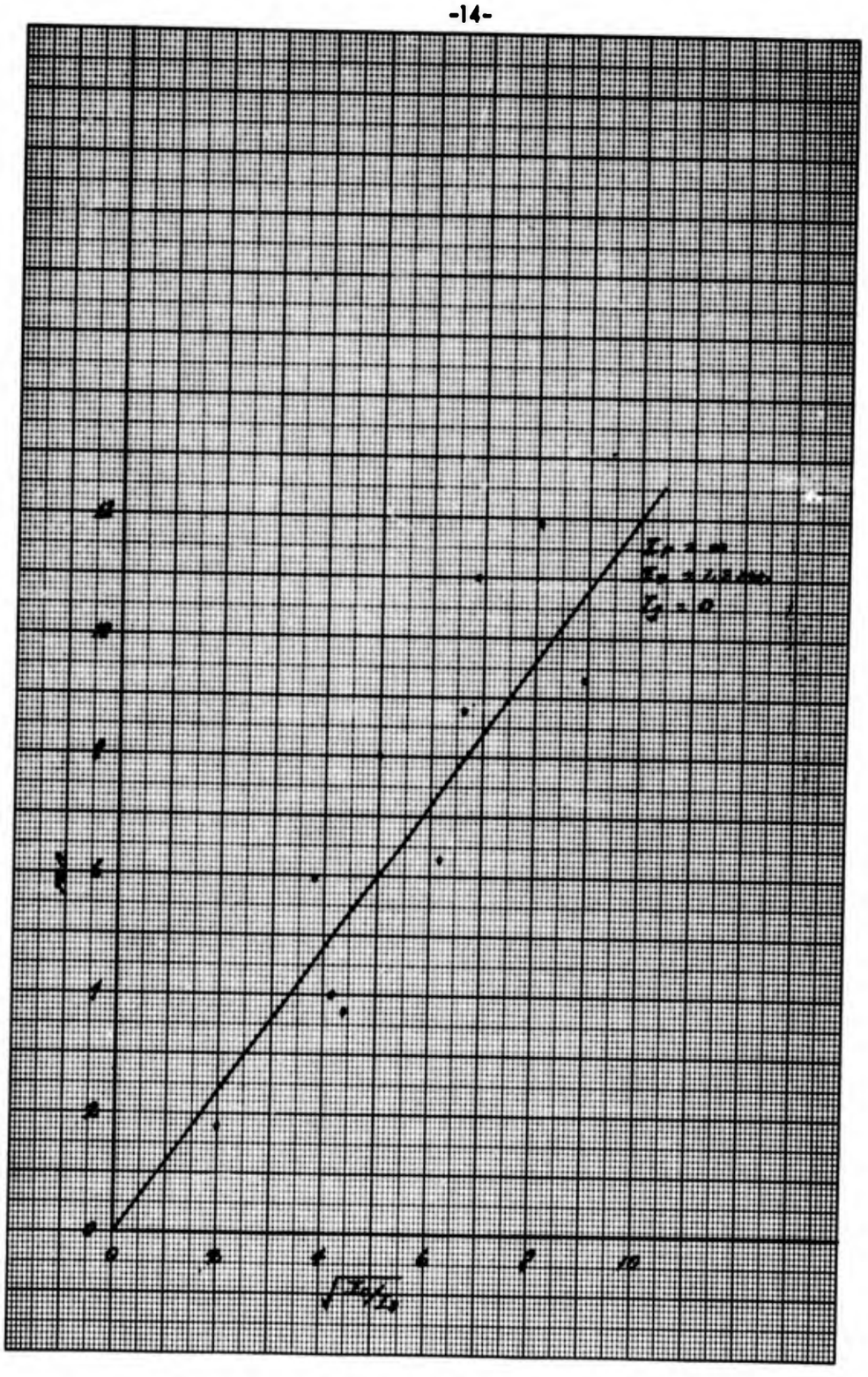

Appendix IV

The preparation of cermet discs that are presently being used in GMR plasma cells are as follows:

A powder mix containing 80 volume per cent UC of 6 w/o carbon and 20 volume per cent niobium are green pressed into 1-inch diameter. The niobium container is coated with carbon by brushing on an Aquadag solution followed by a vacuum drying at 700° F. The green press is then loaded into the carbon-coated niobium can, and pressure bonded for 3 hours at 2600° F under a helium gas pressure of 10,000 psi. After pressure bonding, the cladding is machined to 0.060 in. (minimum) on the bottom and 0.040 in. (minimum) on the diameter. The final dimensions are approximately as sketched below.

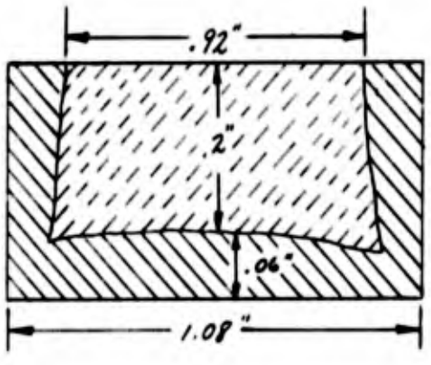

The fuel element is then metallographically polished, examined, and vacuum heated to 3100° F. The sample is then repolished and vacuum heated to 3100° F. The cathode is stored in an argon-filled cotton-packed container.

Calculations by BMI indicate a uranium content of 20.2 gm of U-235. Typical weights are as follows:

Spec. Net Wt.	38.1 gm
(UC + Nb) compact	27.2 gm
UC	23.5 gm
U (total)	22.2 gm
U-235	20.6 gm

Appendix V

I. Introduction

In the conceptual design of this diode (see Fig. #1), three important questions were raised concerning the heat transfer and temperature distributions for the anticipated cathode temperature of 2000° K.

(1) Would the alumina sleeve crack because of severe temperature gradients near the cathode?

(2) Would the temperature at the end of the alumina sleeve be high enough to melt or weaken the metal-to-ceramic braze?

(3) Could the cathode temperature be maintained at 2000° K by a power input of 600 watts or less (600 watts being the maximum power available at the cathode from nuclear considerations of the University of Michigan reactor)?

Calculation of the heat transfer and temperature distributions from radiation theory is extremely difficult, if not impossible, with this complex geometry; hence it was decided to perform preliminary mock-up studies to check the rough calculations and to provide information on the points above.

II. First Mock-up Study

The first mock-up study was designed to provide rough information on temperature distributions along the ceramic sleeve.

A. Apparatus

A schematic diagram of the apparatus is presented in Figure 2. A description of it follows. A laminated tantalum disc 1-1/4" diameter x .100" thick, held at ground potential, was electron bombarded to serve as a heat source at temperatures up to 2000° K. Electron bombardment was accomplished by using a tungsten filament (with a Variac control) tied to the negative side of a variable 2.5 kv D.C. NJE power supply. Concentric with the Ta disc were two Alite (Al_2O_3) cylinders, 3" OD x 9/64" wall x 2-3/4" long, one placed on top of the other and separated by two .060" tungsten rods which supported the Ta disc. Chromel-Alumel thermocouples of .004" wire were fastened to the upper cylinder with Sauereisen cement, as shown in Figure 3, to measure the temperature distribution along the cylinder.

A water-cooled nickel-plated-copper split-ring anode was positioned above the Ta disc. A micrometer adjustment was available to regulate and measure the cathode-anode spacing. The zero spacing was determined electrically by noting a short circuit on a meter installed between the cathode and anode. Other water-cooled heat sinks were: a cylindrical aluminum jacket with a polished reflecting inside surface surrounding the Alite cylinders, and the filament input leads. All water rates were measured by Rotometers and the inlet-outlet temperature differences were measured by Fe-Constantan thermocouples. In this preliminary mock-up study no attempt was made to trap the energy radiating out the open ends of the Alite cylinders. The large CEC bell jar system was used throughout the experiment.

B. Procedure

The variables of the experiment were: the tantalum disc (cathode) temperature, and the cathode-anode (gap) spacing; the top Alite cylinder could be removed to study the effect of heat loss to the aluminum jacket. It was decided to obtain data for three cathode temperatures (maximum of 2000° K) at three gap spacings, and also to obtain some data concerned with the heat loss to the jacket.

The general procedure, once the parameter values were chosen, was to:

(1) Raise the temperature of the Ta disc to the selected value. The input power was regulated to prevent rapid heating and outgassing of the components, since an increased pressure from outgassing often produced an arc at high bombardment voltages. In order to obtain the "true" cathode temperature from the brightness reading, it was necessary to make corrections for the tantalum emissivity and the transmissivities of the glass bell jar and a mirror which were placed in the line of sight.

(2) Obtain the gap spacing by adjusting it to zero spacing and then backing off the prescribed distance.

(3) Adjust water flow rates of anode, jacket and filament leads so that a readable inlet-outlet temperature difference was obtained at steady-state conditions.

(4) Wait until the cylinder thermocouples had reached steady-state values and record data.

C. Results

1. Elimination of Arc Discharges from the Malter Effect

This study was conducted in two parts with slightly different set-ups. In the first set-up the tantalum cylinder shield around the 1/8" cu tubing filament leads was connected electrically to ground. With this set-up, it was found that arc discharges occurred at the higher cathode temperatures where high electron bombardment currents were drawn. Dr. K. H. Kingdon attributed this and corona type discharges observed in previous studies to the "Malter Effect".* In this phenomenon, ions formed in the cell drift toward the negative leads and build up on small non-conducting particles resting on the negative leads. In this manner very high localized fields are built up to initiate discharges from field emission of electrons.

In order to solve this problem, Dr. Kingdon suggested that the tantalum filament lead shield be run at the filament potential. The tantalum shield could be cleaned better than the copper leads, and any surface particles remaining would soon burn off. Therefore, for the second set-up the tantalum filament shield was connected electrically to the filament.

2. Results from First Set-Up

The results from the first set-up are presented in Figure 4. Since these data are also presented graphically with the data of the second set-up, only a brief discussion will be presented here. In Figure 4 the thermocouple temperature is plotted versus the temperature at the edge of the tantalum disc with the thermocouple position as parameter. The total input power is also plotted versus the tantalum disc temperature. Because of the discharges previously discussed, the maximum cathode edge temperature obtained was 2800° F.

Of particular interest in Figure 4 is the indicated temperature at the edge of the Alite cylinder (TC #4) of 970° F at a tantalum disc temperature of 2000° K (3140° F). This is considerably below the maximum operating temperature of 1450° F recommended for the ceramic to metal bond.

3. Results from Second Set-Up

The results from the second set-up are plotted in Figures 5, 6, 7, 8 and 9. Graph 5 is a plot of the total input power necessary to maintain a given cathode temperature, T_c, at various spacings. Graph 6 shows the temperature of thermocouple No. 4 as a function of the cathode temperature at different spacings. (Thermocouple No. 4 was approximately

* L. Malter. Phys.Rev. 50, 48, 1936
Guntherschulze, Zeits. f. Physik, 86, 778, 1933

located at the position of the alumina to metal seal). Graphs 7, 8 and 9 are temperature distribution plots along the cylinder for various cathode temperatures at spacings of~1 mm, 100 mm and ∞ respectively.

The data in Figure 6 indicate that the temperature at the metal to ceramic bond will be tolerable. The high power input (at T_c = 2000° K) of about 900 watt in Figure 5 is attributed to the release of radiant energy from the open ends of the Alite cylinders.

D. Sources of Error

The sources of error in the experiment were:

(1) Optical pyrometry: Beside the usual error from this source, during the data runs at elevated cathode temperatures the hot metal components released surface metal oxides onto the glass bell jar, thus making it difficult to obtain correct cathode temperatures or to duplicate them by optical means.

(2) Emissivity of alumina cylinder: The surface oxides released from the metal components at elevated cathode temperatures were sprayed onto the alumina cylinder causing emissivity changes. The alumina cylinder changed from a white to a grey during the course of the experiment. This, of course, affected the radiation from the cylinder and, thus, the temperature distribution on it.

(3) Thermocouple EMF's: It was noted that while running at elevated cathode temperature, when the bombardment supply was suddenly turned off the thermocouple emf's would suddenly drop several mv. This indicates that during part of the experiment, a portion of the thermocouple emf was caused by electron bombardment.

(4) Thermocouple stability: Prior to Run 59.0, it was noted that thermocouple No. 1 would sometimes read lower than thermocouple No. 2. During Run 59.0, thermocouple No. 1 failed to record. Upon examining the cylinder and thermocouple No. 1, it was found that the thermocouple junction had vanished.

To further improve the accuracy of these heat measurements, which were felt to be most important from the standpoint of ensuring successful operation of the ceramic diode when operated inpile, the following series of experiments were also carried out.

III. Second Mock-up Study

The object of this experiment was to obtain data on heat transfer and temperature distributions for a geometry nearer to that of the proposed diode than the first mock-up.

A. Apparatus

The mock-up of Fig. 10 was constructed. This mock-up differed from that of the first experiment in several significant ways:

(1) Only one alumina cylinder was used to simulate the sleeve.

(2) Tantalum end pieces were included in the mock-up.

(3) A Chromel-Alumel thermocouple was cemented between the end of the sleeve and the tantalum end piece with Pyroceram (#95) cement.

A general description of the mock-up follows, with numbers corresponding to those on Fig. 1.

A laminated tantalum disc (1), 1-1/8" dia. by .100" thick, serving as cathode was Heliarc welded to a tantalum support cylinder (2), a detailed sketch of which is shown in Fig. 11. Another tantalum cylinder with end cap (3), serving as anode for heat transfer purposes, had a 1/8" port (4) through which it was possible to view the cathode and obtain the temperature with an optical pyrometer. The cathode-anode spacing was approximately 3-1/3 mm when the pieces were cold. Concentric with the cathode were the alumina cylinder, 3" OD x 9/64" wall x 2-3/4" long, (5) and an aluminum water-cooled jacket (6) with a polished internal surface. The sleeve and end caps were supported by three evenly spaced alumina rods, (7) 3/16" dia. x 5-1/2" long, which, in turn, were held by an aluminum ring (8) with set screws.

The cathode and support cylinder were held at ground potential. A 10 mil tungsten filament (9) mounted to tantalum strips (11), .020" x .2" x 3", was supplied by a Variac through 1/8" copper tubing (10) and was tied to the negative terminal of a 2.5 KV D.C. supply, thus permitting electron bombardment of the cathode. The filament shield of .005" tantalum (12) was also tied to the negative potential to prevent discharges due to the Malter effect . An insulator (13) connected the filament leads to allow water flow without shorting out the filament. The mock-up rested on a piece of AlSiMag ceramic (14).

A Chromel-Alumel thermocouple of .004" wire (15) was installed between the sleeve and lower end cap with Pyroceram (#95) cement, which was placed only at the thermocouple position in order that the tantalum end cap might expand without undue stress. A thermocouple of the same type was placed at the top of the sleeve (16) but was not cemented. Thermocouple positions on the sleeve and in the water cooling circuit are shown in Fig. 12.

B. Procedure

The procedure, after outgassing and pumping the system down, was to bring the cathode to a temperature of 2000° K, allow the system to reach steady state, and then to record pertinent data.

C. Results

The pyrometer temperatures were corrected for the tantalum emissivity, the bell jar transmittance, and the mirror reflection (assumed equal to the bell jar transmittance) to yield:

$$T_{Cathode}\ (corrected) = 2000° K$$

$$T_{Anode}\ (corrected) = 1230° K$$

The sum of electron bombardment and filament power gives the total input power:

$$P_{Total}\ (in) = 545 \text{ watts}$$

The heat conducted away by the jacket coolant was negligible, but the heat captured by the filament leads was

$$P_{Filament}(out) = 84 \text{ watts}$$

The main results are:

(1) The power input to the cathode, i.e. the total input power corrected for heat loss to the filament leads, required to maintain it at 2000° K, was found to be approximately 460 watts. From the first experiment it was found that an average (corrected) power input of 840 watts to the cathode was needed to maintain it at an average temperature of 2050° K with a gap spacing

of approximately 1 mm. Thus, the conduction along and radiation from the tantalum end plates is 380 watts less than the radiation from the hot cathode to the environment as occurred in the first experiments.

(2) With the cathode at 2000° K, the temperature at the Pyroceramic joint was 1323° F, while the temperature at the uncemented joint at the anode end of the sleeve was 1026° F.

D. Error Sources

It is believed that the errors for this experiment, although identical with those of the first experiment, were mitigated by using an extremely clean bell jar and optical system, and by cleaning the tantalum pieces of oxides according to RLE specifications. The experiment was performed using the Alite sleeve of the first experiment, and a slight emf due to electron bombardment was observed for the sleeve thermocouples.

IV. Conclusions

While the results are within the desired ranges, it is felt that more favorable values for the input power and the joint temperature could be achieved in the Second Reactor Demonstration Diode for the following reasons:

(1) The end caps will be brazed to the sleeve around the circumference of the cylinder so that a larger area than that of this experiment will be available for heat conduction. Thus, the temperature at the joint will be less than measured during the present experiment.

(2) The end caps themselves will have a longer conduction path and a larger radiation area than those used in the present experiment (because of bellows-type geometry). This will further reduce the temperature at the joint.

(3) The emissivity of the clean sleeve will be less than that of the one used during the present experiment. This will reduce the required power but may increase the joint temperature.

(4) Due to problems of alignment, it was impossible to capture all of the radiation from the back of the end cap cylinders. Thus, the experimental value for power input to the cathode is larger than the actual value, and it is hoped that a 2000° K cathode temperature may be maintained with less power.

(5) If the reactor diode contains water-cooled leads to filaments within the cathode and anode support cylinders, these will provide additional heat sinks.

Figure 1

Proposed Second Reactor Demonstration Diode

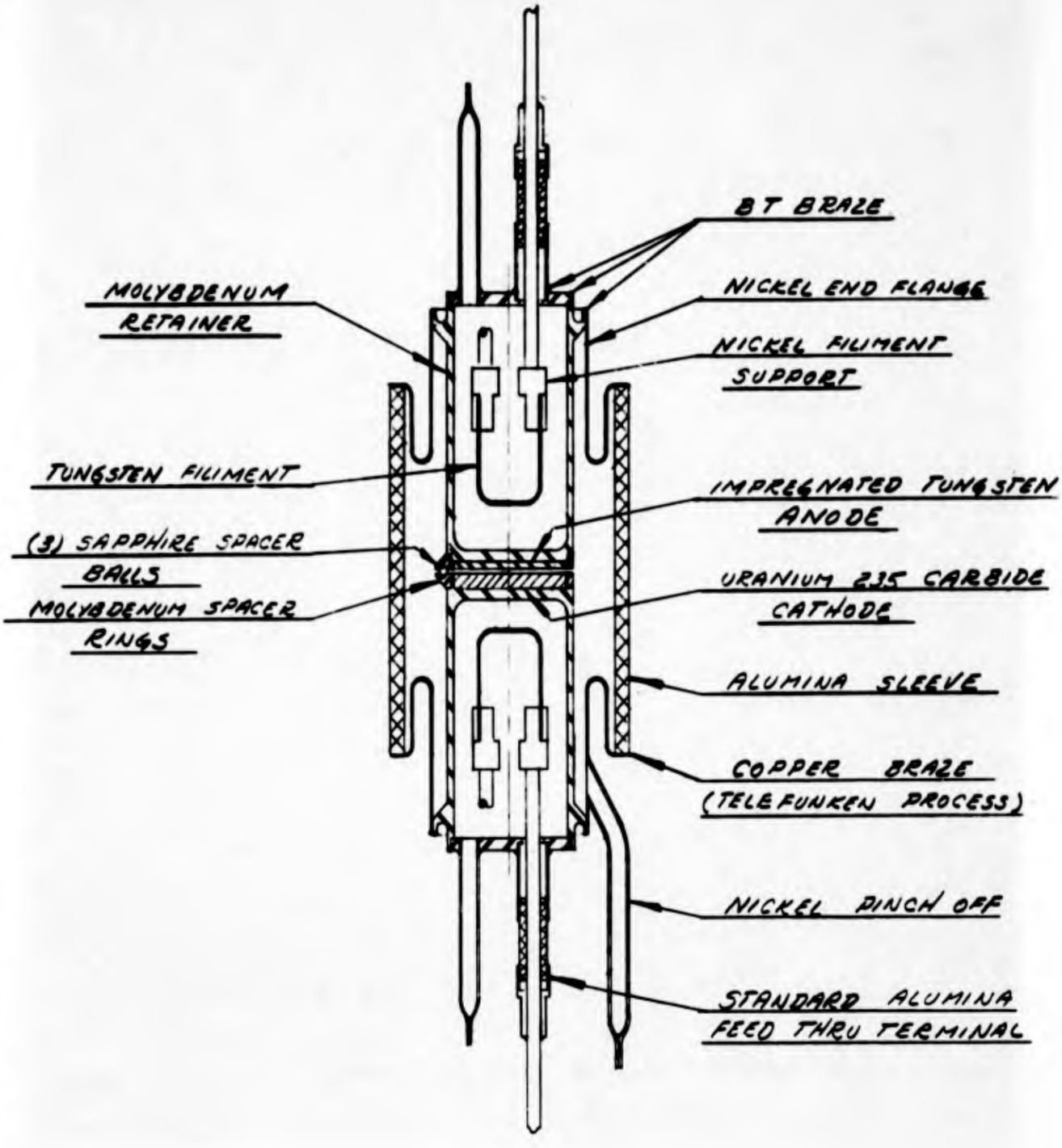

Figure 2
Preliminary Mock-up Study of
Second Reactor Demonstration Diode

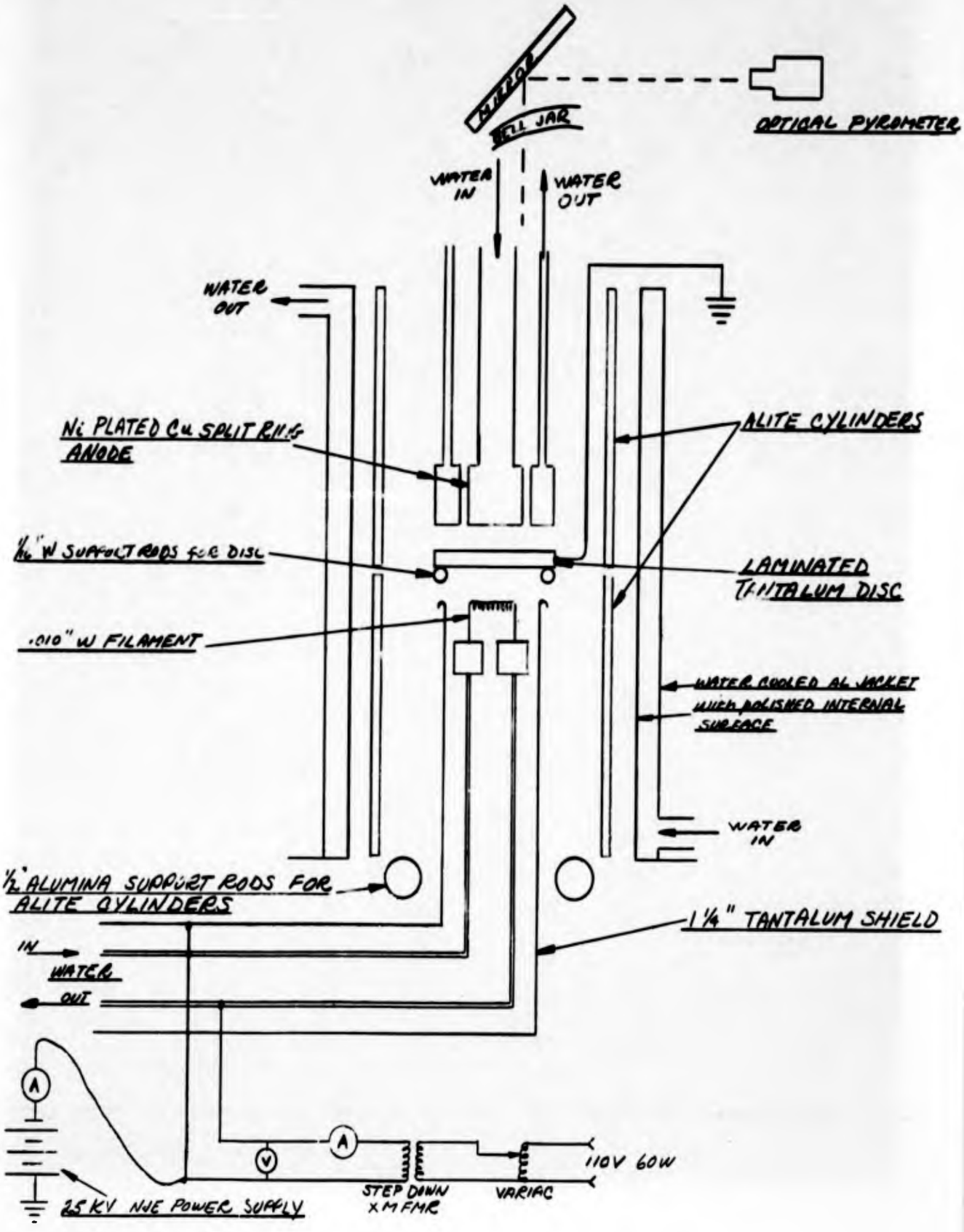

Figure 3
Thermocouple Position on Alite Cylinder

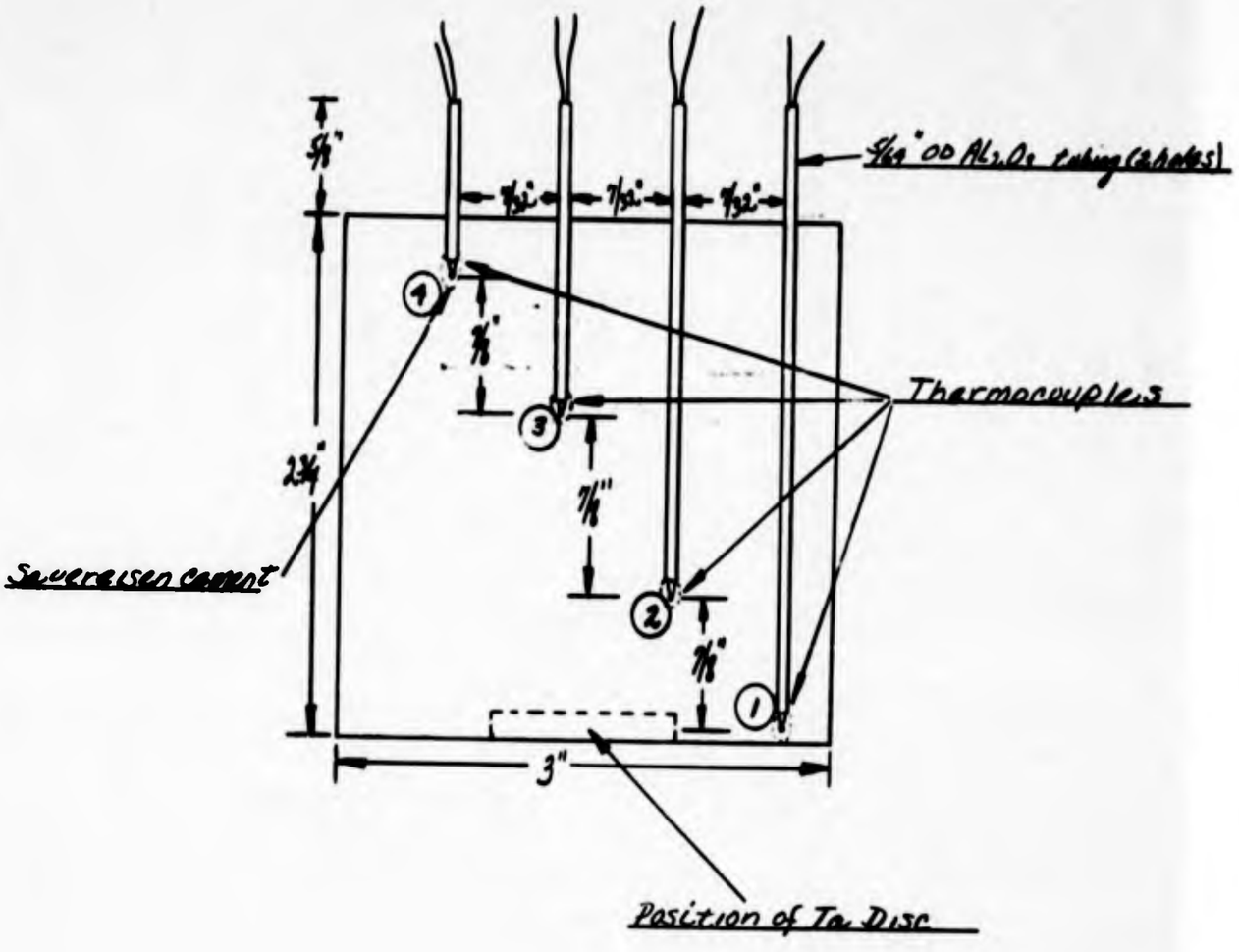

K·E 10 X 10 TO THE CM. 359-14 KEUFFEL & ESSER CO.

Figure 4

TEMPERATURE DISTRIBUTION IN AN ALUMINA CYLINDER

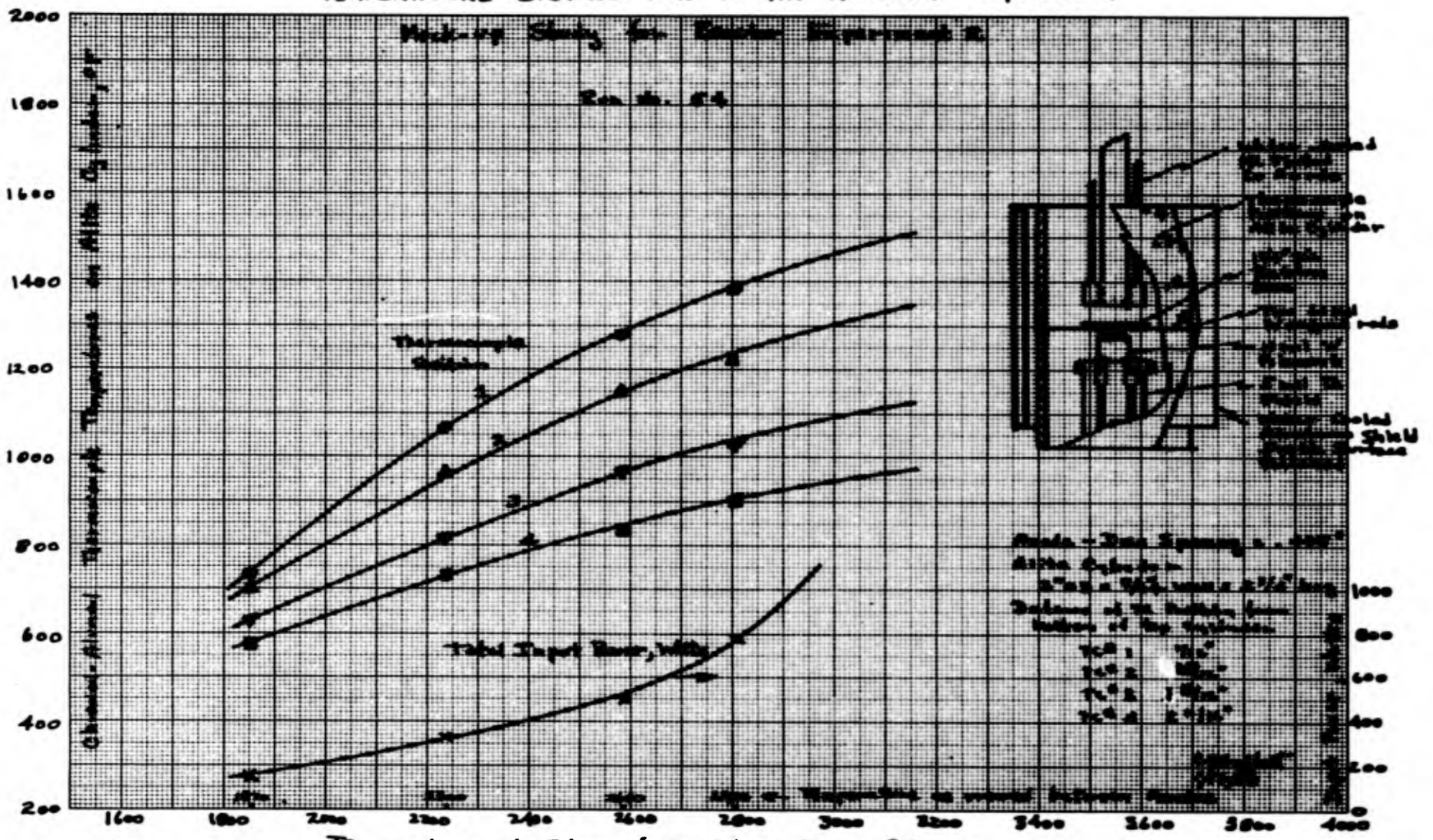

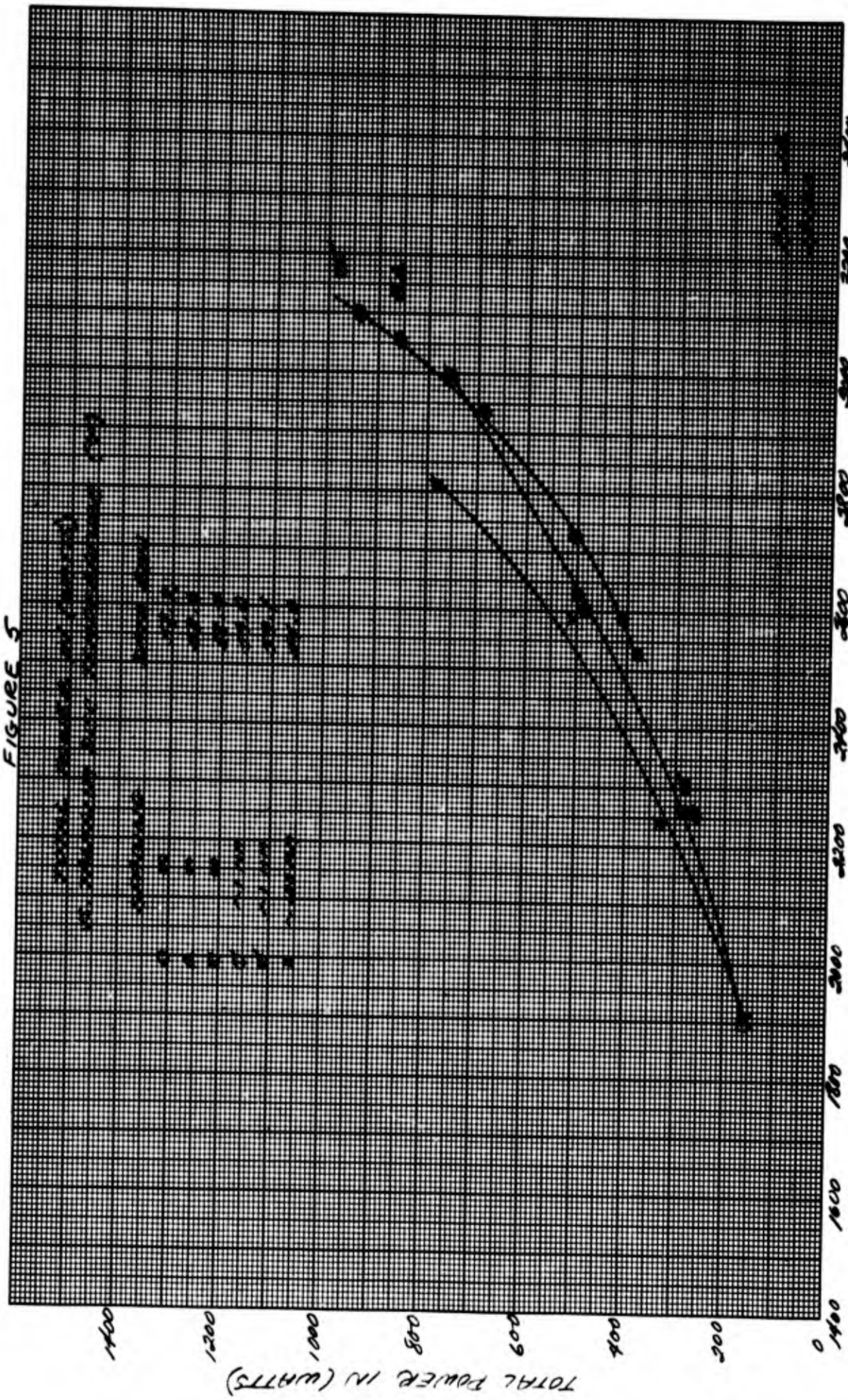

FIGURE 5

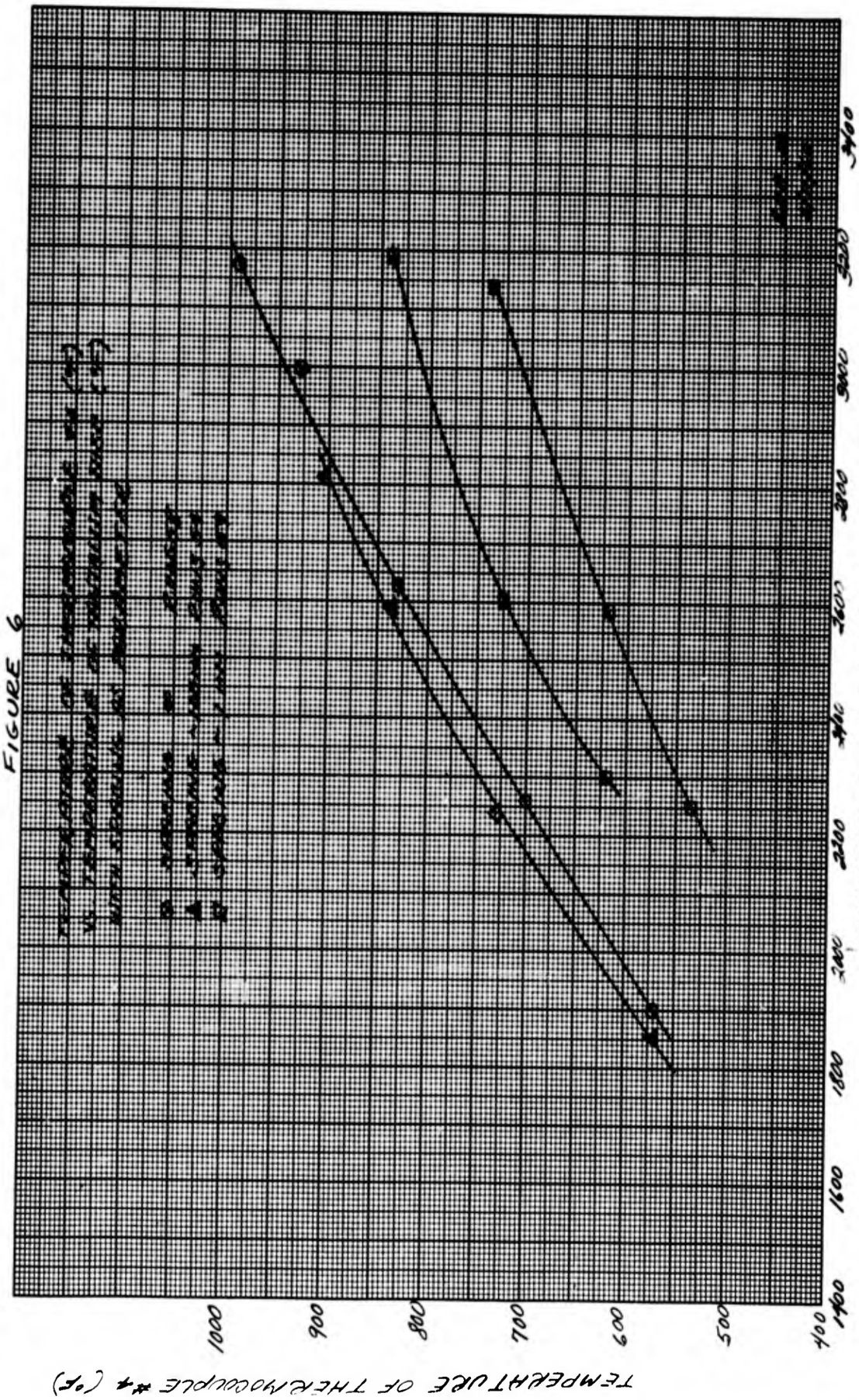
TEMPERATURE OF THERMOCOUPLE #4 (°F)
1000
900
800
700
600
500
400
1400
1600
1800
2000
2200
2400
2600
2800
3000
3200
3400
TEMPERATURE OF TANTALUM DISC (°F)

FIGURE 6

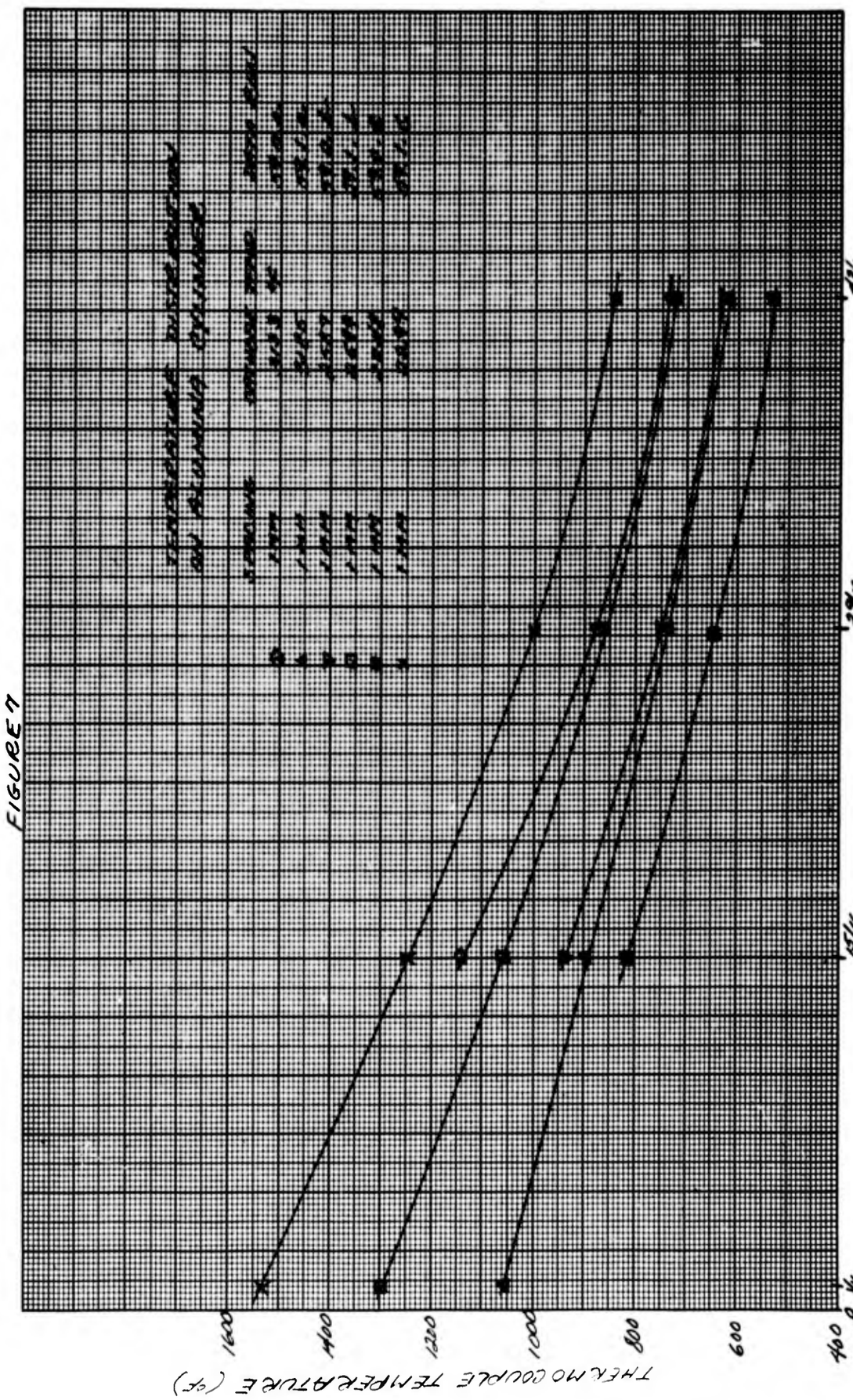
FIGURE 7
THERMOCOUPLE TEMPERATURE (°F)
1600
1400
1200
1000
800
600
400
0 in
5/16
2 3/16
DISTANCE ALONG CYLINDER (in)

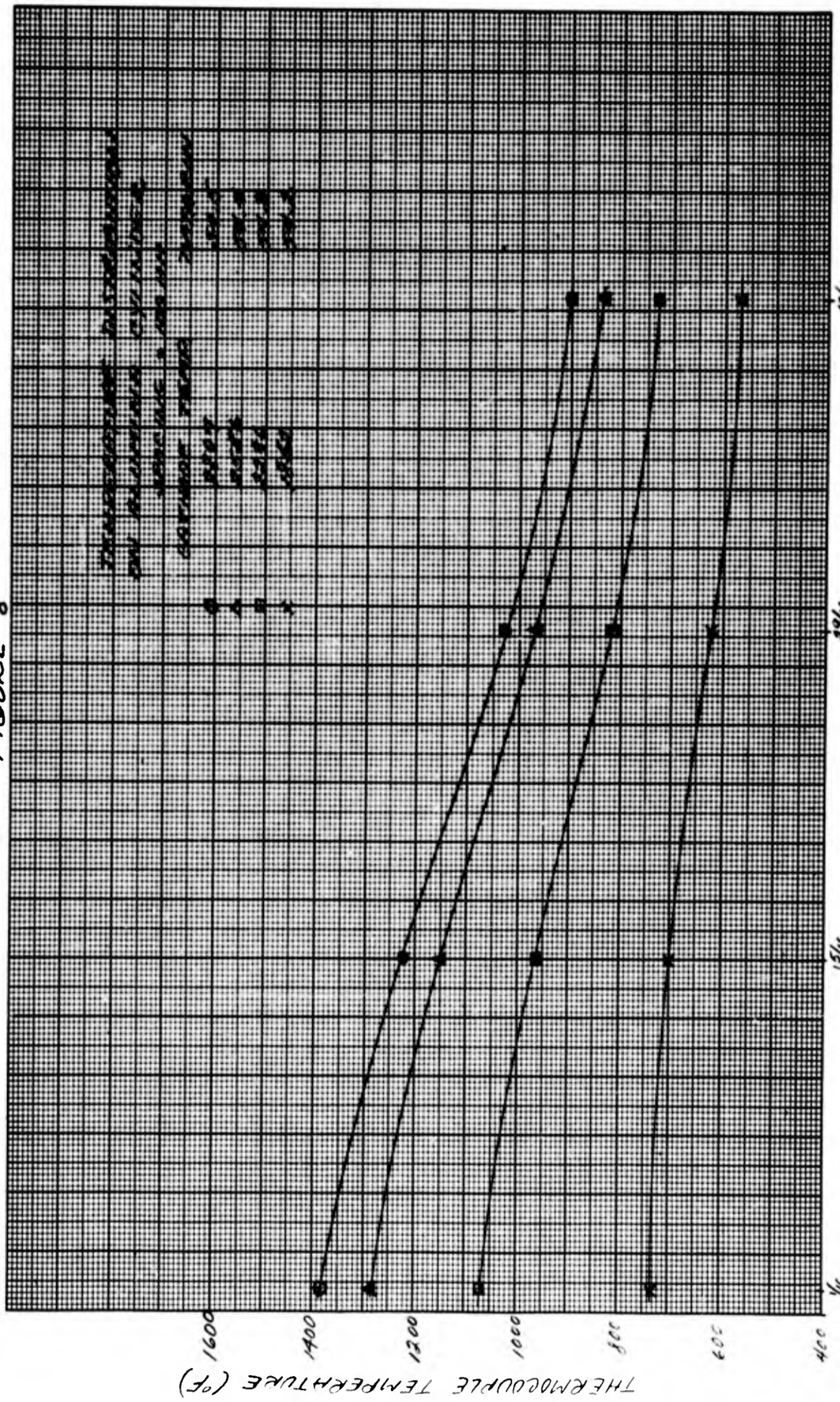
THERMOCOUPLE TEMPERATURE (°F)
1600
1400
1200
1000
800
600
400
1/16
5/16
9/16
13/16
DISTANCE ALONG CYLINDER (IN)

FIGURE 8

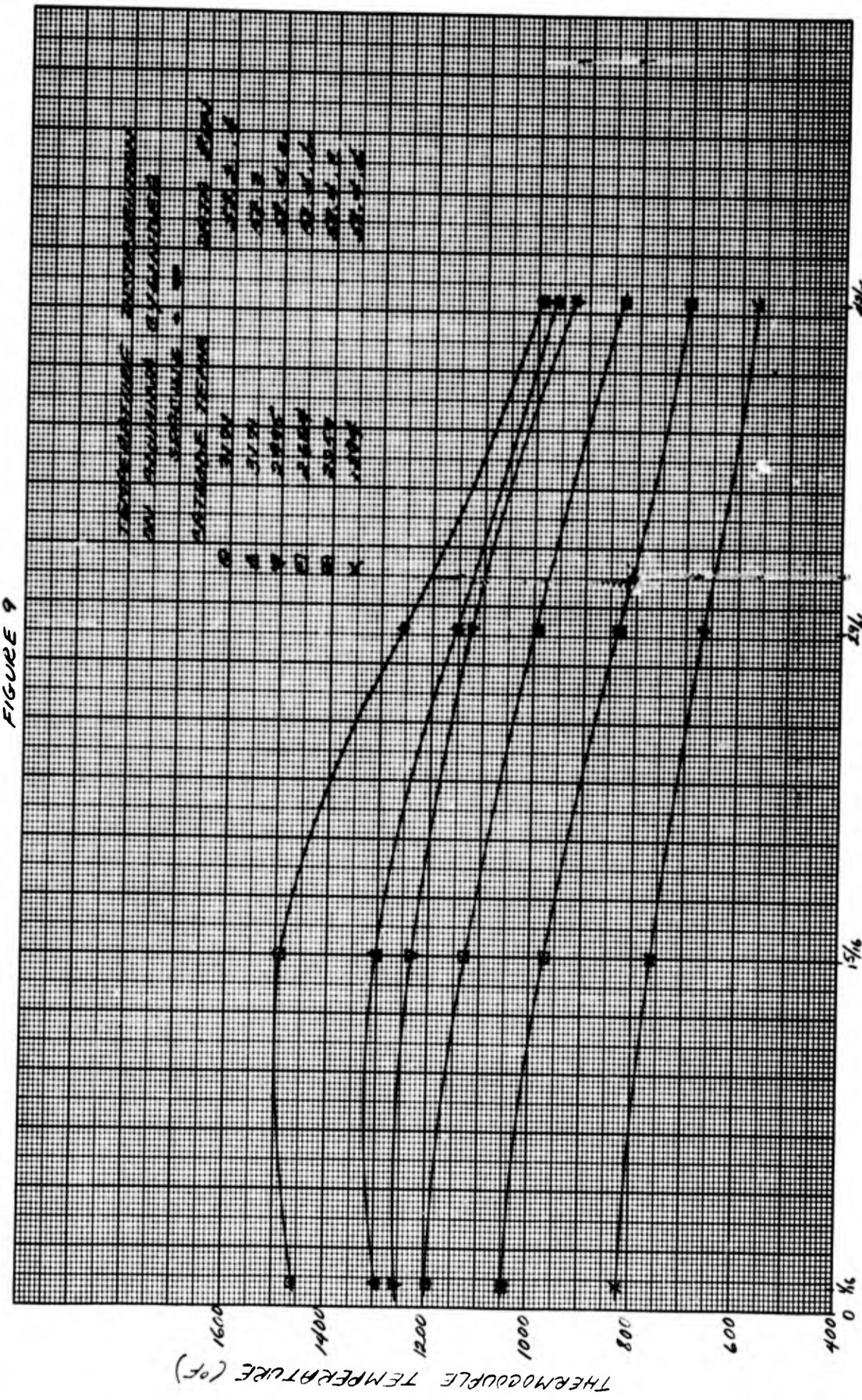
THERMOCOUPLE TEMPERATURE (°F)
1600
1400
1200
1000
800
600
400
0 in
1/16
1/8
3/16
DISTANCE ALONG CYLINDER (IN)

FIGURE 9

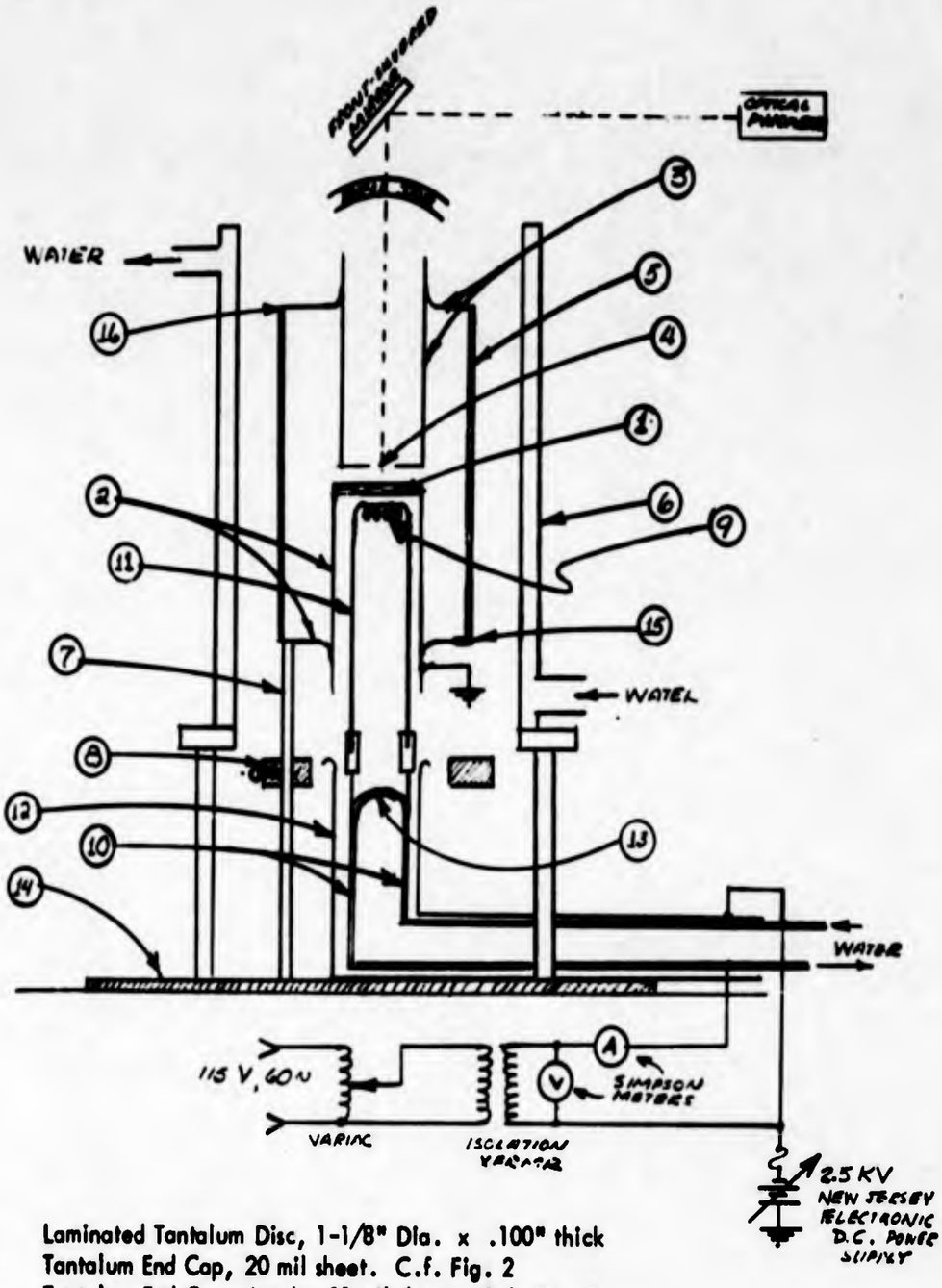

(1) Laminated Tantalum Disc, 1-1/8" Dia. x .100" thick
(2) Tantalum End Cap, 20 mil sheet. C.f. Fig. 2
(3) Tantalum End Cap, Anode, 20 mil sheet. C.f. Fig. 2
(4) 1/8" Dia. Viewing Port
(5) Alite (Al_2O_3) Cylinder, 3" OD x 9/64" Wall x 2-3/4" long
(6) Aluminum Jacket, Polished Internal Surface, 3-1/2" ID x 5-1/2" long
(7) Alumina (Al_2O_3). Support Rods, 3/16" Dia. x 5-1/2"
(8) Aluminum Retaining Ring
(9) Tungsten Filament, 10 mil wire
(10) Copper Tubing, 1/8" OD
(11) Tantalum Strips, .020" x .2" x 3"
(12) Tantalum Filament Shield, 5 mil sheet
(13) Polyflow Insulator
(14) AlSiMag
(15) Chromel-Alumel (.004" wire) Thermocouple, Positioned by Pyroceram(®95) Cement
(16) Chromel-Alumel (.004" wire) Thermocouple, Uncemented Position

Fig. 10. Schematic: Mockup for Proposed Second Reactor Demonstration Diode

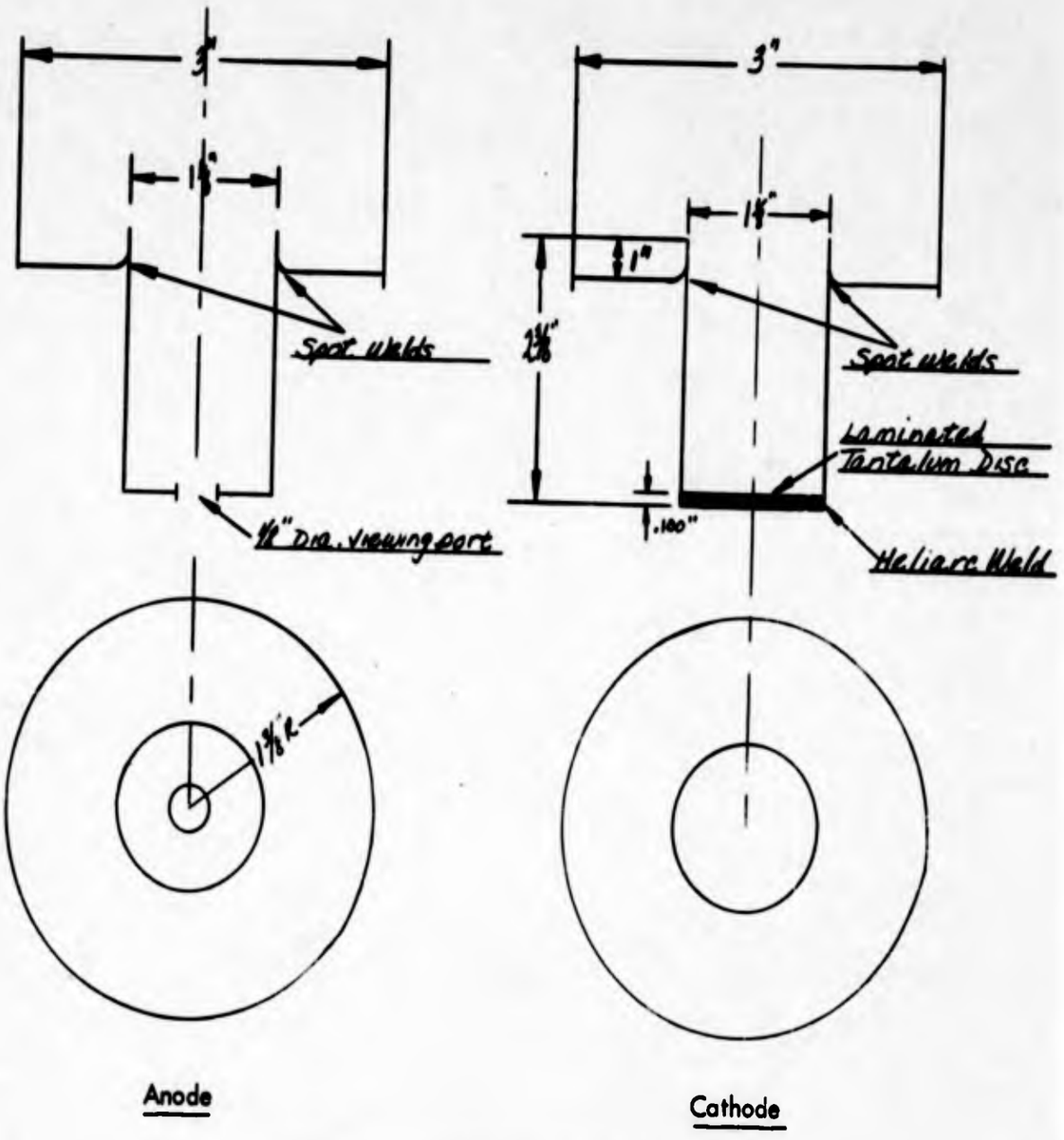

Material: .020" Tantalum Sheet

Fig. 11. Tantalum End Caps: Anode and Cathode: Mockup for Proposed Second Reactor Demonstration Diode

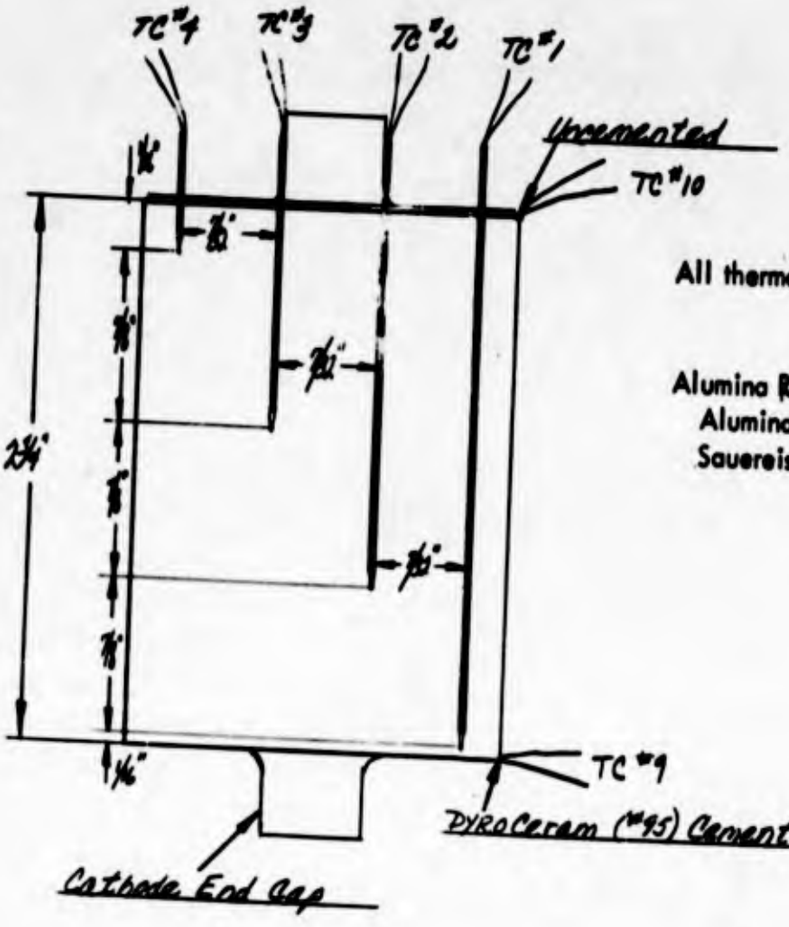

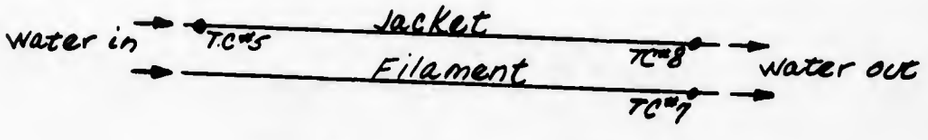

Thermocouples: Iron-Constantan

Fig. 12. Thermocouple Positions: Sleeve and Water Circuit: Mockup for Proposed Second Reactor Demonstration Diode

Appendix VI

One of the problems to be considered in selecting materials for use in low pressure plasma diode experiments is the interaction between the various construction materials and their environment at their operating temperature. Materials that exhibit high vapor pressures or high dissociation pressures may greatly affect the characteristics of the plasma cell. Also reactions between adjoining materials may produce new materials that have poor temperature characteristics. In order to aid in the evaluation and selection of the various plasma diode construction materials, the following thermochemical equilibrium calculations and data are presented.

Chemical Reaction Equilibrium

In reviewing the literature for chemical equilibrium data, one may discover that the data are presented in a variety of different ways. In order to assist in the evaluation of the data, the following thermodynamic relationships are presented.

Knowing the equilibrium states for any chemical system as a function of the three independent variables -- pressure, temperature, and initial composition -- one can predict the equilibrium or maximum possible degree of conversion. The maximum degree of conversion will be attained only when the system has reached equilibrium, which will require an infinite amount of time. Nevertheless, this equilibrium point is of great practical importance since it establishes an absolute limit beyond which the reaction cannot go.

For condensed systems, and particularly at elevated temperatures, it is convenient to express thermochemical functions in terms of temperature and pressure. In general,

a chemical reaction involves changes in heat content and in the entropy of the system. Thus it is convenient to define another quantity, F, the free energy, such that

$$F_T = H_T - TS_T \tag{1}$$

or for any isothermal process

$$\Delta F_T = \Delta H_T - T\Delta S_T \tag{1a}$$

For a given chemical reaction

$$\Delta F_T = \Sigma F_T \text{ (products)} - \Sigma F_T \text{ (reactants)} \tag{2}$$

where ΔF_T is a measure of the tendency for the reaction to occur at temperature, T. If ΔF is negative, the reaction will tend to proceed to the right as written. If ΔF is positive, the reaction tends to proceed to the left as written. If $\Delta F = 0$, there is no tendency to react and the system is in equilibrium.

Absolute values of F or of ΔF are not listed, but a free energy, F°, may be defined relative to some standard or reference state. Normally this standard state is taken to be the pure solid, pure liquid, or pure gas at one atmosphere pressure and at the temperature in which we are interested. Thus $F - F^\circ$ is a measure of the reacting tendency of a substance. We may now introduce another quantity, the activity, α defined by

$$F_T - F_T^\circ = RT \ln \alpha \tag{3}$$

For the standard state, the activity of a substance is unity ($\alpha^\circ = 1$) thus $\ln \alpha^\circ = 0$.

If we now consider a reaction of the type

$$wA + xB = yC + zD$$

the change in free energy at a given temperature becomes

$$\Delta F_T = yF_C + zF_D - (wF_A + xF_B) \tag{4a}$$

Now if the reactants are in their standard states and react completely to give the products in their standard states, the free energy change becomes

$$\Delta F_T^\circ = y F_C^\circ + z F_D^\circ - (w F_A^\circ + x F_B^\circ) \quad (4b)$$

Subtracting reaction (4b) from (4a) we get

$$\Delta F_T - \Delta F_T^\circ = y(F_C - F_C^\circ) + z(F_D - F_D^\circ) - w(F_A - F_A^\circ) - x(F_B - F_B^\circ) \quad (4c)$$

or

$$\Delta F_T - \Delta F_T^\circ = RT \ln \frac{(\alpha_C)^y (\alpha_D)^z}{(\alpha_A)^w (\alpha_B)^x} \quad (4d)$$

At equilibrium ΔF will be equal to zero, thus equation (4d) reduces to the form

$$\Delta F_T^\circ = -RT \ln K \quad (5)$$

where K is called the equilibrium constant and is equal to the equation

$$K = \frac{(\alpha_C)^y (\alpha_D)^z}{(\alpha_A)^w (\alpha_B)^x} \quad (6)$$

In studying the equilibrium yield of a reaction, the first step is to evaluate the equilibrium constant as a function of temperature. This can be accomplished by utilizing thermodynamic data only if the heat of reaction and entropy of the reaction at one temperature and complete heat-capacity data are available. Thus by the relationship

$$\Delta F_T^\circ = \Delta H_T^\circ - T \Delta S_T^\circ \quad (7)$$

ΔF° and therefore K can be calculated if ΔH_T° and ΔS_T° can be evaluated.

If we know the heat of a reaction at some reference temperature, ΔH_{ref}°, we can calculate the heat of reaction at any other desired temperature, ΔH_T°, provided that we know the heat capacities of the reactants and products. This can be accomplished as illustrated in Figure 1.

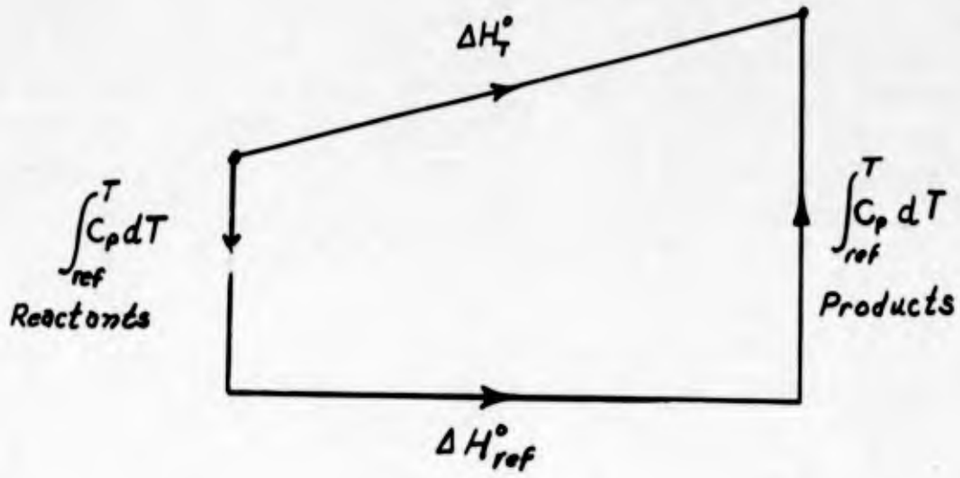

Figure 1

$$\text{Thus } \Delta H_T^\circ = \Delta H_{ref}^\circ + \int_{ref}^{T} \Delta C_p \, dT \qquad (8)$$

In a like manner, the change in entropy can be evaluated by

$$\Delta S_T^\circ = \Delta S_{ref}^\circ + \int_{ref}^{T} \Delta C_p \frac{dT}{T} \qquad (9)$$

where $\Delta C_p = \sum C_p \text{ (products)} - \sum C_p \text{ (reactants)}$

Equation (7) would form a straight line (plotting ΔF_T° against T) if ΔH_T° and ΔS_{ref}° were constant. In many cases their variation with temperature is small enough to allow a straight line plot using average values of ΔH_T° and ΔS_T° which is very useful for most estimating purposes. The assumptions of constant ΔH_T° and ΔS_T° is equivalent to assuming that the total heat capacity of the products of the reaction equals that of the initial reactants, i.e. $\Delta C_p = 0$. This assumption is surprisingly good in a great many cases. Now applying the above assumption to equation (5), we get

$$\ln K = -\frac{\Delta H_{ref}^\circ}{RT} + \frac{\Delta S_{ref}^\circ}{R} \qquad (10)$$

so that a plot of log K as a function of 1/T approximates a straight line.

In cases where complete heat-capacity and entropy data are not available, equations (7) and (10) are presented as

$$\Delta F_T^\circ = \Delta H^\circ_{ref} + IT \tag{11}$$

and

$$\ln K = -\frac{\Delta H^\circ_{ref}}{RT} + C \tag{12}$$

respectively, where I and C are constants whose values are determined from one known value of ΔF_T° and K.

If ΔC_p for a given reaction is found to be constant and independent of temperature, the application of equations (8) and (9) to equation (7) results in the following:

$$\Delta F_T^\circ = (\Delta H^\circ_{ref} - \Delta C_p T_{ref}) - \Delta C_p T \ln T + \left[\Delta C_p (1 + \ln T_{ref}) - \Delta S^\circ_{ref}\right] T \tag{13}$$

In terms of the equilibrium constant, equation (13) reduces to the form

$$\ln K = -\frac{A}{T} + B \ln T + C \tag{14}$$

The above discussion presents the standard approach for calculating thermodynamic equilibria utilizing standard heats and free energies of formation at a reference temperature usually picked at 25 degrees C along with absolute entropies and heat-capacity equations. Another approach used in thermochemical calculations is the utilization of a free-energy-function. The free-energy-function is related to the thermodynamic equation (7) as follows:

$$\text{fef} = \left(\frac{F_T - H_{ref}}{T}\right) = -S_T + \left(\frac{H_T - H_{ref}}{T}\right) \tag{15}$$

where fef = free-energy-function. The change of the free-energy-function, Δfef, at a temperature T is defined as

$$\Delta \text{fef} = \Delta(\text{fef})_{\text{products}} - \Sigma (\text{fef})_{\text{reactants}} \tag{16}$$

and

$$\Delta \text{fef}_T = \frac{\Delta F_T}{T} - \frac{\Delta H_{ref}}{T} \tag{17}$$

If one can obtain $\Delta f e f_T$ from tables, he can make an independent evaluation of the heat of reaction at the reference temperature and thus will have a means for calculating the change in free energy for the reaction in question. The data for free-energy-functions are usually presented at one of two reference temperatures. $(F_T - H_o)/T$ is more easily calculated for gases where $(F_T - H_{298})/T$ is easier to use with calorimetric heats of reaction which are usually measured at room temperature, 298° K. Conversion between these two reference temperatures is a common procedure and requires knowledge only of the relationship $(H_{298} - H_o)$, thus

$$\left(\frac{F_T - H_{298}}{T}\right) + \left(\frac{H_{298} - H_o}{T}\right) = \left(\frac{F_T - H_o}{T}\right) \qquad (18)$$

Some of the reactions encountered may have one or more of the components in the gaseous state. At elevated temperatures and at pressures less than a few atmospheres, gases follow the ideal gas law closely, thus the activity of the gas can be approximated by

$$\alpha = \frac{p}{p_o} \qquad (19)$$

where p is the partial pressure of the gas in atmospheres and p_o is the standard state pressure, namely 1 atmosphere. In vapor pressure calculations where a solid is in equilibrium with its vapor, i.e. $M_{(s)} = M_{(v)}$, the equilibrium constant is equal to the vapor pressure expressed in atmospheres, thus equation (12) would become

$$\ln p = -\frac{\Delta H^\circ_{ref}}{RT} + C \qquad (20)$$

The relationship between vapor pressure and temperature is usually derived from the well-known Clausium-Clapeyron equation

$$\frac{dp}{dt} = \frac{\Delta H_v}{T \Delta V} \qquad (21)$$

An approximate solution of this equation is

$$\ln p = -\frac{A}{T} + B \qquad (22)$$

where A and B are arbitrary constants. Many times, vapor-pressure data are more accurately represented in terms of the free energy of vaporization by

$$\ln p = -\frac{\Delta F_v^\circ}{RT} \qquad (23)$$

It should be noted that equation (23) is very similar to equation (20) depending upon the assumption used in obtaining ΔH_T° and ΔS_T° in the evaluation of ΔF_v°.

Data

Presented in Figure 1 are the free energies of formation and free energies of vaporization of a few materials that have possible application in the plasma diode. The examples presented below show how the free energies listed in Figure 1 can be used to calculate vapor pressure, dissociation pressure and free energy changes in chemical reactions.

Example 1

Calculate the vapor pressure of uranium at 1000° K.

From Figure 1

$$U_s = U_v - \Delta F_v^\circ$$

where $-\Delta F_v^\circ = 71{,}000$ cal/mole at 1000° K

Then $\ln p = -\frac{\Delta F_v^\circ}{RT} = -35.5$

so $p = 3.1 \times 10^{-16}$ atm = $\underline{2.3 \times 10^{-13}\ \text{mm of Hg}}$

Example 2

Calculate the oxygen pressure due to the dissociation of Al_2O_3 at 1000° K.

From Figure 1

$$\frac{2}{3} Al_2O_3 = \frac{4}{3} Al + O_2 \quad - \Delta F^\circ$$

where $= \Delta F^\circ$ - 219,000 cal/mole at 1000° K

Then $\ln p = -110$

so $p = 1.6 \times 10^{-48}$ atm = $\underline{1.2 \times 10^{-45}}$ mm of Hg

Example 3

Calculate the free energy for the chemical reaction between UC and Ta at 2000° K.

$$\begin{array}{r} Ta + C = TaC \quad - 32,000 \text{ cal/mole} \\ \underline{UC = U + C \quad + 10,000 \text{ cal/mole}} \\ Ta + UC = TaC + U - 22,000 \text{ cal/mole} \end{array}$$

Thus the free energy of this reaction indicates that the reaction will proceed to the right with the formation of TaC and free U. This is not the full story, however, for now the free uranium may alloy with any free tantalum thus making the reaction proceed further to the right than indicated. But in any event, it can be said that UC will react with Ta at 2000° K to form free uranium.

Appendix VI

Figure 1

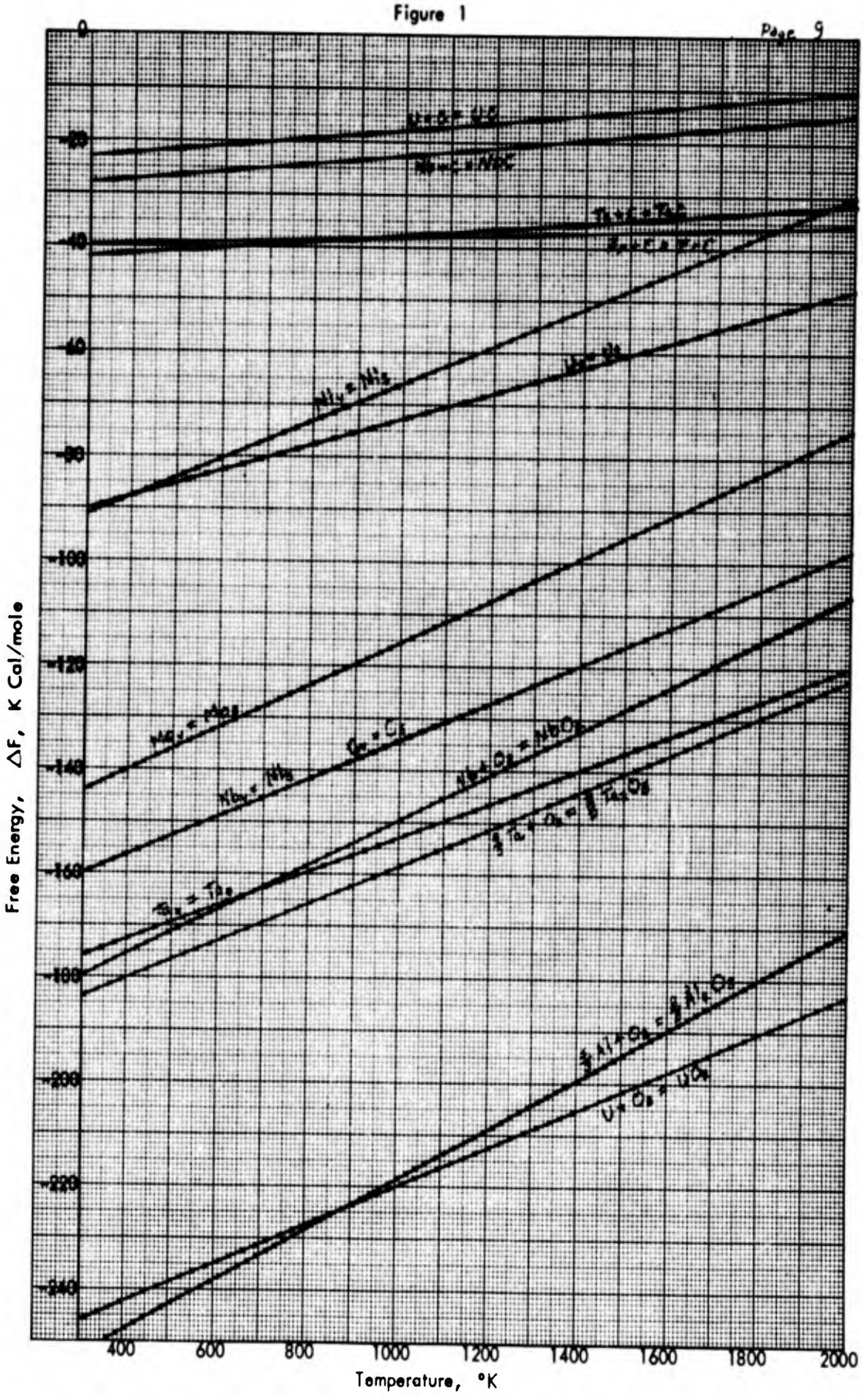

Appendix

Cesium Diode Oscillations

Some preliminary experiments have been carried out on cesium containing diodes. Particularly, the question of plasma oscillations have been studied. Recent experiments in other laboratories have indicated that the efficiency and frequency of oscillation of a cesium diode vary with the emitter-collector spacing.

In particular, the efficiency, defined as the ratio of the measured maximum output power to the input power, corrected for lead loss, has been observed to increase with decreased emitter-collector spacing, and oscillation frequency has been found to increase with decreased spacing. To check out these observations with cylindrical geometry and to obtain more data on the characteristics of cesium diodes, it was decided to construct a triple cesium diode with anode diameters of 0.102 in, 0.218 in, and 0.437 in. See Figs. 1a and 1b.

Each diode has a 10 mil thoriated tungsten filament (about 1 in long) which serves as a cathode surrounded by a cylindrical molybdenum anode 0.5 in long. The filaments are separated and can be heated one at a time, but the anodes are common, being machined in a single molybdenum block. Measurements have been made of the effect of varying bath temperature, filament temperature and the anode diameter on the efficiency, frequencies, and waveforms of the oscillations, and the I-V characteristics. The results of this work are presented here and discussed.

Tube Fabrication and Operation

The molybdenum anode was hydrogen fired prior to assembly on the tube stem, and the thoriated tungsten cleaned and straightened. The filaments are spotted to the molybdenum rod supports and the anode is held mechanically (Fig. 1b). A nickel wire spotted to the anode serves as one leg of a Ni-Mo thermocouple where the Mo leg is one of the anode support rods. The glass bulb is Nonex. The tube was pumped down to $< 10^{-8}$ mm after bakeout at 450° C and after induction outgassing the anode. The Th-W filaments were then activated according to the schedule outlined by Kohl. After seal-off, cesium was released by flashing cesium chromate-silicon getter pellets.

The filament is directly heated by a 60 cycle half wave rectified power supply. Measurement of voltage and current is made during the heating cycle off time to eliminate voltage gradients along the filament.

Measurements

Current-voltage characteristics were measured at various filament and bath temperatures. This operation requires a modified Tektronix 531 scope together with a blanking circuit which, except for one point on the I(t) and V(t) curves, blanks out the whole curve. The I-V characteristic is swept out by varying the load resistor. A typical I-V characteristic is shown in Fig. 2. The region below the knee of the curve that exhibits Lissajou figures indicates a region of oscillation.

The actual experimental set-up used to determine the characteristics is shown in Fig. 3. The TR-10 solid state analog computer was utilized to locate and measure the maximum instantaneous power output point. A block diagram for this set-up is shown in Fig. 4. The TR-10 solid state analog computer multiplies the current and voltage to give the instantaneous power output which, along with the voltage and current, is displayed simultaneously on the Tektronix 555 Scope. By varying the load resistor, R_l, we can easily zero in on the maximum power point. Fig. 5a shows the physical arrangement for these measurements and Fig. 5b shows typical voltage, current and power traces on the Tektronix.

Frequency and waveform of the oscillation at various filament and bath temperatures were observed. The Tektronix 555 scope is ideal for making this measurement because it can pick out any part of the oscillation and display it on a magnified time scale.

In all of the above measurements the power input to the filament is monitored with a Weston 310 wattmeter, which reads both the power dissipated in the wires connecting the wattmeter to the filament, and the actual power dissipated in the filament. To get the actual filament power, it is necessary to subtract from the wattmeter reading the power dissipated in the lead wires.

The filament temperature is determined with an optical pyrometer (L&N), and the bath temperature is controlled by the Capacitrol temperature controller which operated the oven housing the cesium diode. The anode temperature was monitored by a Ta-Mo thermocouple attached to the anode.

Diode Efficiency

The maximum diode efficiency is plotted as a function of cathode input power and bath temperature in Figs. 6, 7 and 8 for the small, medium and large anode diodes respectively. The data of Figs. 7 and 8 do not show as marked a sensitivity to T_b as does that in Fig. 6. These measurements were made using the analog computer circuit of Fig. 4. Power to maintain bath temperature was neglected in this computation. The highest efficiency was measured for the small anode and is 7.5% for T_b = 200° C and T_c = 2190° K (Fig. 9) which is consistent with the value reported by Houston* for a cesium converter using a thorium

* Houston, Report on 20th Annual Conference on Physical Electronics, 72, 1960

dispenser cathode. Houston reports an efficiency of 7% at T_b = 175° C and T_c = 2200° K, a current of 30 amps and power output of 42 watts. Estimating the emitter area, this corresponds to a current density of 3.82 a/cm^2, and power density of 5.3 watts/cm^2. The data for the present tube correspond to a power density of 8.3 watts/cm^2. This possibly corresponds to slightly higher diode current since Houston's 3.82 a/cm^2 is still below the value of saturated emission for Th-W at this temperature.

The efficiency increases with decrease in anode diameter, which indicates plasma resistance is important as emitter to collector spacing increases. This observation is consistent with data reported by others.

It was observed that due to the heat capacity of the anode, and that the thermocouple was located on the periphery of the anode block, there was a thermal lag in measuring anode temperature. This is indicated in Table I which shows anode temperature plotted versus time for fixed heat input. It is believed that the actual inner anode surface comes to thermal equilibrium faster than indicated here, since the I-V characteristics were reproducible over a period of time. Table I also shows the anode temperature as a function of power input to the three anodes individually. These are not necessarily equilibrium values and are used to indicate the range of anode temperature for a given heat input. For most of the data reported here, anode temperature can be taken greater than 600° K.

Table I

Anode Temperature Characteristics for T_b = 100° C

Time min	Anode Temp. °K	Anode Size	Power Input watts	Anode Temp. °K
0	372	S	8	551
5	*	S	10	623
10	513	S	12	658
15	563			
20	590	M	8	533
25	601	M	10	578
30	608	M	12	623
35	610			
40	610	L	8	---
45	612	L	10	511
50	612	L	12	568

* Input power across cathode in small anode of 8 watts applied at 5 min.

From these very preliminary observations made so far on cesium plasma tubes, we may draw the following conclusions:

a. A diode efficiency of 7.5% has been measured for T_b = 200° C, T_c = 2190° K and anode O.D. of 0.1 in. This corresponds to a power density of 8.3 watts/cm^2.

b. Oscillations in the frequency range 3 to 100 kc have been observed for a T_b = 200° C and a T_c = 1400° K over a very limited cathode temperature range.

c. Oscillations for ambient bath temperature decrease in frequency with increased load resistance for a fixed T_c and the range is 100 to 600 kc.

d. Under certain conditions, oscillations do not start at short circuit current but at a finite diode voltage.

e. Oscillation frequency varies very roughly inversely with the square of anode diameter.

Some typical oscillograms, with operating conditions stated, are shown in Figs. 10, 11, 12, 13.

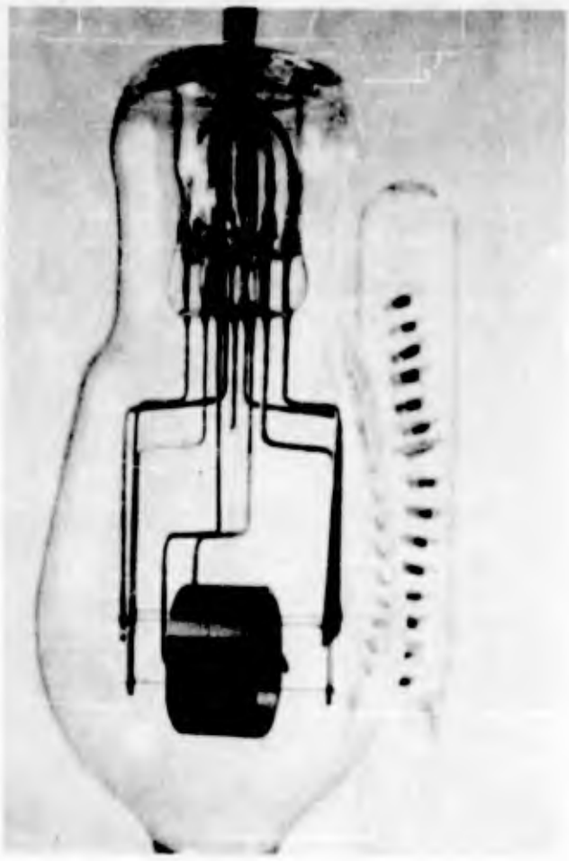

Fig. 1a

Cesium diode #2 (CD-2) before cesium pellets (in the side arm) were fired.

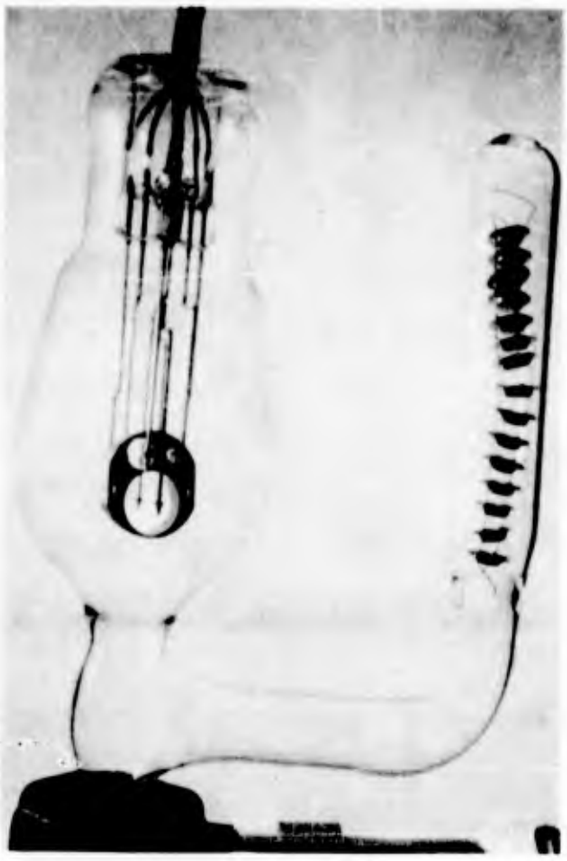

Fig. 1b

Side view of CD-2

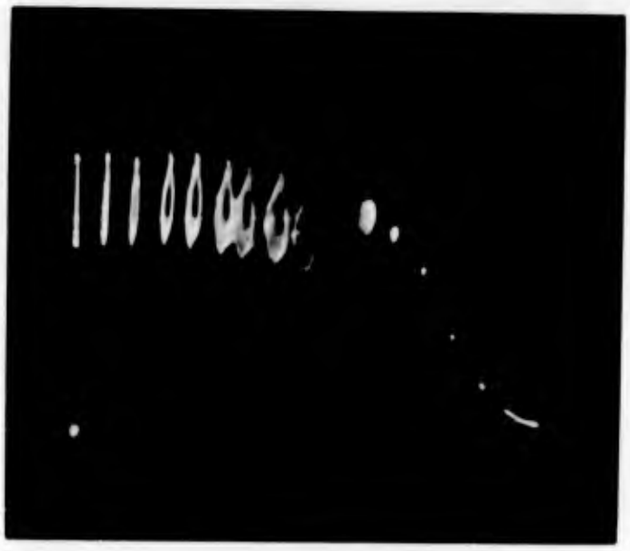

Fig. 2

I -vs V Characteristic

V* = 1 ma/cm T_b = 100° C

H* = 0.5 V/cm T_c = 1955° K

* V refers to vertical oscilloscope sensitivity and H refers to horizontal sensitivity. This is used in subsequent figures as well.

BLOCK DIAGRAM OF EXPERIMENTAL SET UP FOR MEASURING THE CHARACTISTICS OF CESIUM DIODE No. 2

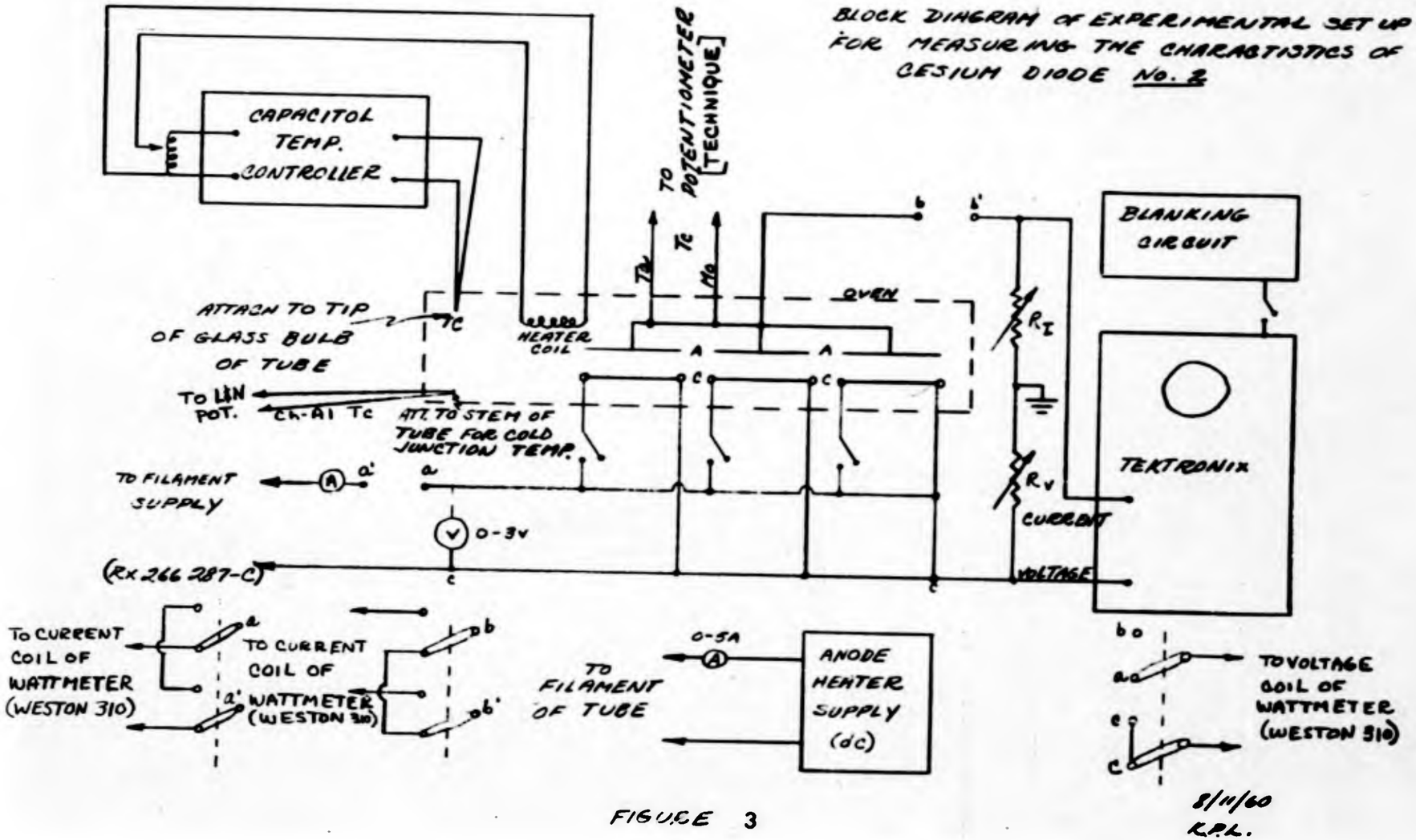

FIGURE 3

8/11/60
R.P.L.

Figure 4

Block diagram of experimental set-up for locating and measuring maximum instantaneous power output of CD-2

$$\text{TR-10 output [volts]} = \frac{(100\,I)\,(2V)}{10} = 20\,VI$$

$$\text{Power output of CD-2 [watts]} = VI = \frac{1}{20} \times \frac{\text{TR-10 output [volts]}}{R_I\ \text{[ohms]}}$$

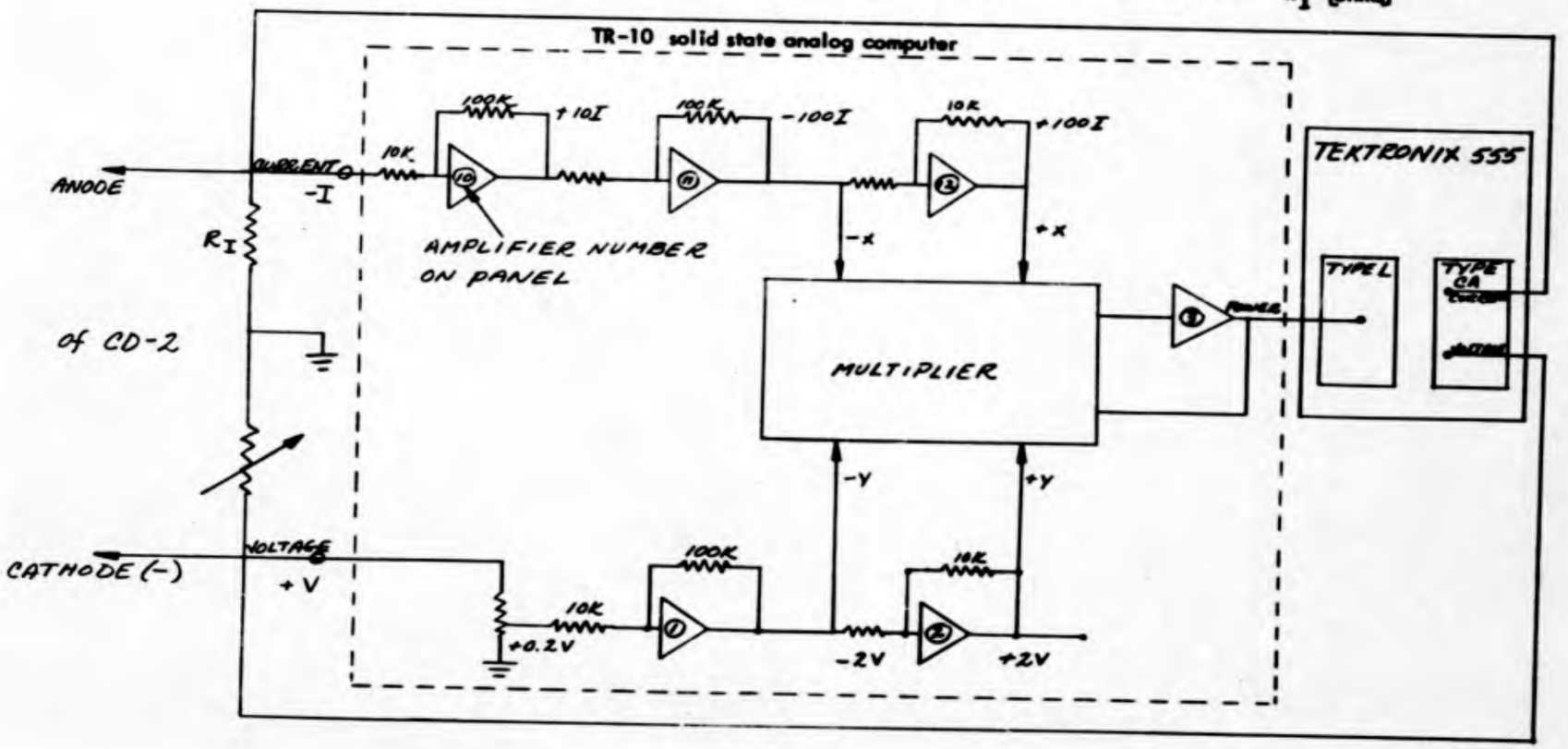

Fig. 5a

Experimental set-up used to measure maximum power output of CD-2.

Fig. 5b

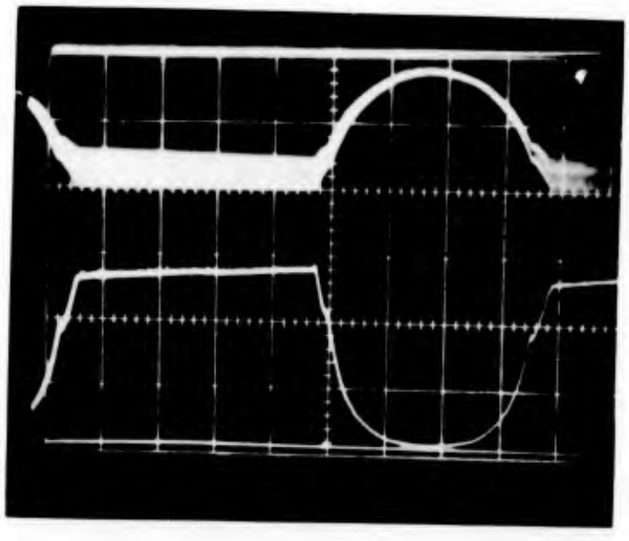

1. Voltage
2. Current

3. Power = Voltage x current

Time is increasing to the left for this and subsequent V-time traces. Note that the D.C. level decreases with time between heating pulses corresponding to filament cooling.

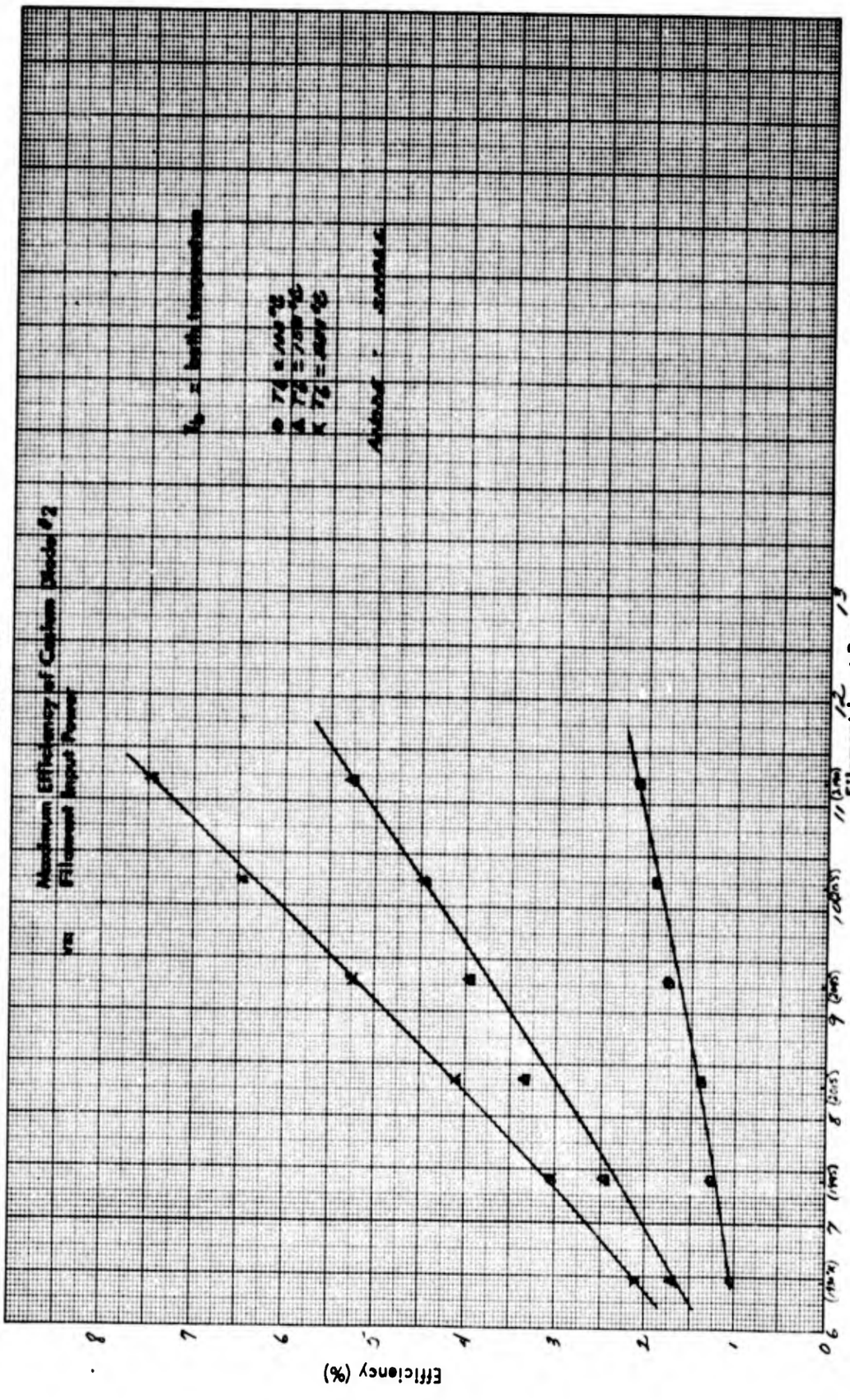

Figure 6

K•E 10 X 10 TO THE CM. KEUFFEL & ESSER CO. ALBANENE % 359T-14

Figure 7

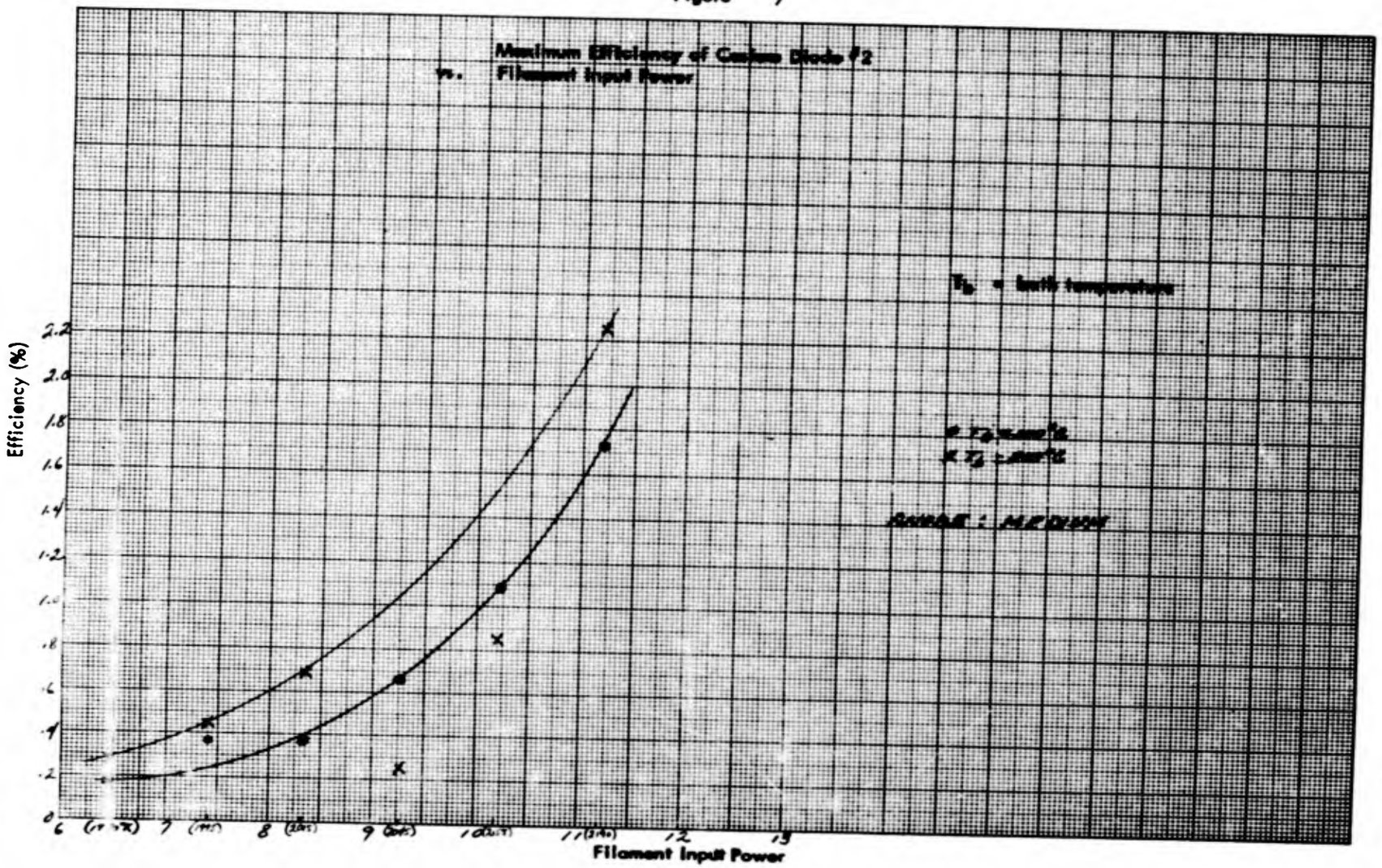

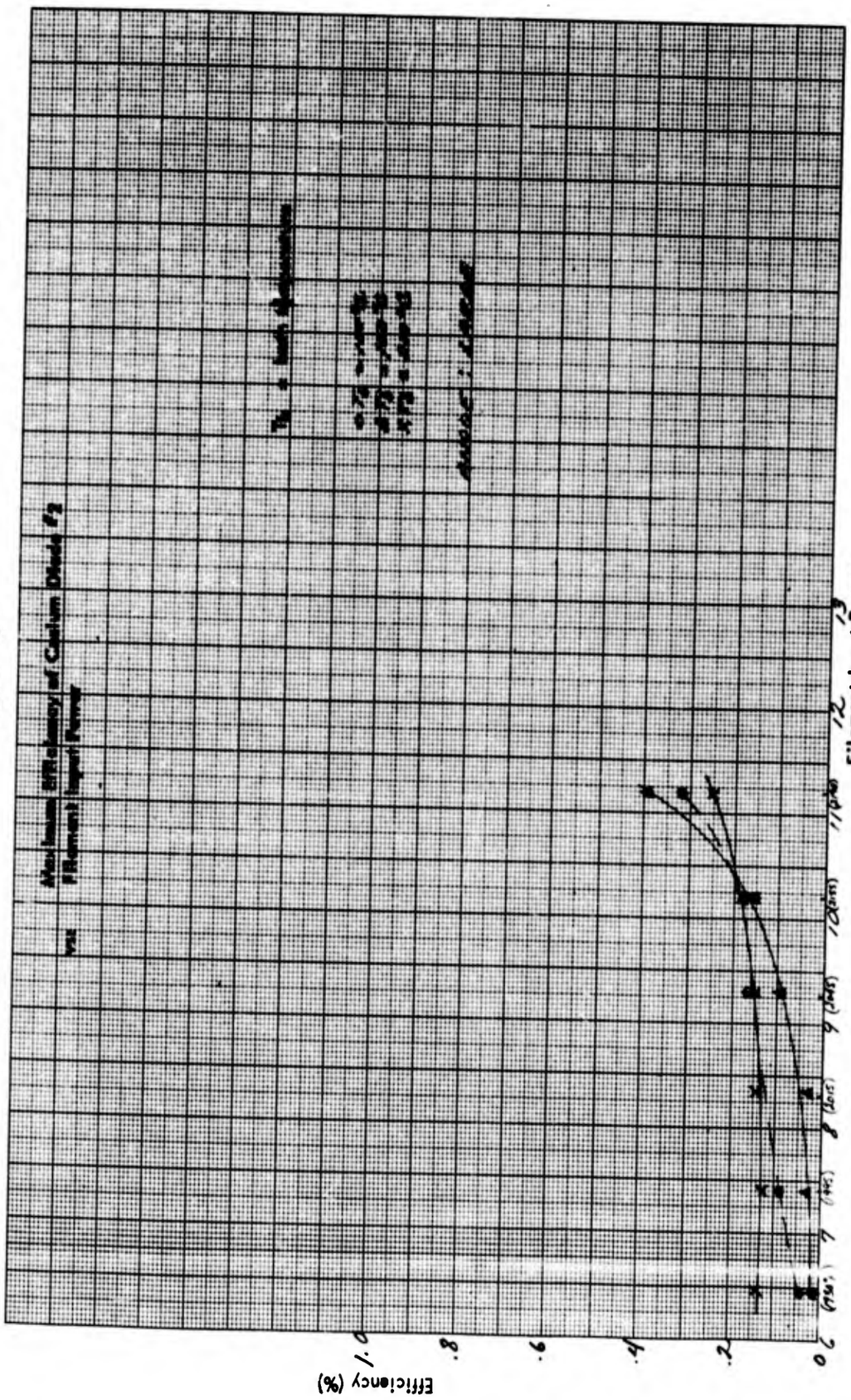

Figure 8

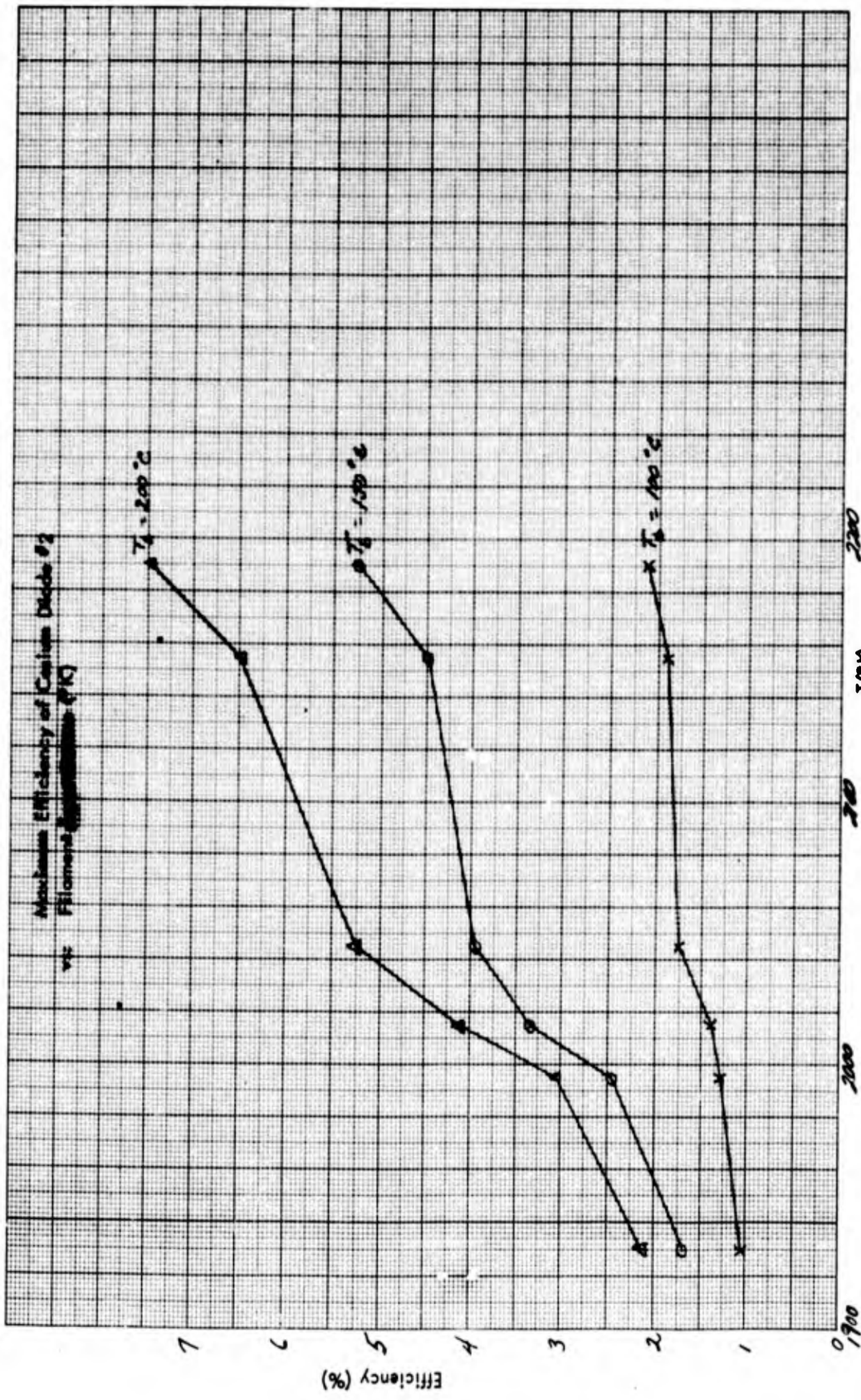

Figure 9

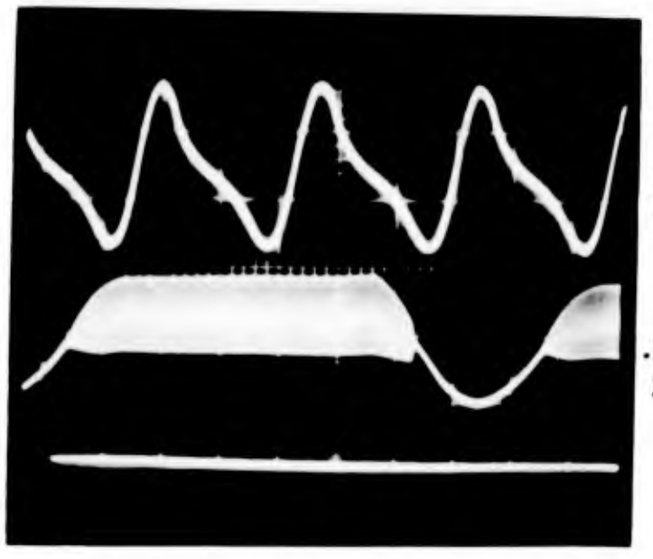

Fig. 10
Anode: Small

1. V = 0.005 V/cm
1. H = 5 μsec/cm
2. V = 0.01 V/cm
2. H = 2 msec/cm

T_b = 200° C
T_c = 1350° K
P_{in} = 2.4 W
R_L = 5 Ω
f = 74.1 kc. No oscillation for $T_f < 1350°$ K

Fig. 11

Anode: Medium

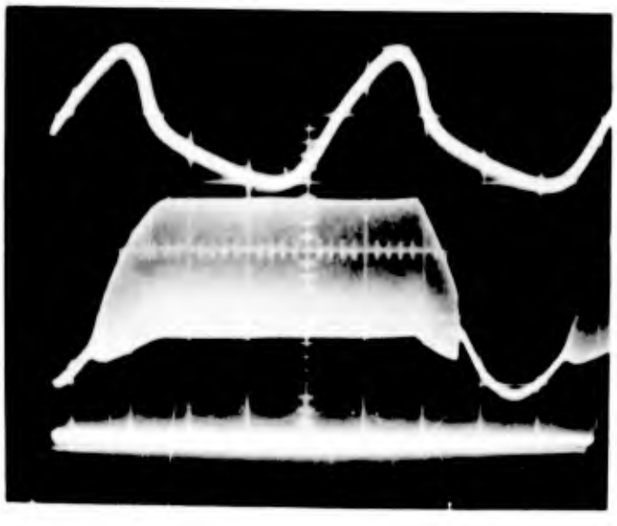

1. V = 0.01 V/cm
1. H = 10 μsec/cm
2. V = 0.01 V/cm
2. H = 2 msec/cm

T_b = 200° C
T_c = 1346° K
P_{in} = 2.3 W
R_L = 5 Ω
f = 21.3 kc
No oscillations for $T_c < 1346°$ K

Fig. 12

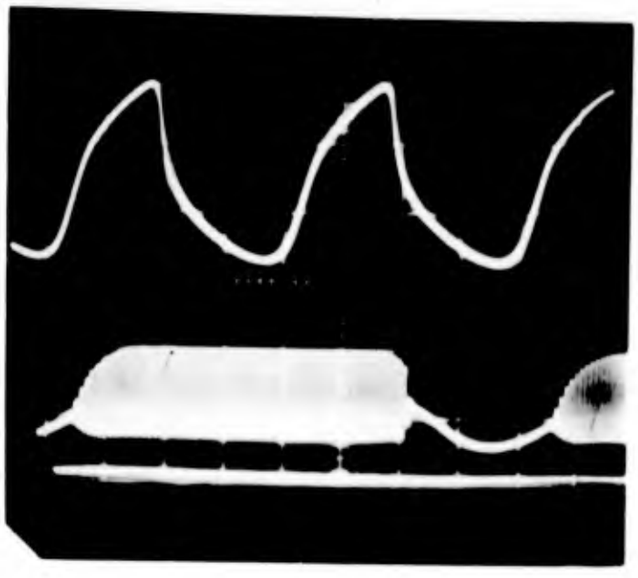

Anode: Large

1. V = 0.01 V/cm
1. H = 50 μsec/cm
2. V = 0.02 V/cm
2. H = 2 msec/cm

T_b = 200° C
T_c = 1410° K
P_{in} = 2.70 W
R_L = 5 Ω
f = 5.1 kc

No oscillations for T_c < 1410° K

Fig. 13

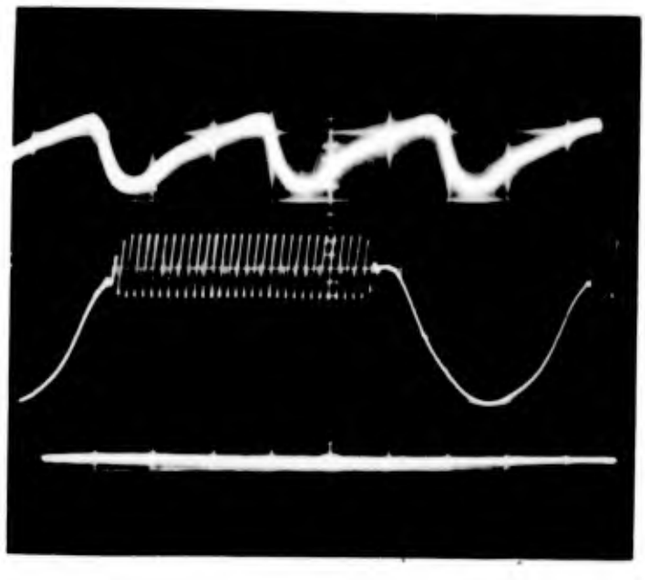

Anode: Large

1. V = 0.005 V/cm
1. H = 100 μsec/cm
2. V = 0.005 V/cm
2. H = 2 msec/cm

T_b = 200° C
T_c = 1780° K
P_{in} = 5.8 W
R_L = 5 Ω
f = 3.4 kc

UNCLASSIFIED